# Optimizing cancer therapy

Gaykema, Sietske

# OPTIMIZING CANCER THERAPY:
## A FOCUS ON MOLECULAR IMAGING

Sietske Bernadette Maria Gaykema

*The research presented in this thesis was supported by the Dutch Cancer Society (grant RUG 2009-4273), Pink Ribbon and a Sisters hope.*

*The printing of this thesis was financially supported by Stichting Werkgroep Interne Oncologie, the Dutch Cancer Society and Mr and Mrs. Gaykema-Ham, and is gratefully acknowledged.*

*Gaykema, Sietske Bernadette Maria*
*Optimizing cancer therapy: a focus on molecular imaging*
*Thesis, University of Groningen, The Netherlands*



*Cover & lay-out: Douwe Oppewal, www.oppewal.nl*
*Printed by: Ipskamp Drukkers, Enschede, The Netherlands*

rijksuniversiteit
groningen

# Optimizing cancer therapy

## A focus on molecular imaging

**Proefschrift**

ter verkrijging van de graad van doctor aan de
Rijksuniversiteit Groningen
op gezag van de
rector magnificus prof. dr. E. Sterken
en volgens besluit van het College voor Promoties.

De openbare verdediging zal plaatsvinden op

maandag 22 september 2014 om 12.45 uur

door

**Sietske Bernadette Maria Gaykema**

geboren op 19 maart 1985
te Emmen

**Promotor**
Prof. dr. E.G.E. de Vries

**Copromotores**
Dr. C.P. Schröder
Dr. A.H. Brouwers
Dr. M.N. Lub-de Hooge

**Beoordelingscommissie**
Prof. dr. R.A.J.O. Dierckx
Prof. dr. E. Vellenga
Prof. dr. J.G.W. Kosterink

**Paranimfen**
W.E. Boertien
R. Talma

# Contents

# CHAPTER 1

## General introduction

# Background

Cancer is one of the leading causes of death in the western World and its incidence is continiously rising. Cancer is treated with chemotherapy, surgery, radiotherapy or targeted and immunotherapeutic anticancer drugs. Given the still disappointing cure rates there is ongoing research to improve efficacy of treatment and reduce treatment time and side effects. Chemotherapeutic drugs have proven efficacy in several tumor types. They damage tumor DNA and subsequently apoptosis of the tumor cell. Chemotherapy affects also normal cells which causes side effects, dose limiting toxicities and therefore a longer treatment time. In most tumor types combination chemotherapy is the most effective strategy. Chemotherapy regimens differ in side effects and therefore much research is done to find the most effective treatment with the fewest side effects.

Another strategy is to try to select patients upfront or early during the course of the disease based on tumor characteristics for optimal treatment. In the last decades, tumor biological research has identified new molecular pathways involved in oncogenesis. This has resulted in the development of targeted anticancer therapies. Currently early tumor response measurements in drug development studies is based on the Response Evaluation Criteria for Solid Tumors (RECIST)[1]. This response measurement was developed with the help of a large ware house found and correlates with overall survival and is as such an early response predictor of drug effect[2]. Response evaluation according to RECIST is in general done after 2-3 cycles of systemic therapy[3]. However, prediction of response before initiation of therapy or earlier during treatment would clearly benefit the patient; patients who will not respond to a certain therapy do not have to suffer from the side-effects and can move on to a better therapy sooner. Molecular characteristics at initiation of treatment and early changes could potentially serve as predictive biomarkers and support treatment decisions at an early stage. Thus, potentially drug development and selection of the right patient for the right treatment could be optimized.

In general for molecular characterization of tumors, a biopsy is required. Unfortunately, biopsies are not always feasible. Furthermore, it provides only static information on the status of a marker in a small part of the tumor and disregards the heterogeneity within remaining tumor tissue and metastases. Characteristics at the tumor cell membrane and in the microenvironment can be targeted with monoclonal antibodies. These are highly specific proteins, which bind to either a ligand or receptor of the (cancer) cell. Molecular imaging with radio-labeled monoclonal antibodies can potentially provide non-invasive whole body information about tumor uptake- and organ distribution of the monoclonal antibodies, and about the presence of the target in all lesions across the patient's body. Molecular imaging with for example positron emission tomography (PET) can be easily serially performed by developing a tracer against a membrane receptor or a ligand.

An example of an important growth factor receptor in breast cancer is the human epidermal receptor (HER)2. Phosphorylation of HER2 leads to cell growth and differentiation. In 20-25% of the breast cancer patients the *HER2* gene is amplified and the protein overexpressed. Targeting this receptor with for example trastuzumab gives a survival benefit in the adjuvant as well as in the metastatic setting[4,5]. It is possible to visualize HER2 with radiolabeled trastuzumab[6,7]. Vascular endothelial growth factor (VEGF)-A is a key factor in angiogenesis and is broadly expressed in different types of cancer. It is the ligand of VEGF-receptors on the endothelial cells. Visualization of VEGF-A is possible e.g. with radiolabeled bevacizumab, which binds to all VEGF-A splice variants.

Next to individual targets for cancer therapy, there is an interest for targeting multiple oncogenic factors at once. Heat shock protein (HSP) 90 is a molecular chaperone which is involvement in all hallmarks of oncogenesis, including HER2 and VEGF-A. HSP90 inhibitors are currently tested in the clinic.

This thesis aims at evaluating the potential clinical applications of an optimal chemotherapeutic regimen in patients with gestational trophoblastic neoplasia in order to improve treatment as well as radio-labeled monoclonal antibody imaging of HER2 and VEGF-A in breast cancer patients, for detection of targets in tumor lesions as well as monitoring treatment response.

# Outline of the thesis

Primary therapy of high-risk gestational trophoblastic neoplasia consists of polychemotherapy. Etoposide (100 mg/m$^2$ days 1-5) and cisplatin (20 mg/m$^2$ days 1-5) (EP) could be a good alternative treatment regimen to etoposide 100 mg/m$^2$ days 1-5, methotrexate 300 mg/m$^2$ day 1, cyclophosphamide 600 mg/m$^2$ day 1, actinomycin D 0.5 mg/m$^2$ day 2 and cisplatin 50 mg/m$^2$ day 4 (EMACP), aiming for comparable effectiveness with a shorter total treatment time.

In **chapter 2** we evaluate the efficacy, treatment time and safety of EP as compared to EMACP. All patients with high risk GTN who were treated with EP in our institution between 2001 and 2013 were included in this retrospectively analysis and compared with the results of patients treated with EMACP between 1984 and 2001. Disease specific survival, duration of therapy and major toxicity were reported.

In **chapter 3**, the roles of current and future potentials of molecular imaging in drug development are reviewed with imaging of HER2 and VEGF-A as role models. We describe in more detail the information that has been obtained with trastuzumab and bevacizumab immuno positron emission tomography (PET) and single photon emission computed tomography (SPECT) imaging. This information could support the use of immunoPET imaging in the development of other antibodies and targeted anticancer agents.

Breast cancer prognosis and response to treatment appear to be partly dependent on microenvironmental characteristics[9]. Therefore, targeting factors in the tumor microenvironment that support the process of tumor progression and development of metastases, may be a rational way to improve therapies to treat cancer patients. In **chapter 4**, we review the targets in the microenvironment that can potentially be modulated to improve patient outcome. Articles for this review were found by searches of PubMed, abstracts American Association for Cancer Research (AACR) and American Society of Clinical Oncology (ASCO) and the clinicaltrials.gov database by use of the terms 'microenvironment' combined with 'metastasis' 'metabolic dysfunction' 'migration' 'immune cells' 'angiogenesis' or 'matrix remodeling' and combinations of these terms with the selected soluble factors. In addition, relevant papers from the reference lists of selected papers were included. Only studies written in English were included.

Loss or gain of HER2 expression can have clear therapeutic consequences, as patients with HER2 positive lesions benefit from anti-HER2 therapy[9,10]. This underlines the necessity to accurately assess HER2 status during the course of metastatic breast cancer. Non-invasive determination of HER2 expression can be performed with molecular imaging. In the clinical setting HER2 imaging is performed with trastuzumab radiolabeled with $^{111}$In and with the positron emitting tomography (PET) isotope zirconium-89 ($^{89}$Zr)[6,7]. One of the hurdles in implementation HER2 imaging in clinical practice is the unknown effect of trastuzumab on *in vivo* molecular HER2 imaging. We previously reported on $^{111}$In-trastuzumab scintigraphy in 17 patients with HER2 overexpressing metastatic breast cancer after the first loading dose of trastuzumab[6]. Part of these patients underwent a second

scintigraphy after treatment. Therefore the aim of the study described in **chapter 5** is to use the serial scintigraphy data to assess the effect of trastuzumab treatment on tumour uptake, biodistribution and radiation dosimetry of $^{111}$In-trastuzumab. $^{111}$In-scintigraphy was performed before and during treatment with paclitaxel and trastuzumab. Patients received 6 once-every-3-weeks cycles trastuzumab (2 mg/kg) and paclitaxel (175 mg/m$^2$) every 3 weeks. $^{111}$In-trastuzumab was injected on day 1 of the first cycle and day 15 of the fourth cycle. Whole-body planar scintigraphy scans were acquired on 4 different time points from 15 minutes until 7 days postinjection. Differences in tumor and organ uptake were determined from radiation dosimetric data and expressed as residence time (defined as area under the curve of radioactivity versus time). Radiation dose of tumors and organs and effective dose were calculated.

**Chapter 5B** describes the clinical value of the $^{89}$Zr-trastuzumab PET in a patient with a diagnostic dilemma.

In **chapter 6**, the clinical feasibility of VEGF-A imaging with $^{89}$Zr-bevacizumab in patients with primary breast cancer is presented. Prior to surgery, breast cancer patients underwent a PET/CT scan of breasts and axillary regions, 4 days after injection of the tracer $^{89}$Zr-bevacizumab administration intravenously. $^{89}$Zr-bevacizumab uptake was quantified as the maximum standard uptake value ($SUV_{max}$). Quantification of $^{89}$Zr-bevacizumab levels in primary tumor lesions, metastatic lymph nodes as well as physiologic uptake in breast and bloodpool is performed. PET images were compared with standard imaging modalities. VEGF-A levels in tumor and normal breast tissues were assessed with Enzyme-Linked Immuno Sorbent Assay (ELISA) and immunohistochemistry and compared with the PET results.

HSP90 chaperones protect key client proteins involved in all hallmarks of breast cancer growth and progression including HER2 and hypoxia inducible transcription factor (HIF)-1$\alpha$[11]. The latter results in downregulation of VEGF-A. Therefore HER2 and VEGF-A downregulation are potential early predictive biomarkers for the response to drug that act as HSP90 inhibitors. Previously, HER2 and VEGF-A imaging following HSP90 inhibition was performed in mice bearing a human xenograft model[12,13]. In **chapter 7,** the study is presented in which patients with metastatic or locally advanced breast cancer (HER2 or ER positive) were treated with the HSP90 inhibitor NVP-AUY922. 70mg/m2 NVP-AUY922 was administered intravenously on a weekly schedule in the University Medical Center Groningen or The Royal Marsden Hospital London. Here, we searched for a biomarker to predict tumor response. $^{18}$F-fluordeoxyglucose (FDG)-PET and CT were performed pre-treatment and at different time points during treatment. In addition, patients underwent an $^{89}$Zr-bevacizumab PET (in estrogen receptor (ER) positive patients) or $^{89}$Zr-trastuzumab PET (in HER2 positive patients) pre-treatment and after 3 weeks. In blood samples, serial HSP70 levels and extracellular form of HER2 (HER2-ECD) were measured. Quantification of $^{89}$Zr-bevacizumab-and trastuzumab levels in all lesions as well as physiologic uptake in organs was performed. PET data were compared with conventional imaging.

In **chapter 8 and 9**, the findings of this thesis are summarized, followed by a general discussion with future perspectives.

# References


1. Eisenhauer EA, Therasse P, Bogaerts J, et al. New response evaluation criteria in solid tumours: revised RECIST guideline (version 1.1). Eur J Cancer 2009; 45:228-47.
2. Jain RK, Lee JJ, Ng C, et al. Change in tumor size by RECIST correlates linearly with overall survival in phase I oncology studies. J Clin Oncol 2012; 30:2684-90.
3. NCCN clinical practice guidelines in clinical oncology. v2013; 2013.
4. Slamon DJ, Clark GM, Wong SG, Levin WJ, Ullrich A, McGuire WL. Human breast cancer: correlation of relapse and survival with amplification of the HER-2/neu oncogene. Science 1987; 235:177-82.
5. Masood S, Bui MM. Prognostic and predictive value of HER2/neu oncogene in breast cancer. Microsc Res Tech 2002; 59:102-8.
6. Perik PJ, Lub-De Hooge MN, Gietema JA, et al. Indium-111-labeled trastuzumab scintigraphy in patients with human epidermal growth factor receptor 2-positive metastatic breast cancer. J Clin Oncol 2006; 24:2276-82.
7. Dijkers EC, Oude Munnink TH, Kosterink JG, et al. Biodistribution of 89Zr-trastuzumab and PET imaging of HER2-positive lesions in patients with metastatic breast cancer. Clin Pharmacol Ther 2010; 87:586-92.
8. Morales M, Planet E, Arnal-Estape A, Pavlovic M, Tarragona M, Gomis RR. Tumor-stroma interactions a trademark for metastasis. Breast 2011; 20 Suppl 3:S50-5.
9. Slamon DJ, Leyland-Jones B, Shak S, et al. Use of chemotherapy plus a monoclonal antibody against HER2 for metastatic breast cancer that overexpresses HER2. N Engl J Med 2001; 344:783-92.
10. Piccart-Gebhart MJ, Procter M, Leyland-Jones B, et al. Trastuzumab after adjuvant chemotherapy in HER2-positive breast cancer. N Engl J Med 2005; 353:1659-72.
11. Workman P, Burrows F, Neckers L, Rosen N. Drugging the cancer chaperone HSP90: combinatorial therapeutic exploitation of oncogene addiction and tumor stress. Ann N Y Acad Sci 2007; 1113:202-16.
12. Nagengast WB, de Korte MA, Oude Munnink TH, et al. 89Zr-bevacizumab PET of early antiangiogenic tumor response to treatment with HSP90 inhibitor NVP-AUY922. J Nucl Med 2010; 51:761-7.
13. Oude Munnink TH, Korte MA, Nagengast WB, et al. (89)Zr-trastuzumab PET visualises HER2 downregulation by the HSP90 inhibitor NVP-AUY922 in a human tumour xenograft. Eur J Cancer 2010; 46:678-84.

# CHAPTER 2

# Cisplatin-based chemotherapy for high risk gestational trophoblastic neoplasia: EP or EMACP?

S.B.M. Gaykema[1]
H.L. Lutgers[2]
H.J.G. Arts[3]
J.A. Gietema[1]
A.K.L Reyners[1]

Departments of Medical Oncology[1], Endocrinology[2] and Gynaecologic Oncology[3], University of Groningen, University Medical Centre Groningen, Groningen, the Netherlands

*Submitted*

# Abstract

**Background:** Therapy of low risk gestational trophoblastic neoplasia (GTN) not responding to monotherapy and primary high risk GTN consists of polychemotherapy. EMACP, a regimen consisting of etoposide (100 mg/m$^2$ d1-5), methotrexate (300 mg/m$^2$ d1), cyclophosphamide (600 mg/m$^2$ d1), dactinomycin (0.5 mg/m$^2$ d2) and cisplatin (50 mg/m$^2$ d4) intravenously, is effective. Etoposide (100 mg/m$^2$ d1-5) and cisplatin (20 mg/m$^2$ d1-5 intravenously; EP) may be an alternative regimen with comparable efficacy and a shorter treatment time. After normalization of the βhCG serum levels, patients treated with EMACP received 2 additional consolidation cycles, which is not the case for EP. In this study we evaluate the safety, efficacy, and treatment time of EP.

**Methods:** All patients with high risk GTN who were treated since 2001 with EP at our institution were included in this retrospectively cohort analysis and compared with the results of patients treated between 1984-2001 with EMACP. Disease specific survival, duration of therapy and major toxicity are reported.

**Results:** Thirteen and 16 patients started treatment with respectively EP and EMACP. With a median follow up duration of 173 months (range 11-344) overall survival rates are comparable for both regimens (EP 92.3%, EMACP 93.8%; $P = 0.88$). Median treatment time was shorter with EP (EP 78, range 63-84 days; EMACP 110, range 84-168 days; ($P = 0.006$). Respectively 3 and 9 patients were hospitalized for pancytopenia ($P = 0.17$). One patient developed an allergic reaction on EMACP. Three patients on EP experienced a thromboembolic event and one patient was hospitalized for diarrhea.

**Conclusion:** In this retrospective single institution analysis of the treatment of high risk GTN the EP regimen has survival rates in the same range as EMACP with comparable toxicity, but with a shorter treatment time.

# Introduction

Gestational trophoblastic disease (GTD) defines a spectrum of tumors originating from the placenta. The resulting proliferative process has the potential to develop into the malignant subset of gestational trophoblastic neoplasia (GTN). The spectrum of GTN is characterized by their aggressive invasion into the myometrum and propensity to metastasize. Histologically, these tumors include invasive mole, choriocarcinoma, placental site trophoblastic tumor and epithelioid trophoblastic tumor. The most common malignant form of GTN is choriocarcinoma, which arises from an antecedent pregnancy, either a molar or normal conceptus. GTN is one of the most chemotherapy-responsive and highly curable cancers, even in the setting of widespread metastatic disease[1].

Low risk GTN, which is defined as a WHO prognostic score of 0-6[2], is treated with methotrexate or dactinomycin. When this fails, or in case of high risk GTN, which is defined as a WHO prognostic score of ≥7, several combination chemotherapy regimens have been advocated[3]. However, the necessity for polychemotherapy is not frequent due to the low incidence of GTN and the effective treatment of low risk GTN with monotherapy. A combination of etoposide, methotrexate, dactinomycin, cyclophosphamide and vincristine (EMA-CO) is the most used polychemotherapy regimen in high-risk GTN with a 80% complete remission rate[4]. The EMA-CO regimen was retrospectively compared with methotrexate plus folate acid and dactinomicin (MTX+Act-D), methotrexate, dactinomycin and cyclophosphamide or chlorambucil (MAC) and cyclophosphamide, hydroxurea, dactinomycin, methotrexate with folate acid, vincristine and doxorubicin (CHAMOCA).

The EMA-CO regimen had the highest complete remission rate with few toxic effects[5]. However, a significant part of patients treated with EMA-CO did require salvage chemotherapy with a platinum containing regimen[1]. Especially in case of liver and/or brain metastases 5-year survival is poor, 35.3% and 70.6% respectively[6]. The 5-year survival of the subgroup of patients with both liver and brain metastases is only 10%[7]. In a recent study, etoposide and cisplatin (EP) followed by etoposide, methotrexate, and dactinomycin weekly alternated with cyclophosphamide and vincristine (EMA-CO) nearly completely prevented early deaths in that phase II study[8]. Besides induction therapy, platinum-based chemotherapy can also be the primary curative regimen. Remission rates in platinum-based chemotherapy, consisting of etoposide, methotrexate, cyclophosphamide, actinomycin D and cisplatin (EMACP), are in the same range as that of EMA-CO[9]. However, both these regimens need two consolidation cycles after normalization of the β-human chorionic gonadotropin (βhCG).

As GTN histologically mimics testicular germ cell tumours, which can be cured with etoposide and cisplatin[10], this compact regimen can also be used as a first line treatment in GTN without the need of consolidation cycles. Here, we report the results of the EP regimen in patients with high-risk GTN treated at our institution from 2001. These results were compared with the results of the EMACP regimen in a comparable patient population treated until 2001.

# Methods

## Study population

Data from patients who were treated at our institution with EP or EMACP for primary high-risk GTN or after failure of previous chemotherapy for low-risk GTN were collected retrospectively. EMACP was standard of treatment from 1984 till 2001, thereafter EP became our first-line polychemotherapy regimen. Patients were classified using the modified WHO prognostic scoring system. Patients with WHO scores of 0 to 6 were considered to have low-risk disease, whereas those with a score of 7 or higher were considered high-risk.

## Treatment

EP was administrated intravenously during five subsequent days in a three-weekly interval: etoposide 100 mg/m$^2$/day and cisplatin 20 mg/m$^2$/day. In this protocol, 3 cycles of EP were administered if the βhCG was normalized at the start of the second cycle; in all other cases the patients received four cycles of EP. Normalization of βhCG was defined as a serum βhCG level below 5 IU/L. This protocol was analogous to the testicular germ cell tumor treatment protocol, except that bleomycin was not given to GTN-patients. In the EMACP regimen, etoposide 100 mg/m$^2$ days 1-5, methotrexate 300 mg/m$^2$ day 1, cyclophosphamide 600 mg/m$^2$ day 1, dactinomycin 0.6 mg/m$^2$ day 2 and cisplatin 60 mg/m$^2$ day 4 were administered intravenously in a four-weekly interval. After normalization of the βhCG serum levels, patients treated with EMACP received 2 additional consolidation cycles. In both regimens, surgical resection of the most suspicious residual tumor focus was considered if the βhCG did not normalize.

## Outcomes

βhCG levels were measured at the start of each cycle and once between two cycles of chemotherapy. Before the year 2000, the immunoradiometric assay from Amersham Buchler, Braunschweig, FRG was used. In 2000 this assay was changed to Architect from Abbot, IL. All values were converted to IU/L. The time to normalization was defined as the time from the first treatment day until the first βhCG value below 5 IU/l. Outcome measures were the overall survival, the mean number of chemotherapy cycles required to achieve complete remission (defined as βhCG value below 5 IU/l) and the duration of therapy. Toxicity was registered using the Common Terminology Criteria for Adverse Events (CTCAE), version 3.0. Data on toxicity were obtained from the medical chart of each individual patient.

## Statistical analysis

Data are presented as median ± standard deviation (SD). Patient characteristics, remission rates and toxicity were compared using Fisher's exact or Chi-square test. Mean age, time to normalization, time of treatment and mean number of chemotherapy cycles were compared using Student t-test or Mann-Whitney U test. A double sided *P*-value <0.05 was considered significant.

# Results

A total of 29 patients with high-risk GTN, or with low-risk disease that failed on prior chemotherapy, have been treated with EP (n=13) or EMACP (n=16) between 1984 and 2013 at our institution. Patient characteristics are summarized in Table 1.

**Table 1.** Patient characteristics at start of the polychemotherapeutic treatment

| | EP (*N*=13) | EMACP (*N*=16) | *P*-value |
|---|---|---|---|
| Age at diagnosis (years) | | | |
| Mean ± SD | 31 ± 4.6 | 31 ± 6.9 | 0.82 |
| Antecedent pregnancy | | | |
| Hydatidiform mole | 8 (61.5%) | 11 (68.8%) | |
| Term pregnancy | 5 (38.5%) | 1 (6.3%) | 0.08 |
| Non-molar abortion | 0 | 3 (18.8%) | |
| IUVD | 0 | 1 (6.3%) | |
| WHO score at primary diagnosis | | | |
| Median (range) | 8 (2-20) | 13 (3-15) | 0.53 |
| βhCG at start of polychemotherapy | | | |
| Median (range) | $1.1*10^4$ ($21-1.2*10^6$) | $1.7*10^4$ ($4-1.5*10^5$) | 0.08 |
| Indication of chemotherapy | | | |
| Single-agent resistant disease | 7 (53.8%) | 14 (87.5%) | 0.09 |
| Primary high-risk disease | 6 (46.2%) | 2 (12.5%) | |

In the EP group, one patient died due to an intracranial bleeding in a brain metastasis after the first EP cycle. The remaining 12 patients achieved complete remission. In the EMACP regimen, 15 of the 16 patients achieved complete remission. One patient died due to sepsis after the first cycle of EMACP. During follow up, no patients developed recurrent disease (median follow-up EP-regimen 93 months, range 11-150; median follow-up EMACP-regimen 280 months, range 170-344). Disease specific survival of EP patients was 92.3% and 93.8% for patients initially treated with EMACP ($P$ = 0.88). Median time to βhCG normalization was 50 days, range 13-177 for the EP regimen compared to a median of 32 days, range 3-72 for EMACP ($P$ = 0.17).

Median treatment time was 78 days (range 63-84) for patients treated with EP compared to 110 days (range 84-168) for patients treated in the EMACP regimen ($P$ = 0.006).

In both treatment regimens one patient died during treatment. A total of 9 patients who received EMACP (56.3%) and 3 who received EP (30.8%) were hospitalized for pancytopenia with neutropenic fever ($P = 0.17$). One patient treated with EMACP developed an allergic reaction, probably due to cisplatin, for which she was successfully treated in the intensive care unit. Three patients treated with EP had a thrombotic event during treatment and one patient was hospitalized for diarrhea grade 4, which subsided within 5 days with supportive treatment (Table 2).

**Table 2.** Toxicity requiring hospitalization

| | EP (*N*=13) | EMACP (*N*=16) | *P*-value |
|---|---|---|---|
| Thromboembolic events | 3 | 0 | |
| Pancytopenia | 4 | 9 | 0.17 |
| Allergic reaction | 0 | 1 | |
| Diarrhea | 1 | 0 | |

# Discussion

To the best of our knowledge, this is the first paper reporting on the results of EP as first line polychemotherapy for high-risk GTN or low risk GTN unresponsive to monotherapy. The present analysis shows that disease specific survival rates of patients treated with EP were in the same range as that of patients treated with EMACP with a shorter total treatment time. Patients treated with EP appeared to have more often thrombotic events and diarrhea. However patients treated with EMACP were hospitalized more frequently for neutropenic fever and thrombocytopenia. This study was too small to study long-term side effects. The relatively high risk of secondary malignancies after polychemotherapy for GTN found in other studies is expected to be related to the cumulative dose of etoposide[9]. Long-term effects of EP are quite extensively studied in patients with testicular cancer[11], in contrast to the long-term effects of EMACP. A total of 82 patients received a cumulative dose of at least 2 g/m$^2$ of etoposide, after which 5 (6.1%) developed leukaemia within 10 years after treatment[12]. Whereas no patients developed leukaemia in a study in which patients received less than 2 g/m$^2$[,13]. Each cycle of EP and EMACP contains the same amount (500 mg/m$^2$) of etoposide. The EMACP regimen required slightly more cycles compared to EP, and thus higher cumulative dose of etoposide, which may have the consequence of a higher risk for secondary leukaemia in EMACP. The higher prevalence of bone marrow toxicity in EMACP compared to EP may be a sign of this increased risk. Although EMACP might encompass a higher risk for secondary malignancies compared to EP, the EP regimen has serious vascular side effects. In the EP regimen, the total cisplatin dose (100 mg/m$^2$ per cycle) is higher compared to the EMACP regimen (60 mg/m$^2$). Cisplatin is associated with thrombotic events during treatment[14]. The long-term effects of cisplatin involve mainly neurotoxicity, renal and vascular toxicity[15], which might be more prominent in patients treated with EP.

The time to βhCG normalization did not differ significantly between the two treatment regimens. However, most patients treated with EMACP were treated before the year 2000, whereas patients treated thereafter mainly received EP. Moreover, more patients treated with EMACP had single-agent resistant disease. At earlier times, less extensive pre-treatment imaging was performed. That way, sites of metastases might be missed which leads to lower WHO scores. The change in the βhCG assay diminishes the uniformity of the assay, but will not influence the time to normalization.

In this study we have shown that EP combination chemotherapy is a feasible treatment for high-risk GTN. The confidence interval of the remission rates and long-term survival of EP are overlapping with EMACP, while the treatment time was shorter with EP. There were no relevant different toxicity profiles for EP and EMACP. It seems feasible to decrease the intensity of the treatment of high-risk GTN and put 3 or 4 cycles of EP as initial treatment. A randomized control trial is needed to confirm the results of this retrospective study prospectively and should encompass long-term side effects.

# References

1. Lurain JR. Gestational trophoblastic disease II: classification and management of gestational trophoblastic neoplasia. Am J Obstet Gynecol 2011; 204:11-18.
2. FIGO Oncology Committee. FIGO staging for gestational trophoblastic neoplasia 2000. FIGO Oncology Committee. Int J Gynaecol Obstet 2002; 77:285-287.
3. El-Helw LM, Hancock BW. Treatment of metastatic gestational trophoblastic neoplasia. Lancet Oncol 2007; 8:715-724.
4. Newlands ES, Bagshawe KD, Begent RH et al. Results with the EMA/CO (etoposide, methotrexate, actinomycin D, cyclophosphamide, vincristine) regimen in high risk gestational trophoblastic tumours, 1979 to 1989. Br J Obstet Gynaecol 1991; 98:550-557.
5. Kim SJ, Bae SN, Kim JH et al. Effects of multiagent chemotherapy and independent risk factors in the treatment of high-risk GTT--25 years experiences of KRI-TRD. Int J Gynaecol Obstet 1998; 60 Suppl 1:S85-96.
6. Bower M, Newlands ES, Holden L et al. EMA/CO for high-risk gestational trophoblastic tumors: results from a cohort of 272 patients. J Clin Oncol 1997; 15:2636-2643.
7. Crawford RA, Newlands E, Rustin GJ et al. Gestational trophoblastic disease with liver metastases: the Charing Cross experience. Br J Obstet Gynaecol 1997; 104:105-109.
8. Alifrangis C, Agarwal R, Short D et al. EMA/CO for high-risk gestationaltTrophoblastic neoplasia: Good outcomes with induction low-dose etoposide-cisplatin and genetic analysis. J Clin Oncol 2013; 88:536-541.
9. Lybol C, Thomas CM, Blanken EA et al. Comparing cisplatin-based combination chemotherapy with EMA/CO chemotherapy for the treatment of high risk gestational trophoblastic neoplasia. Eur J Cancer 2013; 49:860-867.
10. Williams SD, Birch R, Einhorn LH et al. Treatment of disseminated germ-cell tumors with cisplatin, bleomycin, and either vinblastine or etoposide. N Engl J Med 1987; 316:1435-1440.
11. Haugnes HS, Bosl GJ, Boer H et al. Long-term and late effects of germ cell testicular cancer treatment and implications for follow-up. J Clin Oncol 2012; 30:3752-3763.
12. Rustin GJ, Newlands ES, Lutz JM et al. Combination but not single-agent methotrexate chemotherapy for gestational trophoblastic tumors increases the incidence of second tumors. J Clin Oncol 1996; 14: 2769-2773.
13. Smith MA, Rubinstein L, Anderson JR et al. Secondary leukemia or myelodysplastic syndrome after treatment with epipodophyllotoxins. J Clin Oncol 1999; 17:569-577.
14. Travis LB, Beard C, Allan JM et al. Testicular cancer survivorship: research strategies and recommendations. J Natl Cancer Inst 2010; 102:1114-1130.
15. Pliarchopoulou K, Pectasides D. Late complications of chemotherapy in testicular cancer. Cancer Treat Rev 2010; 36:262-267.

# CHAPTER 3

# Molecular imaging of the receptor HER2 and the ligand VEGF as role models for the use of immunoPET in drug development

S.B.M. Gaykema[1]
E.G.E. de Vries[1]
T.H. Oude Munnink[1]
W.B. Nagengast[1]
A.G.T. Terwisscha van Scheltinga[1]
G.A.P. Hospers[1]
R.A.J.O. Dierckx[3]
A.H. Brouwers[3]
C.P. Schröder[1]
M.N. Lub-de Hooge[2,3]

Departments of Medical Oncology[1], Hospital and Clinical Pharmacy[2], and Nuclear Medicine and Molecular Imaging[3], University Medical Center Groningen, University of Groningen, The Netherlands.

*World Scientific, Chapter in Trends on the role of PET in drug development 2012; p681-690*

# Abstract

ImmunoPET is the noninvasive imaging of specific targets with radiolabeled monoclonal antibodies. These tracers can give information about tumor uptake and about presence of the target in all tumor lesions across the patient's body. ImmunoPET can be used to evaluate changes in target as consequence of treatment with monoclonal antibody and non-monoclonal antibody targeted drugs. It can also potentially contribute to optimal patient selection for targeted therapy. In this chapter, we illustrate these potential applications of immunoPET by means of preclinical and clinical imaging studies performed with the radiolabeled monoclonal antibodies trastuzumab and bevacizumab for visualization of the receptor HER2 and the ligand VEGF respectively.

# Introduction



In the last decades, many new targets for anticancer drugs have been identified and this has led to the development of the targeted anticancer therapies. Among them are monoclonal antibodies. Monoclonal antibodies are highly specific proteins, which bind to either a ligand or receptor of the (cancer) cell and several monoclonal antibodies have been approved over the last years for use as therapeutic drug in oncology. Currently there are limited options to predict who is going to respond to these targeted therapies. Even with the progress that has been made in the selection of a high HER2 expression in tumors of patients treated with the monoclonal antibody trastuzumab or selection of wild-type KRAS in patients treated with cetuximab or panitumumab, there is still a need to improve the selection of patients so as to receive the most optimal treatment.

Noninvasive imaging of specific targets with radiolabeled monoclonal antibodies can give information about tumor uptake and organ distribution of the monoclonal antibodies and about the presence of the target in all lesions across the patient's body. Monoclonal antibodies can be radiolabeled with varying radio-isotopes and can, depending on the isotope, be imaged by single photon emission computed tomography (SPECT) or positron emission tomography (PET). The physical half-life of the radio-isotope should suit the kinetics of tumor accumulation and non-tumor clearance of the monoclonal antibodies to allow imaging at the time-point of optimal tumor accumulation. Monoclonal antibodies have a long serum half-life of, often more than ten days. They are predominantly excreted through hepatic clearance, due to their large molecular weight around 150 kDa, which is above the kidney threshold of approximately 50 kDa. Large monoclonal antibodies penetrate slowly but constantly into solid tumor tissue. Because the serum clearance is low, the slow penetration results over days in an increasing tumor accumulation. For adequate visualization with slowly accumulating monoclonal antibodies the isotopes should also have long half-lives, like Indium-111 ($^{111}$In; $t_{1/2}$ 67h) for SPECT and Zirconium-89 ($^{89}$Zr; $t_{1/2}$ 78h) for PET imaging. In order to minimize bone marrow, thyroid, liver or kidney toxicity, the half-life of the isotope should not exceed the biological half-life of the monoclonal antibodies. PET potentially provides a higher spatial resolution, a better signal-to-noise ratio and allows a superior quantification compared to SPECT.

Over the last years we performed pre-clinical as well as clinical imaging studies with radiolabeled trastuzumab, which binds to HER2 and with radiolabeled bevacizumab which binds to all vascular endothelial growth factor (VEGF)-A splice variants.

In this chapter we describe in more detail the information that has been obtained with trastuzumab and bevacizumab immunoPET imaging. This information could support the use of immunoPET imaging in the development of other antibodies and targeted anticancer agents.

# HER2 visualization

HER2 is a member of the ErbB tyrosine kinase receptor family and consists of an extracellular domain, a transmembrane segment and an intracellular protein kinase domain. HER2 is involved in cellular growth, survival, proliferation and maturation in metastases and angiogenesis, and has anti-apoptotic effects. Over-expression of this receptor due to gene amplification occurs in 20-30% of all breast cancers and in a lower percentage in gastric and esophageal cancers[1]. Trastuzumab is a humanized monoclonal antibody targeting the extracellular domain of HER2 and is used in the treatment of patients with HER2 over-expressing breast cancer. The addition of trastuzumab to chemotherapy has increased tumor response rate and survival in the metastatic setting, and disease free- and overall survival in the adjuvant setting. HER2 tumor expression can vary during treatment in an individual patient and can differ between metastatic lesions within a patient. In the metastatic setting almost all patients will develop resistance for this drug.

To allow in vivo HER2 imaging, we developed $^{111}$In-trastuzumab. Tumor uptake and biodistribution of $^{111}$In-trastuzumab was studied in HER2-positive and –negative human tumor-bearing mice. The HER2 positive tumor showed substantially more uptake of $^{111}$In-trastuzumab compared to the HER2 negative tumor. The difference in $^{111}$In-trastuzumab uptake between HER2-positive versus negative tumors was already measurable five hours after injection and was even more pronounced three days after injection. Liver spleen and kidney showed marked non-specific uptake, which is normal for $^{111}$In-labeled antibodies[2].

$^{111}$In-trastuzumab was clinically used in HER2 positive metastatic breast cancer patients. With SPECT imaging we were able to visualize new lesions, previously unidentified with standard staging techniques, in 13 out of 15 patients[3].

A side effect of trastuzumab is cardiotoxicity, which occurs particularly when trastuzumab is combined with anthracyclines. HER2 in the heart plays a key role during embryogenesis. Myocardial HER2 expression may be transiently upregulated by a compensatory mechanism following cardiac stress. In a clinical trial, we evaluated whether myocardial HER2 expression (as measured by $^{111}$In-trastuzumab SPECT) is upregulated by anthracycline-induced cardiac stress or in case of heart failure by chronic pressure or volume overload. To this end, $^{111}$In-trastuzumab scans were performed in breast cancer patients shortly after anthracyclines as well as in patients with non-anthracycline-related heart failure. Shortly after completion of anthracycline treatment, myocardial HER2 overexpression was detectable in 50% of the patients, while none of the non-anthracycline-related heart failure patients showed myocardial uptake[4].

After these $^{111}$In-trastuzumab SPECT studies, the long-lived PET-isotope $^{89}$Zr became available for clinical immunoPET imaging with $^{89}$Zr-labeled antibodies. For labeling of internalizing monoclonal antibodies positron emitting radiometals like $^{89}$Zr are preferable over radiohalogens like $^{124}$I. This is because positron emitting radiometals are retained within the target cell after internalization and intracellular degradation of the tracer. Of the available positron emitting radiometals, $^{89}$Zr has the most favorable half-life of 78.4 hours,

allowing antibody imaging up to seven days postinjection. Pre-clinical evaluation of $^{89}$Zr-trastuzumab displayed equal tumor uptake for $^{89}$Zr-trastuzumab compared to $^{111}$In-trastuzumab, but the superior image quality of $^{89}$Zr-trastuzumab is due to the high spatial resolution and sensitivity of PET, while there was an equal tumor uptake for $^{89}$Zr-trastuzumab and $^{111}$In-trastuzumab. In addition, PET-imaging has the advantage of data quantification and whole body 3D imaging[5].



To investigate the use of $^{89}$Zr-trastuzumab for HER2 PET imaging, a clinical feasibility study was performed to determine required conditions of $^{89}$Zr-trastuzumab antibody dose and timing. HER2-positive metastatic breast cancer patients received 37 MBq $^{89}$Zr-trastuzumab at three trastuzumab protein doses (10 or 50 mg when trastuzumab naïve and 10 mg while on trastuzumab treatment) and underwent ≥ 2 PET-scans around days 2 and 5 post tracer injection. The best moment to assess $^{89}$Zr-trastuzumab tumor uptake was 4-5 days postinjection. Trastuzumab naive patients required 50 mg $^{89}$Zr-trastuzumab and patients on trastuzumab treatment 10 mg. Accumulation of $^{89}$Zr-trastuzumab allowed PET imaging of known tumor lesions in the liver, lung, bone and brain as well as unknown brain and bone metastases. In conclusion $^{89}$Zr-trastuzumab PET at appropriate antibody dose allows visualization and quantification of uptake in HER2 positive lesions in metastatic breast cancer patients[6].

The current practice of trastuzumab dosing for metastatic breast cancer is based on patient body weight. However, there are clues that trastuzumab pharmacokinetics and organ distribution can be affected by extensive tumor load. We showed in a patient with extensive HER2 positive liver metastases that $^{89}$Zr-trastuzumab was predominantly taken up by these liver metastases and rapidly cleared from the circulation. The rapid $^{89}$Zr-trastuzumab clearance in this patient can theoretically be explained by rapid binding of trastuzumab molecules to the many HER2 receptors in the large liver metastases. The HER2 PET scan was repeated after start with trastuzumab in a therapeutic dose. Compared to the first HER2 PET scan, this scan showed less $^{89}$Zr-trastuzumab liver uptake, a higher blood pool level and more uptake in other tumor lesions such as bone metastases[7]. This indicates that only after saturation of the HER2 receptors in the liver metastases are other lesions reached by trastuzumab. This implies that for adequate dosing of trastuzumab, tumor load should presumably be taken into account.

# VEGF visualization

Vascular endothelial growth factor (VEGF), released by tumor cells, is an important factor in angiogenesis. Angiogenesis, the formation of new blood vessels, is important for the growth of tumors. In tumor cells there is an unproportional up-regulation of VEGF production which leads to locally high VEGF levels. The humanized monoclonal antibody bevacizumab blocks VEGF-induced tumor angiogenesis by binding and thereby neutralizing VEGF-A.

To select patients who could benefit from VEGF targeted therapies imaging of VEGF using specific tracers, is of great interest.

We developed $^{111}$In- and $^{89}$Zr-bevacizumab which showed specific tumor uptake in a human ovarian xenograft model. MicroPET imaging using $^{89}$Zr-bevacizumab showed clear tumor localization 72 hours post-injection with maximal uptake 168 hours post-injection, which was similar to ex vivo biodistribution. $^{89}$Zr-bevacizumab tumor uptake could be quantified non-invasively, allowing follow-up of VEGF secretion during therapy[8]. Clinically, $^{89}$Zr-bevacizumab is used in renal cell cancer patients. In these tumor lesions, there is a high tumor-to-background ratio[9]. In melanoma patients $^{111}$In-bevacizumab was used to compare $^{111}$In uptake before and after treatment with bevacizumab. A single dose of bevacizumab slightly decreased $^{111}$In-bevacizumab uptake[10].

# Imaging drug effects

ImmunoPET could also be used to follow *in vivo* pharmacodynamic effects of other targeted drugs. Heat Shock Protein 90 (HSP90) is a molecular chaperone that assists in the structural formation and folding of a wide variety of oncogenic client proteins including HER2 and HIF-1$\alpha$ (which drives VEGF excretion). Currently, there are several inhibitors of HSP90 in clinical development. In tumors, HSP90 exists in an activated state, with higher affinity for HSP90 inhibitors, compared with normal cells. HER2 down-regulation is a potential biomarker for early response to HSP90-targeted therapies, therefore we used $^{89}$Zr-trastuzumab to quantify the alterations in HER2 tumor expression after NVP-AUY922 treatment, a potent HSP90 inhibitor. The HER2 over-expressing human SKOV-3 ovarian tumor cell line was used for *in vitro* experiments and as xenograft model in nude athymic mice. For *in vivo* evaluation, mice received 50 mg/kg NVP-AUY922 intra-peritoneally every other day. $^{89}$Zr-trastuzumab was injected intravenously six days before NVP-AUY922 treatment and after three NVP-AUY922 doses. MicroPET imaging was performed at 24, 72 and 144 hours post-tracer injection followed by *ex vivo* biodistribution and immunohistochemical staining. PET tumor quantification showed a mean reduction of 41% ($P$ = 0.0001) in $^{89}$Zr-trastuzumab uptake, 144 hours post-tracer injection after NVP-AUY922 treatment. PET results were confirmed by *ex vivo* $^{89}$Zr-trastuzumab biodistribution and HER2 immunohistochemical staining. Thus it was shown that down-regulation of

HER2, by means of HSP90 inhibition, can be non-invasively monitored and quantified with $^{89}$Zr-trastuzumab PET[11,12].

VEGF expression is regulated by HIF-1α, which is also a client protein of HSP90. Therefore, we investigated whether the effect of HSP90 inhibition could also be evaluated by means of visualizing VEGF downregulation *in vivo*. We performed $^{89}$Zr-bevacizumab micro-PET in a mouse model with A2780 human ovarian tumor, pre- and post-NVP-AUY922 treatment. *Ex vivo* tumor VEGF levels and histological response were used as verification. Two weeks of NVP-AUY922 treatment decreased $^{89}$Zr-bevacizumab tumor uptake with 44% ($P = 0.0003$) compared to pre-treatment values. The same downregulation pattern was observed when tumor VEGF levels were measured with ELISA, and mean vessel density following NVP-AUY922 treatment[12]. This technique is currently under clinical evaluation in an ongoing clinical study to investigate whether $^{89}$Zr-labeled trastuzumab or bevacizumab visualization of HER2 and VEGF can serve as an early biomarker for HSP90 inhibition in HER2 positive metastatic breast cancer patients. Sunitinib is an anti-angiogenic compound which targets the VEGF receptor and has shown activity against various tumor types. Currently no biomarkers are available to select patients or function as early response predictor. Previously, we showed that radiolabeled ranibizumab, an anti-VEGF Fragment antibody (Fab) tracer with high affinity for all VEGF-A isoforms, allows non-invasive, frequent, quantitative and rapid insight in VEGF levels in the tumor and its microenvironment. Therefore, radiolabeled ranibizumab was used to monitor sunitinib treatment to obtain insight in locoregional changes in tracer uptake during therapy. Direct cytotoxicity of sunitinib was evaluated *in vitro* in a high VEGF producing human A2780 ovarian tumor cell line. Nude mice were inoculated with A2780 cells. When the tumor was established, mice were treated once daily with sunitinib (60 mg/kg intraperitoneally) or vehicle for seven days followed by a stop week, thus reflecting the patient regimen, or sunitinib/vehicle was continued for seven days. $^{89}$Zr-ranibizumab (or control $^{89}$Zr-Fab-IgG for aspecific uptake) was injected at baseline, following seven or 14 days of treatment. MicroPET images were made 0, 6 and 24 hours post-injection of the tracer. $^{89}$Zr-ranibizumab revealed an inhomogeneous change in tumor uptake with a rebound phenomenon after stopping sunitinib treatment, resulting in 59% increased tracer uptake which corresponded with rapid tumor growth and an increase of plasma human VEGF levels. Clinically, VEGF PET is a good candidate to be explored for individual guidance of optimal anti-angiogenic therapy[13].

# Conclusion

ImmunoPET can serve as a tool in drug development. We addressed results with this sensitive PET technique. The newly developed tracers can potentially play a role as biomarker in drug development. There are several tumor characteristics candidate for development of tumor specific tracers. Imaging drug targets, such as illustrated by several studies performed with radiolabeled trastuzumab and bevacizumab, can be used to evaluate the presence of the target in every lesion. Further studies should define whether these imaging techniques can indeed lead to successfully patient tailored therapy.

# References

1. Moasser MM. The oncogene HER2: Its signaling and transforming functions and its role in human cancer pathogenesis. Oncogene 2007; 26:6469-6487.
2 Lub-de Hooge MN, Kosterink JG, Perik PJ, et al. Preclinical characterisation of 111In-DTPA-trastuzumab. Br J Pharmacol 2004; 143:99-106.
3 Perik PJ, Lub-De Hooge MN, Gietema JA, et al. Indium-111-labeled trastuzumab scintigraphy in patients with human epidermal growth factor receptor 2-positive metastatic breast cancer. J Clin Oncol 2006; 24:2276-2282.
4. de Korte MA, de Vries EG, Lub-de Hooge MN, et al. 111Indium-trastuzumab visualises myocardial human epidermal growth factor receptor 2 expression shortly after anthracycline treatment but not during heart failure: A clue to uncover the mechanisms of trastuzumab-related cardiotoxicity. Eur J Cancer 2007; 43:2046-2051.
5. Dijkers EC, Kosterink JG, Rademaker AP, et al. Development and characterization of clinical-grade 89Zr-trastuzumab for HER2/neu immunoPET imaging. J Nucl Med 2009; 50:974-981.
6. Dijkers EC, Oude Munnink TH, Kosterink JG, et al. Biodistribution of 89Zr-trastuzumab and PET imaging of HER2-positive lesions in patients with metastatic breast cancer. Clin Pharmacol Ther 2010; 87:586-592.
7. Oude Munnink TH, Dijkers EC, Netters SJ, et al. Trastuzumab pharmacokinetics influenced by extent human epidermal growth factor receptor 2-positive tumor load. J Clin Oncol 2010.
8. Nagengast WB, de Vries EG, Hospers GA, et al. In vivo VEGF imaging with radiolabeled bevacizumab in a human ovarian tumor xenograft. J Nucl Med 2007; 48:1313-1319.
9. Oosting SF, Brouwers AH, Van Es SC, et al. 89Zr-bevacizumab PET imaging in metastatic renal cell carcinoma patients before and during antiangiogenic treatment. J Clin Oncol 2012; (Meeting Abstracts) suppl abstr 10581.
10. Nagengast WB, Hooge MN, van Straten EM, et al. VEGF-SPECT with 111in-bevacizumab in stage III/IV melanoma patients. Eur J Cancer 2011; 47:1595-1602.
11. Oude Munnink TH, Korte MA, Nagengast WB, et al. (89)zr-trastuzumab PET visualises HER2 downregulation by the HSP90 inhibitor NVP-AUY922 in a human tumour xenograft. Eur J Cancer 2010; 46:678-684.
12. Nagengast WB, de Korte MA, Oude Munnink TH, et al. 89Zr-bevacizumab PET of early antiangiogenic tumor response to treatment with HSP90 inhibitor NVP-AUY922. J Nucl Med 2010; 51:761-767.
13. Nagengast WB, Lub-de Hooge MN, Oosting SF, et al. VEGF-PET imaging is a noninvasive biomarker showing differential changes in the tumor during sunitinib treatment. Cancer Res 2011; 71:143-153.

# CHAPTER 4

# Targeting breast cancer through its microenvironment: current status of preclinical and clinical research in finding relevant targets

H.H. Nienhuis[1]
S.B.M. Gaykema[1]
H. Timmer-Bosscha[1]
M. Jalving[1]
A.H. Brouwers[2]
M.N. Lub-de Hooge[2,3]
B. van der Vegt[4]
B. Overmoyer[5]
E.G.E. de Vries[1]
C.P. Schröder[1]

Departments of [1]Medical Oncology, [2]Nuclear Medicine and Molecular Imaging, [3]Hospital and Clinical Pharmacy, [4]Pathology, University Medical Center Groningen, University of Groningen, The Netherlands and Department of Medical Oncology, Dana-Farber Cancer Institute, Harvard Medical School, Boston, MA, USA.

*Manuscript in preparation*

# Abstract

It is increasingly evident that not only breast cancer cells, but also the tissue embedding these cells: the tumor microenvironment, plays an important role in tumor progression, metastasis formation and treatment sensitivity. This review focuses on the current knowledge of processes by which the microenvironment affects breast cancer, including formation of the metastatic niche, metabolic stimulation, stimulation of tumor cell migration, immune modulation, angiogenesis and matrix remodeling. The number of drugs targeting key factors in these processes is expanding, and the available clinical data is increasing. Therefore current strategies for intervention and prediction of treatment response are outlined. At present, targeting the formation of the metastatic niche and metabolic stimulation by the breast cancer microenvironment, are already showing clinical efficacy. Intervening in the stimulation of tumor cell migration and immune modulation by the microenvironment are upcoming fields of great research interest. In contrast, targeting microenvironmental angiogenesis or matrix remodeling appears to be of limited clinical relevance in breast cancer treatment so far. Further research is warranted to optimize intervention strategies and develop predictive tests for the relevance of targeting involved factors within the microenvironment in order to optimally personalize breast cancer treatment.

# Introduction

Breast cancer is the most common cause of cancer death among women worldwide[1]. In 2010, 207,090 women were diagnosed with breast cancer in the United States[2]. Approximately 6% of all breast cancer patients have metastatic disease at the time of diagnosis, and currently 20% will eventually develop metastatic breast cancer (MBC)[3]. Once metastasized, breast cancer is generally incurable.



Recent treatment strategies focus on induction of tumor cell death using chemotherapeutic, anti-hormonal and targeted agents. However, it is increasingly recognized that not only the tumor cells, but also the tissue embedding the tumor cells; their microenvironment, plays an important role in tumor progression and metastasis. This role in the complexity of metastasis[4] can be assumed from the metastatic pattern of breast cancer to specific organs[5]. The importance of the cancer microenvironment is underlined by the recent inclusion of the microenvironment in the so called "hallmarks of cancer"[6,7]. Furthermore, microenvironmental characteristics affect breast cancer prognosis and chemosensitivity, and as such are increasingly incorporated in gene expression profiles[8,9]. Novel drugs targeting key factors in the microenvironment are being developed.

The tumor microenvironment includes soluble factors, extracellular matrix (ECM) and stromal cells[10]. Involved soluble factors comprise growth factors, hormones, immunoglobulins, cytokines and chemokines[10]. The ECM contains proteoglycans, hyaluronic acid and fibrous proteins (collagen, fibronectin and laminin). Involved stromal cells include fibroblasts, (pre-)adipocytes, cells of the vascular system (endothelial cells) and immune cells[11,12]. Combinations of different cellular, extracellular and soluble factors can act to support multiple processes in the breast cancer microenvironment that promote progression and metastasis. This review focuses on the current knowledge of processes involved in the breast cancer microenvironment, and how they affect breast cancer progression and metastasis. These processes include: formation of the metastatic niche, metabolic stimulation, stimulation of tumor cell migration, immune modulation, angiogenesis and matrix remodeling. We will place them in order of importance as targets for breast cancer therapy, with the currently available (pre) clinical evidence (Table 1). Furthermore, we will outline present data with regard to strategies for monitoring treatment effect. Finally, we will describe potential future directions exploiting the microenvironment in breast cancer treatment.

**Table 1.** Currently available (pre)clinical evidence for targeting microenvironmental processes

| Process | Factor | Targeting | Level of evidence* | References | Possible biomarker |
|---|---|---|---|---|---|
| Accommodation of distant metastases | TGFβ | Anti-TGFβ1 antibodies (1D11, GC1008[1]), TGFβR TKI (Ki26894, LY215799, LY2109761), bisphosphonates# (zoledronic acid [2-6]) | 4, 1 | (21, 31) | PSmad2 level PBMCs, TGFβ response gene signature |
| | RANK/ RANKL/ OPG | Anti-RANKL antibody (denosumab [7-10]) | 1 | (47) | Urine NTX level |
| Metabolic stimulation | E2 | Dietary fat reduction [11-14], ER antagonist (tamoxifen), aromatase inhibitor | 1 | (54) | Circulating E2 level, aromatase level |
| | Insulin | biguanide (metformin [15-24]) | 1 | (91) | |
| | IGF-1 | Anti-IGF-1R antibodies (ganitimumab[25,26], dalotuzumab[27,28], R1507[29]) | 2 | (98) | |
| Stimulation of tumor cell migration | HGF | cMET TKIs (cabozantinib[30,31], foretinib[32,33], tivantinib[34,35]) anti cMET antibody (onartuzumab[36]), anti-HGF antibody (AMG102) | 3 | (114) | Circulating HGF level |
| | SDF-1 | Anti-SDF-1 antibody, Anti-CXCR4 antibody (44717.111), CXCR4 inhibitors (plerixafor, CTCE-9908) | 4 | (118) | |
| Immune modulation | PD-1 | Anti-PD-1 antibodies (BMS-936558[37], AMP-514[38], AMP-224[39], MK-3475[40]), anti-PD-L1 antibodies (MPDL3280A[41], MSB0010718C[42], MEDI4736[43,44], BMS-936559[45]) | 3 | (149, 189) | |
| | CTLA-4 | Anti-CTLA4 antibodies (ipilimumab[46,47], tremelimumab) | 3 | (153) | |
| | TAM | Bisphosphonate (zoledronic acid[2-6]) | 4 | (152) | |
| Angiogenesis | VEGF-A | Anti-VEGF-A antibody (bevacizumab[48-68]), anti-VEGFR TKI (sunitinib[69-73]) | 2 | (160, 167) | $^{89}$Zr-bevacizumab PET |
| Matrix remodeling | MMP | Various MMP inhibitors (NSC-683551[74]) | 2 | (180, 181) | |
| | Integrins | Integrin inhibitor: cyclized pentapeptide (Cilengitide[75-78]), anti-α5ß1 integrin antibody (volociximab) | 4, 3 | (182) | |
| | LOX | Anti-LOXL antibody AB0024[79] | 3 | (186) | |

*Level of evidence:
1 Clinical evidence. Treatment effect in breast cancer patients.
2 Clinical evidence. No treatment effect in breast cancer patients.
3 Clinical evidence. Treatment effect in non-breast cancer patients.
4 Preclinical evidence. Treatment effect in breast cancer models.
5 Preclinical evidence. Treatment effect in non-breast cancer models.
#Indirect effect. Anti tumor effect of bisphosphonates not fully proven to be TGFβdependent.

| | | | | | |
|---|---|---|---|---|---|
| 1 | NCT01401062 | 28 | NCT01234857 | 55 | NCT00887536 |
| 2 | NCT01323933 | 29 | NCT00796107 | 56 | NCT01303679 |
| 3 | NCT00512993 | 30 | NCT01441947 | 57 | NCT00333775 |
| 4 | NCT01129336 | 31 | NCT01738438 | 58 | NCT00408408 |
| 5 | NCT00127205 | 32 | NCT01138384 | 59 | NCT00929240 |
| 6 | NCT00295646 | 33 | NCT01147484 | 60 | NCT00567554 |
| 7 | NCT01864798 | 34 | NCT01575522 | 61 | NCT01250379 |
| 8 | NCT01545648 | 35 | NCT01542996 | 62 | NCT01663727 |
| 9 | NCT01077154 | 36 | NCT01186991 | 63 | NCT01094184 |
| 10 | NCT01952054 | 37 | NCT01928394 | 64 | NCT00448591 |
| 11 | NCT00002564 | 38 | NCT02013804 | 65 | NCT00391092 |
| 12 | NCT00068458 | 39 | NCT01352884 | 66 | NCT00600340 |
| 13 | NCT00925652 | 40 | NCT01295827 | 67 | NCT00545077 |
| 14 | NCT00811824 | 41 | NCT01375842 | 68 | NCT01426880 |
| 15 | NCT01310231 | 42 | NCT01943461 | 69 | NCT00513695 |
| 16 | NCT01589367 | 43 | NCT01938612 | 70 | NCT00824538 |
| 17 | NCT01101438 | 44 | NCT01975831 | 71 | NCT00270413 |
| 18 | NCT01627067 | 45 | NCT00729664 | 72 | NCT00570908 |
| 19 | NCT01905046 | 46 | NCT00083278 | 73 | NCT00078000 |
| 20 | NCT01885013 | 47 | NCT01502592 | 74 | NCT00001683 |
| 21 | NCT01477060 | 48 | NCT00433511 | 75 | NCT01276496 |
| 22 | NCT01566799 | 49 | NCT00785291 | 76 | NCT00077155 |
| 23 | NCT01042379 | 50 | NCT00601900 | 77 | NCT00004258 |
| 24 | NCT01929811 | 51 | NCT00520975 | 78 | NCT00022113 |
| 25 | NCT01042379 | 52 | NCT01935492 | 79 | NCT01323933 |
| 26 | NCT00626106 | 53 | NCT01131195 | | |
| 27 | NCT01605396 | 54 | NCT00028990 | | |

[1,2,3 etc] : Currently in clinical trial in breast cancer patients. Clinicaltrials.gov identifier

## Search strategies and selection criteria

Articles for this review were found by searches of PubMed, abstracts american association for cancer research (AACR) and american society of clinical oncology (ASCO) and the clinicaltrials.gov database by use of the terms 'breast cancer', 'microenvironment' combined with 'metastasis' 'metabolic dysfunction' 'migration' 'immune cells' 'angiogenesis' or 'matrix remodeling' and combinations of these terms with the selected soluble factors. In addition, relevant papers from the reference lists of selected papers were included. Only studies written in English were included.

# Formation of the metastatic niche

The importance of the interaction of the breast cancer cells with their microenvironment has long been suggested by the specificity of the metastatic pattern[4]. In MBC patients, metastasis patterns even differ per breast cancer subtype[5]. In general however, bone is by far the most common metastatic site involving 65% of patients with MBC[5,13,14]. Crucial factors involved in the development of bone metastases are transforming growth factor (TGF)β and receptor activator of nuclear factor κB ligand (RANKL) (Figure 1A).

The cytokine **TGFβ** has tumor suppressive properties in the physiological setting. However, during malignant progression, TGFβ signaling promotes growth, progression and invasion of the tumor[15]. Both cancer and cancer associated fibroblasts (CAF)s excrete TGFβ by autocrine as well as paracrine secretion, giving rise to a tumor-promoting microenvironment (Figure 1A.1 and 1A.2)[16,17]. Activated TGFβ binds to the TGFβI- and TGFβII-receptor (-R) which both induce Smad2 phosphorylation which in turn activates transcriptional factors[18].

High circulating plasma levels of TGFβ1, measured by enzyme-linked immunosorbent assay, reflected a worse prognosis in 117 and 439 (mainly early stage) primary breast cancer patients[19,20]. TGFβ is highly expressed in the bone tissue surrounding bone metastases[21]. Bisphosphonates are commonly used as supportive treatment in MBC patients with bone metastases. In a metastatic mouse model with human breast cancer cells, treatment with bisphosphonates reduced TGFβ in the environment of bone metastases[22] (Figure 1A.3). Three clinical trials studied the effect of the biphosphonate zoledronic acid in the adjuvant setting. In the ABCSG-12 trial involving 1,803 patients, disease free survival at 62 months was increased from 88% to 92% (hazard ratio (HR) 0.68; 95% confidence interval (CI) 0.51–0.91; $P = 0.009$) by the addition of the biphosphonate to endocrine therapy[23]. The ZO-FAST study compared immediate with delayed (after fracture or high risk thereof) zoledronic acid administered with adjuvant endocrine therapy. The disease free survival increased by immediate zoledronic acid administration from 92% to 95%, (HR 0.588; 95% CI 0.361–0.959; $P = 0.0314$) at 36 months follow up[24]. In the AZURE trial however, amongst 3,360 patients no difference was seen[25]. In this study the majority of patients received chemotherapy rather than endocrine therapy alone. A subgroup analysis in patients being postmenopausal for more than 5 years showed an increase in disease free survival from 71% to 78.2% (adjusted HR 0.75; 95% CI 0.59 to 0.96; $P = 0.02$) 5 years after randomization. In the NEO-ZOTAC study, amongst 250 human epidermal growth factor receptor (HER)2 negative breast cancer patients, no difference in pathologic response rate was seen with or without zoledronic acid, administered in the neo-adjuvant setting[26]. A meta-analysis amongst 17,751 from 41 randomized clinical trials compared outcome of breast cancer patients with and without adjuvant bisphosphonate treatment and found reduction of breast cancer mortality and bone recurrence in post-menopausal patients[27]. Currently, several trials are ongoing to further study the anti-cancer effect of zoledronic acid (Table 1).

Lowered estrogen levels promote bone turnover activity[28], this could lead to the release of bisphosphonate from the bone matrix[29]. In bone-trope xenograft mouse models, more bone metastases developed in ovariectomized mice compared to control mice. Zoledronic acid treatment reduced tumor growth only in the oophorectomized mice[30]. These findings support the clinical findings and suggest that the development of bone metastasis and the effect of zoledronic acid are estradiol (E2) dependent. With regard to other compounds that influence TGFβ signaling, only preclinical data are available. In human triple negative breast cancer (TNBC) metastatic models in mice, reducing TGFβ signaling, either pharmacologically (with pan-TGFβ antibody 1D11 or TGFβ receptor inhibitor Ki26894 or LY2109761 or molecularly (with a short hairpin against Smad4), reduced metastases[22,31,32] (Figure 1A.3). However, in a metastatic human luminal breast cancer mouse models, targeting TGFβ signaling with 1D11 did not influence metastasis formation after intracardiac breast cancer cell injection[33]. Moreover, deletion of the TgfβII receptor gene in mouse mammary epithelial cells increased tumor and pulmonary metastasis formation[34]. This suggests not only that targeting of TGFβ in early phases of tumorigenesis has tumor promoting effects, but also that there is likely to be a breast cancer subtype specific aspect to this.



With regard to biomarkers for effective TGFβ targeting , there are limited data available. In a syngeneic rat tumor model, *ex vivo* pSmad2 protein levels in peripheral blood mononuclear cells correlated with change in tumor pSmad2 protein levels in response to TGFβR tyrosine kinase inhibitor (TKI) LY2157299[35]. A TGFβ response gene signature retrieved from primary breast tumors comprising 153 genes was developed to identify tumors with high TGFβ signaling activity. In a cohort of 368 samples, tumors positive for this gene set did indeed show higher mRNA levels of TGFβ1 and TGFβ2[36]. In estrogen receptor (ER) negative tumors, this response signature correlated with recurrent disease in the lungs. A study in 12 glioblastoma patients using zirconium-89 ($^{89}$Zr) labeled GC1008, an antibody against active isoforms of TGFβ, for visualization TGFβ showed a 15 times higher median standardized uptake value $(SUV)_{max}$ in tumor lesions than in normal brain tissue of[37]. There is one ongoing phase I/II trial in MBC patients with GC1008 in combination with local radiotherapy (Table 1) (Figure 1A.3).

As mentioned previously, another crucial factor involved in the development of bone metastases is receptor activator of nuclear factor κB ligand (RANKL). The role of the RANK/RANKL/*osteoprotegerin* (OPG) pathway in promoting and sustaining breast cancer bone metastases is supported by an increasing amount of preclinical and clinical data. The development of bone metastasis is caused by a vicious cycle involving interplay between cancer cells and their surroundings (Figure 1A.1 and 1A.2). Cancer cells secrete parathyroid hormone-related protein (PTHrP)[38]. PTHrP subsequently stimulates microenvironmental osteoblasts to produce RANKL, which in turn stimulates osteolytic activity by osteoclasts. Enhanced osteolysis releases growth factors, such as TGFβ, from the bone matrix. This induces tumor growth, and thereby PTHrP excretion, completing the vicious cycle. Data from small clinical studies (56 patients) suggest that PTHrP levels, measured

**Figure 1.** Processes in breast cancer microenvironment that promote progression and metastasis.

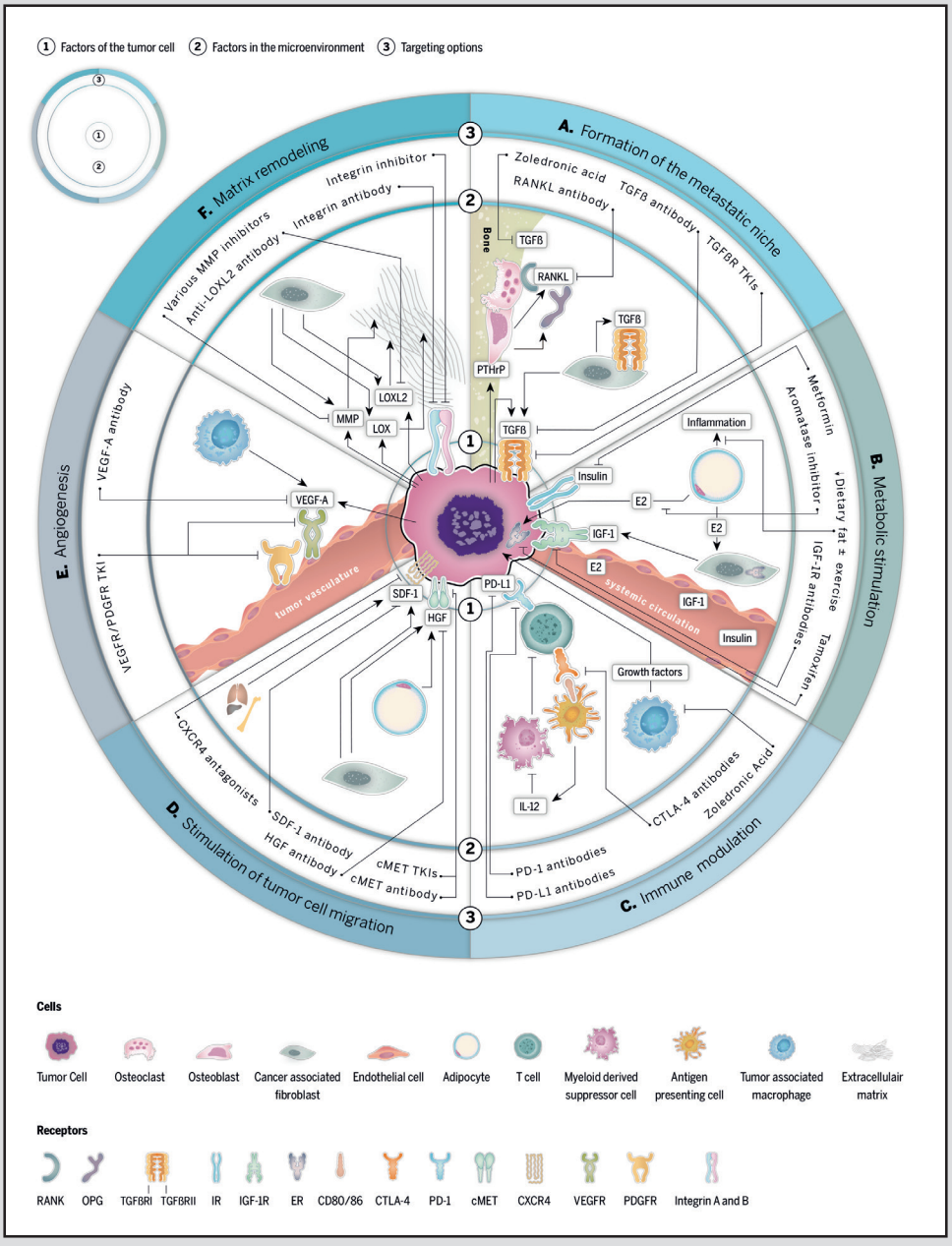

**Legend of Figure 1**| Processes in breast cancer microenvironment that promote progression and metastasis.

**A** | *Formation of the metastatic niche.* 1) Factors on the tumor cell membrane are transforming growth factor receptor (TGFβR) I and TGFβRII and the secreted TGFβ and parathyroid hormone-related protein (PTHrP). 2) Factors in the breast cancer microenvironment are TGFβ, receptor activator of nuclear factor κB (RANK), RANK ligand (RANKL) and osteoprotegerin (OPG). TGFβ is excreted by cancer associated fibroblasts (CAFs) and is stored in the bone matrix. RANK is expressed by osteoclasts. Osteoblasts excrete RANKL and OPG. 3) Targeting options are an anti-TGFβ antibody, TGFβ tyrosine kinase inhibitors (TKI) s, zoledronic acid and anti-RANKL antibody.
**B** | *Metabolic stimulation.* 1) Factors on the tumor are the cytoplasmic estrogen receptor (ER) and the membrane bound insulin receptor (IR) and insulin-like growth factor 1 receptor (IGF-1R). 2) Factors in the breast cancer microenvironment are inflammation, estradiol (E2), insulin and IGF-1. Obesity leads to inflammation of adipocytes. E2 is excreted by adipocytes. IGF-1 is secreted by CAFs. E2, insulin and IGF-1 are also produced elsewhere in the body and reach the breast microenvironment via the systemic circulation. 3) Targeting options are dietary fat reduction with our without physical exercise, tamoxifen, aromatase inhibitor, metformin and anti IGF-1R antibodies.
**C** | *Immune modulation.* 1) Factor on the tumor cell is membrane bound programmed death ligand (PD- L)1. 2) Factors in the breast cancer microenvironment are PD-1, Cytotoxic T lymphocyte-associated antigen (CTLA)-4 and interleukin (IL)-12. PD-1 and CTLA-4 are membrane bound proteins on T-cells. IL-12 is secreted by antigen presenting cells (APCs) and blocks myeloid derived supressor cells (MDSCs). CD80/86 are membrane bound receptors on the APC. Tumor associated macrophages (TAMs) secrete tumor promoting growth factors. 3) Targeting options are PD-L1 antibodies, PD-1 antibodies, CTLA-4 antibodies and zoledronic acid.
**D** | *Stimulation of tumor cell migration.* 1) Factors on the tumor cell are cell membrane receptors c-mesenchymal-epithelial transition factor (cMET) and chemokine C-X-C motif receptor 4 (CXCR4). 2) Factors in the breast cancer microenvironment are hepatocyte growth factor (HGF) and stromal derived growth factor (SDF)-1. HGF is secreted by CAFs and adipocytes. SDF-1 is expressed by CAFs and liver, lung and bone. 3) Targeting options are an anti cMET antibody, cMET TKIs, an HGF antibody, SDF-1- antibodies and CXCR4 antagonists.
**E** | *Angiogenesis.* 1) The factor of the tumor cell is vascular endothelial growth factor (VEGF)-A, which is excreted. 2) Factors in the breast cancer microenvironment are the ligand VEGF-A and the receptors VEGF-R and platelet derived growth factor receptor (PDFGR). VEGF is also being excreted by TAMs. VEGFR and PDFGR are expressed by endothelial cells. 3) Targeting options are an VEGF antibody and a VEGFR and PDFGR TKI.
**F** | *Matrix remodeling.* 1) Factors on the tumor cell are the membrane bound integrin A and B and the excreted matrix metalloproteases (MMPs), lysyl oxidases (LOX) and LOX ligand (LOXL)2. 2) Factors in the breast cancer microenvironment are the extracellular matrix (ECM), integrins, MMPs, LOX and LOXL2. Integrins are bound to the ECM. MMPs, LOX and LOXL2 are secreted by CAFs. 3) Targeting options are an anti-integrin antibody, an integrin inhibitor, various MMP inhibitors and an anti-LOXL2 antibody.



immunohistochemically, are higher in bone metastases compared to primary breast cancers[39,40]. Under physiological circumstances, excessive bone resorption is prevented by *OPG*. *OPG* is secreted by osteoblasts and competes with RANKL in binding to RANK[41] (Figure 1A.1 and 1A.2). In tumors, OPG can be down regulated via different mechanisms such as reduced synthesis[42]. The RANK/RANKL/OPG axis also plays a role in primary breast cancer development. In breast tissue progesterone can induce RANKL expression in mammary epithelial cells[43], thereby exerting a mitogenic effect. A murine anti RANKL antibody reduced tumor formation in a spontaneous mouse mammary tumor model[44]. RANKL treatment of SKBR3 breast cancer cells stimulated proliferation and led to protection from cell death in response to irradiation and doxorubicin *in vitro*[45]. High RANK and low OPG mRNA expression in 295 primary breast cancer tumors was correlated with worse

overall survival[46]. High RANK expression, measured by immunohistochemistry in 93 breast cancer samples, was associated with earlier onset of bone metastases development[46].

The importance of RANKL in the development of skeletal related events has been proven with denosumab, a monoclonal antibody that binds human RANKL to inhibit bone destruction[47] (Figure 1A.3). A randomized double blind study in 2,046 MBC patients with at least one bone metastasis, showed superiority of denosumab compared to zoledronic acid in delaying time to first on-study skeletal-related event[48]. Time to disease progression, overall survival and adverse events rates were similar between these groups. Denosumab is now part of standard clinical care to supplement the treatment of bone metastasis in MBC. Clinical trials are ongoing to study the anti-cancer effect of denosumab (Table 1).

Data on biomarkers for targeting RANKL are limited, and assessment is mostly based on clinical grounds: skeletal related events, recurrence and death. Denosumab treatment decreased urine N-terminal telopeptide levels in MBC patients with bone metastases[49]. However, serum levels RANK/RANKL/OPG levels did not correlate with these endpoints in 30 MBC patients treated with bisphosphonates[50].

In conclusion, bone is clinically the most seductive environment for breast cancer. The formation of the metastatic niche by the microenvironment there, is affected by TGFβ and RANK/RANKL/OPG signaling. Standard treatment options in MBC that may at least in part exert their effect by influencing these factors are bisphosphonates and denosumab. TGFβ inhibitors are currently investigated in clinical trials.

## Metabolic stimulation

The metabolic environment can profoundly affect breast cancer behavior. Microenvironmental factors contributing in the process of metabolic stimulation of breast cancer are obesity and metabolic dysfunction. Soluble factors involved in this are E2, insulin and insulin-like growth factor (IGF)-1[51] (Figure 1B).

**Obesity** increases the risk of death due to breast cancer. In a prospective, population based study in almost 500,000 women, the relative risk of breast cancer death was 2.1 in obese women with a body mass index (BMI) of at least 40 compared to normal weight women[52]. Moreover in patients with ER positive breast cancer, obesity is a risk factor for recurrence of breast cancer[53] and development of metastases[54]. Furthermore, dietary fat reduction seems to prolong disease free survival in women with resected breast cancers independently of ER presence (Figure 1B.3). In a group of 2,437 women with resected early stage breast cancer, patients were randomized between dietary intervention and control groups. In the dietary intervention group, 9.8% relapsed compared to 12.4% in the control group ($P = 0.034$)[55]. A preclinical study described a link between high fat diet and breast cancer growth[56]. The cholesterol metabolite named 27-hydroxycholesterol, which mimics estrogen in certain tissues, resulted in faster tumor growth and more metastasis formation after administration to MMTV-PyMT mice. On a high fat, high cholesterol diet these mice showed also more rapid tumor growth compared to mice on a normal diet. Clinical trials are ongoing to study the anti-cancer effect of dietary fat reduction (Table 1). In a prospective observational study, physical activity equivalent to 3-5 hours walking a week improved survival in 2,987 breast cancer patients[57]. The exact mechanism behind this effect remains to be speculated about[58].

The mechanisms linking obesity and breast cancer development and outcome are multifactorial involving inflammation, hormonal inbalance and metabolic dysfunction. Obesity leads to **inflammation** of adipose tissue which is characterized by necrotic adipocytes surrounded by macrophages[59] and the level of breast inflammation is correlated with BMI[60] (Figure 1B.2). Chronic inflammation is related to the development of various cancer types[61]. In two case-control studies with in total almost 2000 post-menopausal women, systemic levels of the aspecific inflammatory marker C-reactive protein (CRP) or soluble tumor necrosis factor receptor (sTNFR)2 were associated with overweight and increased breast cancer risk[62,63]. In a randomized trial amongst 439 obese and overweight women, weight loss alone or in combination with exercise resulted in reduction of the inflammatory biomarkers IL-6, serum amyloid A and high sensitivity-CRP compared to baseline and compared to controls[64].

Presumably the most powerful factor by which elevated body weight promotes breast cancer, is **E2**[65]. The conversion from testosterone by aromatase enzyme cytochrome p450 leads to the production of E2[66]. During the fertile phase E2 is primarily produced in the ovaries, while various cells including adipocytes in the breast, excrete E2 in postmenopausal women[67,68]. E2 binds to the nuclear ER present on breast cancer cells and CAFs[69-72]

(Figure 1B.1 and 1B.2), leading to cancer cell proliferation. Increased aromatase activity in fat tissue leads to elevated E2 levels in breast tumors compared to normal breast tissue[68]. Interestingly, high BMI in postmenopausal women is associated with higher aromatase activity leading to high E2 levels and augmented breast cancer risk[65]. Weight loss alone or in combination with exercise, on the other hand, reduced systemic E2 levels in overweight patients[73]. This phenomenon is proposed as a cause for the worse prognosis observed in women who experience weight gain after breast cancer treatment[74]. The effect of physical exercise alone on E2 levels is inconsistent, although modest at most[73,75]. E2 signaling can be targeted using aromatase inhibitors or ER antagonists (such as fulvestrant or tamoxifen) (Figure 1B.3). Studies comparing treatment efficacy of estrogen targeting between obese and normal weight patients showed contradicting results[54,76]. As can be expected, ER positive tumor cells can indirectly be influenced by oophorectomy. Lowering circulating E2 by oophorectomy in unaffected BRCA1 mutation carriers also reduces the risk of breast cancer by 56%[77]. This is very intriguing as the majority of BRCA1 associated breast cancers is ER negative[78]. The discrepancy might be explained by E2 responsiveness of luminal progenitor cells of BRCA1 associated basal tumors[79]. This may explain the reduced incidence of secondary breast cancers by tamoxifen in BRCA1 or BRCA2 carriers with breast cancer (OR= 0.50, 95% CI: 0.28-0.89)[77]. Another potential explanation is the fact that in the breast, ER is expressed in epithelial- as well as in stromal cells and stromal ER expression can affect tumor growth[80-82].

In addition to the endocrine importance of adipose tissue in the breast, obesity is related to metabolic dysfunction, which can also affect tumor progression[83,84]. In obesity, non-esterified fatty acids compete with glucose as a metabolic fuel, inducing **insulin** resistance leading to high glucose and insulin levels. Insulin is being produced by pancreatic ß-cells and binds to the insulin receptor on the cell membrane of nearly all cell types (Figure 1B.1 and 1B.2). Insulin binding to the insulin receptor on breast cancer cells activates the PI3K and MAPK signaling pathways and results in a cascade of proliferative and anti-apoptotic events. The PI3K pathway mediates the glucose regulatory effects of insulin but is inhibited in insulin resistance and, therefore, hyperinsulinemia, leading to increased signal transduction, is required to restore normal PI3K pathway activity. Since signaling via the MAPK pathway is preserved despite insulin resistance, high insulin levels in the microenvironment of breast cancer cells lead to hyperactivation of this pathway and enhanced cellular proliferation[85]. In insulin resistance and diabetes mellitus in patients, insulin responsive tissues, such as skeletal muscle, become insulin resistant, stimulating insulin production. Epithelial cells including breast cancer cells probably remain relatively insulin sensitive and the consequent increased insulin-mediated signaling can lead to enhanced proliferation in cell line models[86]. In animal models and humans, both insulin resistance and exogenous insulin injections have been associated with an increased risk of cancer and cancer recurrence[87]. Insulin and hyperinsulinemia can also promote tumorigenesis indirectly by influencing the levels of other modulators, such as IGFs, sex hormones, inflammatory processes and adipokines[88]. Insulin resistance and

hyperinsulinemia suppress the production of sex hormone-binding globulin by the liver[89]. This can lead to increased availability of free sex hormones favoring breast cancer development and progression[90].

Metformin, which belongs to the biguanide class of oral hypoglycemic agents, is prescribed to over 120 million type 2 diabetic patients worldwide. It reduces insulin resistance, and leads to lower insulin and glucose levels which may also reduce tumor cell growth (Figure 1B.3). Metformin indeed diminishes the growth of breast cancer cells in vitro[91]. Retrospectively, patients with breast cancer who received neoadjuvant chemotherapy were studied; diabetic cancer patients receiving metformin during their neoadjuvant chemotherapy had a higher pathologic complete response rate compared to diabetic patients not receiving metformin (24% vs 8%; $P = 0.007$)[92]. Several trials are ongoing to further study the anti-cancer effect of metformin (Table 1).

A related metabolic factor is **IGF-1**, which is produced by the liver as well as by CAFs[93] (Figure 1B.1 and 1B.2). IGF-1 activates, by binding to its receptor IGF-1R at the tumor cell membrane, the PI3K/AKT pathway. AKT is phosphorylated which leads to cell proliferation and inhibition of apoptosis of the tumor cell. Insulin resistance can result in high IGF-1 levels through various mechanisms[94]. High IGF-1 levels in the microenvironment promote cancer cell growth. IGF-1R is overexpressed in numerous solid tumors including breast cancer[95], and is implicated (in both clinical and preclinical studies) in resistance to hormonal therapy and human HER2 targeting[95,96]. BRCA1 mutation carriers primarily develop TNBC (80%), and these tumors express elevated IGF-1R levels. Mutated BRCA1 fails to suppress IGF-1R, whereas tumors with wild-type BRCA1 are able to suppress IGF-1R[97]. In effect, the large majority of TNBCs express cytoplasmic and membranous IGF-1R[95,98], which is associated with a worse prognosis[95]. By targeting IGF-1R on the tumor cells, the binding of IGF-1 to its receptor is blocked (Figure 1B.3). Despite a strong rationale to intervene with IGF1-R, clinical trials in (breast) cancer with anti IGF-1R antibodies have until now failed to show significant clinical relevance[99]. Clinical trials studying the effect of IGF-1R inhibition in breast cancer are ongoing (Table 1).

In conclusion, metabolic stimulation of breast cancer is induced by obesity, E2, insulin and IGF-1 in the breast cancer microenvironment. Intervention strategies, including weight and dietary fat reduction and metformin treatment, have proven to benefit breast cancer patients. No clinical benefit from IGF-1R inhibitors has been seen so far. Clinical trials studying inhibition of this factor are ongoing.

## Stimulation of tumor cell migration

After tumor cells have invaded into their surroundings, the next step of tumor progression is migration to and through the circulation. The breast cancer microenvironment contains several factors that stimulate tumor cell migration, including hepatocyte growth factor (HGF) and stromal derived growth factor (SDF-1) (Figure 1D).

**HGF** is a soluble factor that is being secreted by CAFs and adipocytes and binds to the c-mesenchymal-epithelial transition factor (cMET) tyrosine kinase receptor on cancer cells [100] (Figure 1D.1 and 1D.2). Binding of the cMET receptor triggers several downstream pathways in tumor cells, including MAPK and PI3K, inducing proliferation and migration[101]. Transcription of both HGF and cMET is induced by several stromal cytokines such as interleukin (IL)-1, IL-6, tumor necrosis factor (TNF)-α and TGF-β[102]. High cMET expression determined immunohistochemically in 930 and 330 primary breast tumors, respectively, was more frequently present in deceased or metastasized patients[103] and correlated with worse disease related survival[104]. Also, high cMET expression, based on protein arrays from lysates of 257 fine needle aspirates of primary breast cancers, is associated with worse disease free and overall survival[105]. Presurgical serum HGF levels were 1.5 fold higher in 124 mainly stage II and III breast cancer patients compared to 35 women with benign breast tumors[106].

HGF added to breast cancer cells induced migration and invasion *in vitro*[107,108]. *In vivo,* lung metastasis formation was enhanced when tumor cells were incubated with HGF before inoculation[109]. Transgenic mice in which HGF expression was elevated by HGF cDNA in their mammary epithelium, developed invasive mammary tumors and pulmonary metastases[110]. Moreover, HGF can play a role in sensitivity to certain drugs. HGF lowered sensitivity to the HER2 and Epidermal Growth Factor Receptor (EGFR)1 TKI lapatinib in HER2 positive breast cancer cells[111]. Inhibiting HGF excretion by fibroblasts studied with hammerhead ribozymes reduced invasiveness of breast cancer cells *in vitro*[112,113]. Using the same technique, cMET inhibition reduced migration and invasion of breast cancer cells *in vitro* in response to HGF[112]. In addition, growth of human breast cancer xenografts co-injected with cells from a human fetal fibroblast cell line in mouse models was decreased when HGF excretion by these fibroblasts was inhibited[112,113]. Tivantinib, a selective cMET inhibitor, reduced bone metastasis formation in mice after injection of MDA-MB-231 tumor cells into the systemic circulation[114].

These results have prompted clinical trials with compounds targeting the HGF/cMET axis (Figure 1D.3). In a phase 1 trial with the TKI tivantinib, 14 out of 51 advanced solid tumor patients had stable disease for over 4 months[115]. Two other TKIs, cabozantinib and foretinib (both against vascular endothelial growth factor receptor (VEGFR)2 and cMET), are currently being tested in breast cancer patients with ER positive and HER2 overexpressing tumors (Table 1). Phase 2 trials are ongoing in TNBC patients with tivantinib, cabozantinib, foretinib and the cMET monovalent antibody onartuzumab (Table 1). With regard to the prediction of response to anti-cMET therapy, in a human glioblastoma xenograft in mice,

the level of autocrine HGF excretion was predictive for the response to anti cMET therapy by a TKI[116]. For molecular imaging, both cMET and HGF can be visualised pre-clinically. Mouse agonistic human cMET antibody DN30 was radiolabeled with $^{89}$Zr. In nude mice bearing a human gastric- or head-and-neck cancer cell line xenograft, $^{89}$Zr-DN30 injection resulted in a maximum tumor to blood ratio of 5[117]. Anti-HGF nanobodies (1E2-Alb8 and 6E10-Alb8) were labeled with $^{89}$Zr and used as a positron emission tomography (PET) tracer in nude mice bearing human glioblastoma xenografts. Tumor uptake of the tracer remained stable, while blood levels of the tracer gradually decreased over time, suggesting specific tumor uptake. The nanobodies inhibited tumor growth[118]. With regard to biomarkers for evaluating the effect of cMET of HGF targeting, no clinical molecular imaging data are available.



**SDF-1** (also known as CXCL12) is produced by CAFs and acts as chemo-attractant for tumor cells expressing chemokine C-X-C motif receptor 4 (CXCR4)[119,120] (Figure 1D.1 and 1D.2). Organs expressing SDF-1, such as lung, bone marrow and liver, can thus lure CXCR4 expressing tumor cells to migrate towards them[121]. High SDF-1 expression determined immunohistochemically in breast cancer tissue of stage I-III patients, was prognostic for worse disease free- and overall survival in three retrospective studies involving a total of 628 patients[122-124]. The correlation between CXCR4 expression in breast cancer tissue and patient outcome has been studied frequently, with contradictory results[125-127]. Targeting SDF-1 or CXCR4 with antibodies or peptide inhibitors decreased breast cancer cell motility *in vitro* and reduced tumor growth and metastasis formation *in vivo*[119,128] (Figure 1D.3). This makes clinical data with the CXCR4 antagonist plerixafor also of interest for breast cancer though no clinical data for breast cancer exists to date. A phase I/II clinical trial using plerixafor, administered in addition to chemotherapy showed the safety of this combination in 46 relapsed acute myeloid leukemia patients[129]. To compare tumor levels of CXCR4 with the physiological expression, several CXCR4 targeting imaging agents have been developed in the preclinical setting (reviewed in[130,131]). Small molecules, antibodies and peptides directed against CXCR4 have been radiolabeled and show CXCR4 expression level dependent tumor uptake in several xenograft mouse models, including breast tumors[132-136]. None of these tracers have reached the clinical setting at this point.

In conclusion, stimulation of tumor cell migration by the microenvironment involves HGF and SDF-1 signaling. Intervention strategies including cMET, HGF and CXCR4 inhibitory agents are moving into the clinical arena in an investigational setting.

# Immune response modulation

The immune system plays a major role in cancer development. Although the host immune system should act against tumor cells, various factors in the tumor microenvironment in fact act in favor of the cancer cells, by modulating the this immune response. In breast cancer, key immunological players are T-cells, immune checkpoint receptors and tumor associated macrophages (TAM)s (Figure 1C).

T-cells can recognize and destroy cancer cells. Infiltration by memory T-cells seen in a large cohort of primary tumors, including breast cancer, was the strongest positive prognostic factor in favor of disease free survival and overall survival at all disease stages[137]. In HER+ or TNBC breast cancer patients neoadjuvantly treated with chemotherapy with our without trastuzumab, the presence of TILs was associated with higher treatment response[138,139]. Myeloid-derived suppressor cells (MDSC) and immune checkpoint receptors suppress T-cell activation in the microenvironment. **IL-12** is excreted by dendritic cells and promotes antitumor immune response and blocks MDSC [140] (Figure 1C.2). Programmed cell death **(PD)-1** is present on T-cells and functions as an immune checkpoint receptor which plays a role in tumor progression[141] (Figure 1C.1 and 1C.2). After binding to its ligand PD-L1, that is present on tumor cells, the T-cell is inactivated, enabling tumor cells to evade the host's immune system[142]. PD-L1 is electively expressed by many solid tumors and by isolated tumor cells within the microenvironment in response to inflammatory stimuli. Blockade of the interaction between PD-1 and PD-L1 potentiates immune response *in vitro*. In immunocompetent MMTV-ErbB-2 transgenic mice PD-1 antibody improved the therapeutic activity of anti-HER2 therapy[143]. Half of 44 human breast cancer specimens showed PD-L1 expression immunohistochemically. PD-L1 expression in these specimens correlated with a more aggressive tumor histology[144]. The presence of PD-1 positive tumor infiltrating lymphocytes, measured by immunohistochemistry in 660 breast cancer samples was correlated with lower overall patient survival[145]. Cytotoxic T lymphocyte-associated antigen **(CTLA)-4** is also present on T-cells and binds to CD80 on cancer cells, thereby transmitting an inhibitory to the T-cell (Figure 1C.1 and 1C.2). Blocking of CTLA-4 by an inhibitory antibody lead to tumor regression *in vivo*[146]. CTLA-4 levels, measured by immunohistochemistry and on mRNA level in 90 samples, were higher in breast cancer tissue compared to normal breast tissue[147]. Another group of immune cells are **TAMs** derived from CD34+ bone marrow progenitors. TAMs can increase the survival and proliferative capacity of cancer cells, by secreting growth factors (Figure 1C.1 and 1C.2). In breast cancer, the presence of TAMs is associated with a worse prognosis[148].

The importance of targeting the immunological support of tumor cells by the microenvironment is increasingly supported by clinical data. In a phase I trial involving various HER2 positive metastatic cancers, including seven patients with MBC, patients received a combination of paclitaxel, trastuzumab and IL-12. Among the seven MBC patients, one experienced a complete response and two a partial response[149]. There was increased activation of extracellular signal-regulated kinases in peripheral blood

mononuclear cells and increased levels of interferon (IFN)γ and several chemokines in patients achieving a clinical benefit compared to patients with progressive disease[149]. Whether these factors may be useful future biomarkers for response prediction will have to be shown in larger trials. Anti-PD-L1 antibody BMS-936559 was administered to 207 extensively pretreated patients, including four with breast cancer (Figure 1C.3). The overall objective response rate was 13% and 34% had prolonged disease stabilization[150]. PD-L1 expression, measured immunohistochemically, correlated to clinical activity of anti PD-1 as well as anti PD-L1 antibodies[151]. However, patients without PD-L1 staining still showed a response rate of 13-17%, compared to 39%-44% of patients with PD-L1 expression[151,152]. Several phase 1 trials with PD-1 and PD-L1 antibodies in solid cancer patients are ongoing (Table 1). High PD-L1 gene expression levels in patients treated neoadjuvantly with trastuzumab, pertuzumab or both were associated with a lower complete response rate. These results provide a rationale for combining HER2-targeted treatments with immune-modulating agents and may allow the prediction of treatment benefit[153]. Tremelimumab and ipilimumab block the activity of T-cell suppressor CTLA-4 (Figure 1C.3). In a phase I study in which 26 MBC patients received tremelimumab and exemestane, 11 experienced stable disease as best response[154]. Ipilimumab studies in MBC patients are ongoing (Table 1). TAMs are derived from the same cell lineage as osteoclasts, therefore the effect of bisphosphonates on TAMs was studied. In mice transgenic for HER2, the number of TAMs was lower in the tumor microenvironment in parallel with the decrease in tumor vascularization after bisphosphonate administration (reviewed in[155]) (Figure 1C.3).
In conclusion, key players in the immunological microenvironment of breast cancer are T-cells, IL-12, immune checkpoint receptors and TAMs. Modulation of adequate T cell response to breast cancer is effected by CTLA-4 and PD-1. Targeting this process, by compounds such as IL12, tremelimumab, ipilimumab and PD-1/PD-L1 inhibitors, is a promising strategy in breast cancer treatment

## Angiogenesis

The tumor microenvironment instigates new vessel formation in response to pro-angiogenic factors secreted by cancer cells[156] (Figure 1E). These tumor vessels show leakiness and a chaotic structure. As a result, angiogenic stimuli are increased which leads to an even more defective vascular system. In the earliest breast cancer stages, angiogenesis is already implicated. VEGF-A is secreted by cancer cells and TAMs and binds to the VEFGRs on endothelial cells[156,157] (Figure 1E.1 and 1E.2). **VEGF-A** expression in normal glandular epithelial structures of the human breast is lower than in (pre)malignant lesions. Expression increased with tumor dedifferentiation (mean number of VEGF-A positive cells 2.5% ± 0.4% in normal lobules versus 10.4% ± 6.6% malignant lesions, $P < 0.001$)[158].

*In vivo* experiments using different non-breast cancer human xenografts in mice showed anti-tumor effect of a monoclonal murine anti-human VEGF-A antibody[159]. Bevacizumab, the most widely used anti-angiogenic drug, is an anti-VEGF-A humanized monoclonal

antibody[160] (Figure 1E.3). A meta-analysis of 7 trials involving 4,032 MBC patients, studied the effect of combining bevacizumab with first line chemotherapeutic drugs and showed a progression free survival prolongation of 1.4 to 5.8 months (HR 0.67; 95% CI 0.61 to 0.73) *w*hile overall survival was not increased[161]. In the RIBBON-2 trial bevacizumab was combined with standard chemotherapy compared to chemotherapy alone as second line treatment in patients with HER2 negative MBC[162]. Progression free survival was prolonged from 5.1 to 7.2 months, but again overall survival was not affected. A subgroup analysis of the RIBBON-2 trial in TNBC patients showed a trend towards increased overall survival[163]. Whether there is truly a benefit with bevacizumab for this subtype in the metastatic setting is currently being investigated (Table 1). The negative BEATRICE trial does not support a role for bevacizumab in the adjuvant treatment for TNBC patients[164]. Also, no additional value was found when bevacizumab was combined with either anti-HER2 or endocrine therapy in a subset of HER2 positive and ER positive MBC patients[165,166]. Multiple phase III trials with bevacizumab in breast cancer patients are still ongoing (Table 1).

Anti-angiogenic agent sunitinib is a TKI against platelet derived growth factor receptors (PDGFR) and VEGFRs (Figure 1E.3). In MBC patients, sunitinib did not prolong progression free survival in phase III trials, and monotherapy sunitinib had an inferior progression free survival compared to capecitabine[167,168]. Clinical trials with sunitinib in breast cancer patients are ongoing. However, so far none of these anti-angiogenic drugs seem to play a clinically relevant role in any of the studied breast cancer subgroups.

While the clinical relevance of targeting VEGF in breast cancer is limited, measuring angiogenic factors may be used for tumor identification of a susceptible subtype. Plasma VEGF-A levels showed no clear relationship with clinical effect of angiogenesis inhibitors[169-171]. However, circulating levels of VEGF-A, may not reflect what is happening at the level of the tumor since VEGF-A binds locally to the ECM[172]. By radiolabeling the anti-VEGF antibody bevacizumab with $^{89}$Zr, VEGF can be visualized with PET. Preclinically, there was tumor specific uptake in human breast and ovarian xenografts in mice[173,174]. In patients, $^{89}$Zr-bevacizumab uptake on PET was shown in 25 of 26 primary breast tumors[175]. Interestingly, $^{89}$Zr-bevacizumab uptake in the primary breast tumors was relatively low, compared to tumor uptake in a series of 22 metastatic renal cell cancers (mean $SUV_{max}$ 1.85 *vs* 10.1)[175,176]. This difference in VEGF-A tumor levels between renal cell and breast cancer lesions, may possibly be related to the difference in efficacy of targeting angiogenesis in these tumor types.

In conclusion, angiogenesis in the microenvironment to support breast cancer growth, is effected by VEGF-A and its receptors. Targeting strategies, including bevacizumab and sunitinib, have been studied in breast cancer; however, so far limited effects have been seen for this therapeutic strategy in breast cancer treatment.

## Extracellular matrix remodeling

The ECM prevents tumor cells from invading the surrounding tissues, and remodeling of the ECM is therefore an obvious process by which the microenvironment might support tumor cells. Numerous factors are involved in this process, including integrins, lysyl oxidase (LOX) and matrix metalloproteases (MMPs) (Figure 1F).

**Integrins** at the tumor cell membrane are a family of heterodimeric, transmembrane glycoproteins consisting of one α and one β subunit. Each family member binds multiple ECM ligands which activates intracellular signaling pathways[177] (Figure 1F.1 and 1F.2). **MMPs** are a family of (secreted or membrane bound) proteolytic enzymes which are expressed by a variety of cells including cancer cells and CAFs and have the ability to degrade ECM components[178-180] (Figure 1F.1 and 1F.2). Despite a strong rationale for targeting factors involved in ECM remodeling, clinical trials with anti-integrin and anti-MMP strategies have so far failed to show meaningful results[181-186] (Figure 1F). Several phase I studies with a MMP inhibitor and integrin inhibitors are ongoing in metastatic solid cancer patients (Table 1).

A potential alternative might be to target **LOX**. Members of the LOX family are secreted by cancer and stromal cells in response to hypoxia and modify the ECM (Figure 1F.1 and 1F.2). LOX crosslinks collagen IV in the basement membrane of the ECM, recruits CD11b+ cells to distant metastatic sites and induces expression of MMPs. Both up-and down regulation of LOX family members have been associated with cancer progression. This paradoxical role of the LOX family is possibly due to their multiple temporal and spatial expression patterns, which may confer differential functions[187]. However, more evidence suggests that the extracellular activity of these proteins in remodeling the ECM facilitates tumor cell invasion and metastasis. Preclinical models showed a decrease in metastases formation after inhibition of LOX and LOXL2[187], without affecting tumor growth. The LOXL2 antibody, AB0024 is currently tested in a phase 1 clinical trial (Table 1) (Figure 1F.3).

In conclusion, extracellular matrix remodeling by the microenvironment is effected by integrins, LOX and MMPs. Targeting strategies including anti-integrin, anti-MMP and up- and down regulation of LOX have so far not been successful in supporting the relevance of this process in breast cancer.

## Discussion and future perspectives

The focus of this review was to describe the current knowledge of processes involved in the breast cancer microenvironment, and how these processes affect breast cancer progression and metastasis. We described the formation of the metastatic niche, metabolic stimulation, stimulation of tumor cell migration, immune modulation, angiogenesis and matrix remodeling. Increasing evidence is supporting the significance of targeting the breast cancer microenvironment. However, different levels of evidence for targeting the described processes are apparent. Targeting the process of formation of the metastatic niche and metabolic stimulation by the breast cancer microenvironment, is already showing clinical efficacy. Intervening with stimulation of tumor cell migration and immune modulation by the microenvironment, is an upcoming field of great interest and research. In contrast, targeting of microenvironmental angiogenesis or matrix remodeling appears to be of limited clinical relevance in breast cancer treatment so far.

To optimize targeting the microenvironment for maximal anti-cancer effect, more detailed knowledge of the interaction between environment and cancer is needed. Preclinical models that allow investigation of this interaction in a species specific manner are currently in development. Furthermore, as many of the described processes take place in parallel, combining agents directed at multiple microenvironmental factors, administered in combination with standard anti-cancer directed treatments such as chemotherapy, may ensure the best clinical result. In addition, differences between breast cancer subtypes are becoming more and more apparent[188] and selecting the appropriate study population could maximize treatment results.

In view of the fact that microenvironmental factors usually do not consistently have a "good" or "bad" impact during cancer progression, it is vital to study the optimal timing of administering microenvironment targeting agents in future studies. With regard to predictive markers for treatment response, tissue and blood assessments may be suitable for this purpose. However, these are static measurements that may not suit the dynamics of targeting microenvironment-cancer interactions. Molecular imaging, although not generally available, can provide local real time information about the *in vivo* interaction of the tumor and its microenvironment. As PET imaging results in whole body images, it may also offer information regarding intra- and inter lesion heterogeneity[155,189]

In summary, targeting the breast cancer microenvironment is an upcoming field of research. For some of the processes involved in the tumor-stroma interaction, clinical evidence for useful intervention is already present, supporting the concept of targeting these processes. Further optimization of this approach is warranted, with regard to combinations of agents, timing, improved knowledge of breast cancer subtype specific-aspects, and predictive markers, to improve this approach for comprehensive implementation in breast cancer care.

## Acknowledgements

Supported by Dutch Cancer Society grant RUG 2010-4739 and the ERC advanced grant OnQview

# References

1. Jemal A, Siegel R, Xu J, Ward E. Cancer statistics, 2010. CA Cancer J Clin 2010; 60:277-300.
2. Howlader N, Noone AM, Krapcho M, Neyman N, Aminou R, Altekruse SF, et al. SEER Cancer Statistics Review, 1975-2009 (Vintage 2009 Populations). *http://seercancergov/csr/1975_2009_pops09/*. 2012; based on November 2011 SEER data submission, posted at the SEER web site, April 2012.
3. Fidler IJ. The pathogenesis of cancer metastasis: the 'seed and soil' hypothesis revisited. Nat Rev Cancer 2003; 3:453-8.
4. Kennecke H, Yerushalmi R, Woods R, Cheang MC, Voduc D, Speers CH, et al. Metastatic behavior of breast cancer subtypes. J Clin Oncol 2010; 28:3271-7.
5. Hanahan D, Weinberg RA. Hallmarks of cancer: the next generation. Cell 2011; 144:646-74.
6. Hanahan D, Coussens LM. Accessories to the crime: functions of cells recruited to the tumor microenvironment. Cancer Cell 2012; 21:309-22.
7. Fumagalli D, Sotiriou C. Treatment of pT1N0 breast cancer: multigene predictors to assess risk of relapse. Ann Oncol 2010; 21 Suppl 7:vii103-6.
8. Morales M, Planet E, Arnal-Estape A, Pavlovic M, Tarragona M, Gomis RR. Tumor-stroma interactions a trademark for metastasis. Breast 2011; 20 Suppl 3:S50-5.
9. Egeblad M, Nakasone ES, Werb Z. Tumors as organs: complex tissues that interface with the entire organism. Dev Cell 2010; 18:884-901.
10. Wiseman BS. Stromal effects on mammary gland development and breast cancer. Science 2002; 296:1046-9.
11. Polyak K, Kalluri R. The role of the microenvironment in mammary gland development and cancer. Cold Spring Harb Perspect Biol 2010; 2:a003244.
12. Chaudary MA. Patterns of recurrence in Western and Japanese women with breast cancer. Breast Cancer Res Treat 1991; 18 Suppl 1:S115-8.
13. Jain S, Fisher C, Smith P, Millis RR, Rubens RD. Patterns of metastatic breast cancer in relation to histological type. Eur J Cancer 1993; 29A:2155-7.
14. Massagué J. TGFβ in cancer. Cell 2008; 134:215-30.
15. Kojima Y, Acar A, Eaton EN, Mellody KT, Scheel C, Ben-Porath I, et al. Autocrine TGF-beta and stromal cell-derived factor-1 (SDF-1) signaling drives the evolution of tumor-promoting mammary stromal myofibroblasts. Proc Natl Acad Sci U S A 2010; 107:20009-14.
16. Guido C, Whitaker-Menezes D, Capparelli C, Balliet R, Lin Z, Pestell RG, et al. Metabolic reprogramming of cancer-associated fibroblasts by TGF-beta drives tumor growth: connecting TGF-beta signaling with "Warburg-like" cancer metabolism and L-lactate production. Cell Cycle 2012; 11:3019-35.
17. Padua D, Massague J. Roles of TGFβ in metastasis. Cell Res 2009; 19:89-102.
18. Grau AM, Wen W, Ramroopsingh DS, Gao YT, Zi J, Cai Q, et al. Circulating transforming growth factor-β-1 and breast cancer prognosis: results from the Shanghai Breast Cancer Study. Breast Cancer Res Treat 2008; 112:335-41.
19. Dave H, Shah M, Trivedi S, Shukla S. Prognostic utility of circulating transforming growth factor beta 1 in breast cancer patients. Int J Biol Markers 2012; 27:53-9.
20. Kang Y, He W, Tulley S, Gupta GP, Serganova I, Chen CR, et al. Breast cancer bone metastasis mediated by the Smad tumor suppressor pathway. Proc Natl Acad Sci U S A 2005; 102:13909-14.
21. Korpal M, Yan J, Lu X, Xu S, Lerit DA, Kang Y. Imaging transforming growth factor-β signaling dynamics and therapeutic response in breast cancer bone metastasis. Nat Med 2009; 15:960-6.
22. Gnant M, Mlineritsch B, Stoeger H, Luschin-Ebengreuth G, Heck D, Menzel C, et al. Adjuvant endocrine therapy plus zoledronic acid in premenopausal women with early-stage breast cancer: 62-month follow-up from the ABCSG-12 randomised trial. Lancet Oncol 2011; 12:631-41.
23. Eidtmann H, de Boer R, Bundred N, Llombart-Cussac A, Davidson N, Neven P, et al. Efficacy of zoledronic acid in postmenopausal women with early breast cancer receiving adjuvant letrozole: 36-month results of the ZO-FAST study. Ann Oncol 2010; 21:2188-94.
24. Coleman RE, Marshall H, Cameron D, Dodwell D, Burkinshaw R, Keane M, et al. Breast-cancer adjuvant therapy with zoledronic acid. N Engl J Med 2011; 365:1396-405.
25. Charehbili A, Van de Ven S, Liefers GJ, Smit VT, Wasser MN, Meershoek-Klein Kranenbarg EM, et al. Clinical and pathological response after neoadjuvant chemotherapy with or without zoledronic acid for patients with HER2-negative large resectable or stage II or III breast cancer. European Cancer Congress 2013 Abstract Book in the European Journal of Cancer 2013; 49.
26. Coleman RE, Gnant M, Paterson A, Powles T, von Minckwitz G, Pritchard K, et al. Effects of bisphosphonate treatment on recurrence and cause-specific mortality in women with early breast cancer: A meta-analysis of individual patient data from randomised trials. Cancer Res 2013; SABCS 2013:abstract nr S4-07.
27. Nicks KM, Fowler TW, Akel NS, Perrien DS, Suva LJ, Gaddy D. Bone turnover across the menopause transition : The role of gonadal inhibins. Ann N Y Acad Sci 2010; 1192:153-60.
28. Gnant M. Role of bisphosphonates in postmenopausal women with breast cancer. Cancer Treat Rev 2013; [Epub ahead of print].

29. Holen I, Wang N, Reeves K, Fowles A, Croucher P, Eaton C, et al. Zoledronic acid specifically inhibits development of bone metastases in the post-menopausal setting – evidence from an in vivo breast cancer model. Cancer Res 2012; 72(24 Suppl.).
30. Ganapathy V, Ge R, Grazioli A, Xie W, Banach-Petrosky W, Kang Y, et al. Targeting the transforming growth factor-β pathway inhibits human basal-like breast cancer metastasis. Mol Cancer 2010; 9:122.
31. Ehata S, Hanyu A, Fujime M, Katsuno Y, Fukunaga E, Goto K, et al. Ki26894, a novel transforming growth factor-β type I receptor kinase inhibitor, inhibits in vitro invasion and in vivo bone metastasis of a human breast cancer cell line. Cancer Sci 2007; 98:127-33.
32. Ganapathy V, Banach-Petrosky W, Xie W, Kareddula A, Nienhuis H, Miles G, et al. Luminal breast cancer metastasis is dependent on estrogen signaling. Clin Exp Metastasis 2012; 29:493-509.
33. Bierie B, Stover DG, Abel TW, Chytil A, Gorska AE, Aakre M, et al. Transforming growth factor-β regulates mammary carcinoma cell survival and interaction with the adjacent microenvironment. Cancer Res 2008; 68:1809-19.
34. Farrington DL, Yingling JM, Fill JA, Yan L, Qian YW, Shou J, et al. Development and validation of a phosphorylated SMAD ex vivo stimulation assay. Biomarkers 2007; 12:313-30.
35. Padua D, Zhang XH, Wang Q, Nadal C, Gerald WL, Gomis RR, et al. TGFβ primes breast tumors for lung metastasis seeding through angiopoietin-like 4. Cell 2008; 133:66-77.
36. Den Hollander MW, Bensch F, Glaudemans AWJM, Enting RH, Bunskoek S, Oude Munnink TH, et al. $^{89}$Zr-GC1008 PET imaging and GC1008 treatment of recurrent glioma patients. J Clin Oncol 2013; 31:(suppl; abstr 2050).
37. Kingsley LA, Fournier PG, Chirgwin JM, Guise TA. Molecular biology of bone metastasis. Mol Cancer Ther 2007; 6:2609-17.
38. Linforth R, Anderson N, Hoey R, Nolan T, Downey S, Brady G, et al. Coexpression of parathyroid hormone related protein and its receptor in early breast cancer predicts poor patient survival. Clin Cancer Res 2002; 8:3172-7.
39. Powell GJ, Southby J, Danks JA, Stillwell RG, Hayman JA, Henderson MA, et al. Localization of parathyroid hormone-related protein in breast cancer metastases: increased incidence in bone compared with other sites. Cancer Res 1991; 51:3059-61.
40. Boyce BF, Xing L. Functions of RANKL/RANK/OPG in bone modeling and remodeling. Arch Biochem Biophys 2008; 473:139-46.
41. Dougall WC. Molecular pathways: osteoclast-dependent and osteoclast-independent roles of the RANKL/RANK/OPG pathway in tumorigenesis and metastasis. Clin Cancer Res 2012; 18:326-35.
42. Fata JE, Kong YY, Li J, Sasaki T, Irie-Sasaki J, Moorehead RA, et al. The osteoclast differentiation factor osteoprotegerin-ligand is essential for mammary gland development. Cell 2000; 103:41-50.
43. Gonzalez-Suarez E, Jacob AP, Jones J, Miller R, Roudier-Meyer MP, Erwert R, et al. RANK ligand mediates progestin-induced mammary epithelial proliferation and carcinogenesis. Nature 2010; 468:103-7.
44. Schramek D, Leibbrandt A, Sigl V, Kenner L, Pospisilik JA, Lee HJ, et al. Osteoclast differentiation factor RANKL controls development of progestin-driven mammary cancer. Nature 2010; 468:98-102.
45. Santini D, Schiavon G, Vincenzi B, Gaeta L, Pantano F, Russo A, et al. Receptor activator of NF-kB (RANK) expression in primary tumors associates with bone metastasis occurrence in breast cancer patients. PLoS One 2011; 6:e19234.
46. Kostenuik PJ, Nguyen HQ, McCabe J, Warmington KS, Kurahara C, Sun N, et al. Denosumab, a fully human monoclonal antibody to RANKL, inhibits bone resorption and increases BMD in knock-in mice that express chimeric (murine/human) RANKL. J Bone Miner Res 2009; 24:182-95.
47. Stopeck AT, Lipton A, Body JJ, Steger GG, Tonkin K, de Boer RH, et al. Denosumab compared with zoledronic acid for the treatment of bone metastases in patients with advanced breast cancer: a randomized, double-blind study. J Clin Oncol 2010; 28:5132-9.
48. Lipton A, Steger GG, Figueroa J, Alvarado C, Solal-Celigny P, Body JJ, et al. Randomized active-controlled phase II study of denosumab efficacy and safety in patients with breast cancer-related bone metastases. J Clin Oncol 2007; 25:4431-7.
49. Mountzios G, Terpos E, Syrigos K, Papadimitriou C, Papadopoulos G, Bamias A, et al. Markers of bone remodeling and skeletal morbidity in patients with solid tumors metastatic to the skeleton receiving the biphosphonate zoledronic acid. Transl Res 2010; 155:247-55.
50. Sung MK, Yeon JY, Park SY, Park JH, Choi MS. Obesity-induced metabolic stresses in breast and colon cancer. Ann N Y Acad Sci 2011; 1229:61-8.
51. Calle EE, Rodriguez C, Walker-Thurmond K, Thun MJ. Overweight, obesity, and mortality from cancer in a prospectively studied cohort of U.S. adults. N Engl J Med 2003; 348:1625-38.
52. de Azambuja E, McCaskill-Stevens W, Francis P, Quinaux E, Crown JP, Vicente M, et al. The effect of body mass index on overall and disease-free survival in node-positive breast cancer patients treated with docetaxel and doxorubicin-containing adjuvant chemotherapy: the experience of the BIG 02-98 trial. Breast Cancer Res Treat 2010; 119:145-53.

53. Ewertz M, Jensen MB, Gunnarsdottir KA, Hojris I, Jakobsen EH, Nielsen D, et al. Effect of obesity on prognosis after early-stage breast cancer. J Clin Oncol 2011; 29:25-31.
54. Chlebowski RT, Blackburn GL, Thomson CA, Nixon DW, Shapiro A, Hoy MK, et al. Dietary fat reduction and breast cancer outcome: interim efficacy results from the Women's Intervention Nutrition Study. J Natl Cancer Inst 2006; 98:1767-76.
55. Nelson ER, Wardell SE, Jasper JS, Park S, Suchindran S, Howe MK, et al. 27-Hydroxycholesterol links hypercholesterolemia and breast cancer pathophysiology. Science 2013; 342:1094-8.
56. Holmes MD, Chen WY, Feskanich D, Kroenke CH, Colditz GA. Physical activity and survival after breast cancer diagnosis. Jama 2005; 293:2479-86.
57. McTiernan A. Mechanisms linking physical activity with cancer. Nat Rev Cancer 2008; 8:205-11.
58. Weisberg SP, McCann D, Desai M, Rosenbaum M, Leibel RL, Ferrante AW, Jr. Obesity is associated with macrophage accumulation in adipose tissue. J Clin Invest 2003; 112:1796-808.
59. Morris PG, Hudis CA, Giri D, Morrow M, Falcone DJ, Zhou XK, et al. Inflammation and increased aromatase expression occur in the breast tissue of obese women with breast cancer. Cancer Prev Res (Phila) 2011; 4:1021-9.
60. Schottenfeld D, Beebe-Dimmer J. Chronic inflammation: a common and important factor in the pathogenesis of neoplasia. CA Cancer J Clin 2006; 56:69-83.
61. Gross AL, Newschaffer CJ, Hoffman-Bolton J, Rifai N, Visvanathan K. Adipocytokines, inflammation, and breast cancer risk in postmenopausal women: a prospective study. Cancer Epidemiol Biomarkers Prev 2013; 22:1319-24.
62. Ollberding NJ, Kim Y, Shvetsov YB, Wilkens LR, Franke AA, Cooney RV, et al. Prediagnostic leptin, adiponectin, C-reactive protein, and the risk of postmenopausal breast cancer. Cancer Prev Res (Phila) 2013; 6:188-95.
63. Imayama I, Ulrich CM, Alfano CM, Wang C, Xiao L, Wener MH, et al. Effects of a caloric restriction weight loss diet and exercise on inflammatory biomarkers in overweight/obese postmenopausal women: a randomized controlled trial. Cancer Res 2012; 72:2314-26.
64. Cleary MP, Grossmann ME. Minireview: Obesity and breast cancer: the estrogen connection. Endocrinology 2009; 150:2537-42.
65. Simpson ER, Mahendroo MS, Means GD, Kilgore MW, Hinshelwood MM, Graham-Lorence S, et al. Aromatase cytochrome P450, the enzyme responsible for estrogen biosynthesis. Endocr Rev. 1994; 15:342-55.
66. Nilsson S, Koehler KF, Gustafsson JA. Development of subtype-selective oestrogen receptor-based therapeutics. Nat Rev Drug Discov 2011; 10:778-92.
67. Simpson ER. Sources of estrogen and their importance. J Steroid Biochem Mol Biol 2003; 86:225-30.
68. Jensen EV, Cheng G, Palmieri C, Saji S, Makela S, Van Noorden S, et al. Estrogen receptors and proliferation markers in primary and recurrent breast cancer. Proc Natl Acad Sci U S A 2001; 98:15197-202.
69. Mueller SO, Clark JA, Myers PH, Korach KS. Mammary gland development in adult mice requires epithelial and stromal estrogen receptor α. Endocrinology 2002; 143:2357-65.
70. Palmieri C, Saji S, Sakaguchi H, Cheng G, Sunters A, O'Hare MJ, et al. The expression of oestrogen receptor (ER)-β and its variants, but not ERα, in adult human mammary fibroblasts. J Mol Endocrinol 2004; 33:35-50.
71. Heldring N, Pike A, Andersson S, Matthews J, Cheng G, Hartman J, et al. Estrogen receptors: how do they signal and what are their targets. Physiol Rev 2007; 87:905-31.
72. Campbell KL, Foster-Schubert KE, Alfano CM, Wang CC, Wang CY, Duggan CR, et al. Reduced-calorie dietary weight loss, exercise, and sex hormones in postmenopausal women: randomized controlled trial. J Clin Oncol 2012; 30:2314-26.
73. Demark-Wahnefried W, Campbell KL, Hayes SC. Weight management and its role in breast cancer rehabilitation. Cancer 2012; 118:2277-87.
74. Friedenreich CM, Woolcott CG, McTiernan A, Ballard-Barbash R, Brant RF, Stanczyk FZ, et al. Alberta physical activity and breast cancer prevention trial: sex hormone changes in a year-long exercise intervention among postmenopausal women. J Clin Oncol 2010; 28:1458-66.
75. Pfeiler G, Stoger H, Dubsky P, Mlineritsch B, Singer C, Balic M, et al. Efficacy of tamoxifen +/- aminoglutethimide in normal weight and overweight postmenopausal patients with hormone receptor-positive breast cancer: an analysis of 1509 patients of the ABCSG-06 trial. Br J Cancer 2013; 108:1408-14.
76. Eisen A, Lubinski J, Klijn J, Moller P, Lynch HT, Offit K, et al. Breast cancer risk following bilateral oophorectomy in BRCA1 and BRCA2 mutation carriers: an international case-control study. J Clin Oncol 2005; 23:7491-6.
77. Atchley DP, Albarracin CT, Lopez A, Valero V, Amos CI, Gonzalez-Angulo AM, et al. Clinical and pathologic characteristics of patients with BRCA-positive and BRCA-negative breast cancer. J Clin Oncol 2008; 26:4282-8.
78. Lim E, Vaillant F, Wu D, Forrest NC, Pal B, Hart AH, et al. Aberrant luminal progenitors as the candidate target population for basal tumor development in BRCA1 mutation carriers. Nat Med 2009; 15:907-13.

79. Pequeux C, Raymond-Letron I, Blacher S, Boudou F, Adlanmerini M, Fouque MJ, et al. Stromal estrogen receptor-α promotes tumor growth by normalizing an increased angiogenesis. Cancer Res 2012; 72:3010-9.
80. Iyer V, Klebba I, McCready J, Arendt LM, Betancur-Boissel M, Wu MF, et al. Estrogen promotes ER-negative tumor growth and angiogenesis through mobilization of bone marrow-derived monocytes. Cancer Res 2012; 72:2705-13.
81. Gupta PB, Kuperwasser C. Contributions of estrogen to ER-negative breast tumor growth. J Steroid Biochem Mol Biol 2006; 102:71-8.
82. Mantovani A, Allavena P, Sica A, Balkwill F. Cancer-related inflammation. Nature 2008; 454:436-44.
83. Luo J, Solimini NL, Elledge SJ. Principles of cancer therapy: oncogene and non-oncogene addiction. Cell 2009; 136:823-37.
84. Godsland IF. Insulin resistance and hyperinsulinaemia in the development and progression of cancer. Clin Sci (Lond) 2010; 118:315-32.
85. Pollak M. Insulin and insulin-like growth factor signalling in neoplasia. Nat Rev Cancer 2008; 8:915-28.
86. Giovannucci E, Harlan DM, Archer MC, Bergenstal RM, Gapstur SM, Habel LA, et al. Diabetes and cancer: a consensus report. CA Cancer J Clin 2010; 60:207-21.
87. Jalving M, Gietema JA, Lefrandt JD, de Jong S, Reyners AK, Gans RO, et al. Metformin: taking away the candy for cancer? Eur J Cancer 2010; 46:2369-80.
88. Plymate SR, Matej LA, Jones RE, Friedl KE. Inhibition of sex hormone-binding globulin production in the human hepatoma (Hep G2) cell line by insulin and prolactin. J Clin Endocrinol Metab 1988; 67:460-4.
89. Pugeat M, Crave JC, Elmidani M, Nicolas MH, Garoscio-Cholet M, Lejeune H, et al. Pathophysiology of sex hormone binding globulin (SHBG): relation to insulin. J Steroid Biochem Mol Biol 1991; 40:841-9.
90. Zakikhani M, Dowling R, Fantus IG, Sonenberg N, Pollak M. Metformin is an AMP kinase-dependent growth inhibitor for breast cancer cells. Cancer Res 2006; 66:10269-73.
91. Jiralerspong S, Palla SL, Giordano SH, Meric-Bernstam F, Liedtke C, Barnett CM, et al. Metformin and pathologic complete responses to neoadjuvant chemotherapy in diabetic patients with breast cancer. J Clin Oncol 2009; 27:3297-302.
92. Yang Y, Yee D. Targeting insulin and insulin-like growth factor signaling in breast cancer. J Mammary Gland Biol Neoplasia 2012; 17:251-61.
93. Ibrahim YH, Yee D. Insulin-like growth factor-I and cancer risk. Growth Horm IGF Res 2004; 14:261-9.
94. Hartog H, Wesseling J, Boezen HM, van der Graaf WT. The insulin-like growth factor 1 receptor in cancer: old focus, new future. Eur J Cancer 2007; 43:1895-904.
95. Milano A, Dal Lago L, Sotiriou C, Piccart M, Cardoso F. What clinicians need to know about antioestrogen resistance in breast cancer therapy. Eur J Cancer 2006; 42:2692-705.
96. Maor S, Yosepovich A, Papa MZ, Yarden RI, Mayer D, Friedman E, et al. Elevated insulin-like growth factor-I receptor (IGF-IR) levels in primary breast tumors associated with BRCA1 mutations. Cancer Lett 2007; 257:236-43.
97. Lerma E, Peiro G, Ramon T, Fernandez S, Martinez D, Pons C, et al. Immunohistochemical heterogeneity of breast carcinomas negative for estrogen receptors, progesterone receptors and Her2/neu (basal-like breast carcinomas). Mod Pathol 2007; 20:1200-7.
98. Kaufman P, Ferrero J, Bourgeois H, Kennecke H, De Boer R, Jacot W, et al. A Randomized, double-blind, placebo-controlled, phase 2 study of AMG 479 with exemestane (E) or fulvestrant (F) in postmenopausal women with hormone-receptor positive (HR+) metastatic (M) or locally advanced (LA) breast cancer (BC). Cancer Res 2010; 70:Abstract nr S1-4.
99. Tyan SW, Kuo WH, Huang CK, Pan CC, Shew JY, Chang KJ, et al. Breast cancer cells induce cancer-associated fibroblasts to secrete hepatocyte growth factor to enhance breast tumorigenesis. PLoS One 2011; 6:e15313.
100. Bhowmick NA, Neilson EG, Moses HL. Stromal fibroblasts in cancer initiation and progression. Nature 2004; 432:332-7.
101. Trusolino L, Bertotti A, Comoglio PM. MET signalling: principles and functions in development, organ regeneration and cancer. Nat Rev Mol Cell Biol 2010; 11:834-48.
102. Garcia S, Dales JP, Charafe-Jauffret E, Carpentier-Meunier S, Andrac-Meyer L, Jacquemier J, et al. Overexpression of c-Met and of the transducers PI3K, FAK and JAK in breast carcinomas correlates with shorter survival and neoangiogenesis. Int J Oncol 2007; 31:49-58.
103. Kang JY, Dolled-Filhart M, Ocal IT, Singh B, Lin CY, Dickson RB, et al. Tissue microarray analysis of hepatocyte growth factor/Met pathway components reveals a role for Met, matriptase, and hepatocyte growth factor activator inhibitor 1 in the progression of node-negative breast cancer. Cancer Res 2003; 63:1101-5.
104. Raghav KP, Wang W, Liu S, Chavez-MacGregor M, Meng X, Hortobagyi GN, et al. cMET and phospho-cMET protein levels in breast cancers and survival outcomes. Clin Cancer Res 2012; 18:2269-77.
105. Sheen-Chen SM, Liu YW, Eng HL, Chou FF. Serum levels of hepatocyte growth factor in patients with breast cancer. Cancer Epidemiol Biomarkers Prev 2005; 14:715-7.

106. Kim EJ, Eom SJ, Hong JE, Lee JY, Choi MS, Park JH. Benzyl isothiocyanate inhibits basal and hepatocyte growth factor-stimulated migration of breast cancer cells. Mol Cell Biochem 2012; 359:431-40.
107. Trusolino L, Cavassa S, Angelini P, Ando M, Bertotti A, Comoglio PM, et al. HGF/scatter factor selectively promotes cell invasion by increasing integrin avidity. Faseb J 2000; 14:1629-40.
108. Lee WJ, Chen WK, Wang CJ, Lin WL, Tseng TH. Apigenin inhibits HGF-promoted invasive growth and metastasis involving blocking PI3K/Akt pathway and β4 integrin function in MDA-MB-231 breast cancer cells. Toxicol Appl Pharmacol 2008; 226:178-91.
109. Gallego MI, Bierie B, Hennighausen L. Targeted expression of HGF/SF in mouse mammary epithelium leads to metastatic adenosquamous carcinomas through the activation of multiple signal transduction pathways. Oncogene 2003; 22:8498-508.
110. Wilson TR, Fridlyand J, Yan Y, Penuel E, Burton L, Chan E, et al. Widespread potential for growth-factor-driven resistance to anticancer kinase inhibitors. Nature 2012; 487:505-9.
111. Jiang WG, Grimshaw D, Lane J, Martin TA, Abounader R, Laterra J, et al. A hammerhead ribozyme suppresses expression of hepatocyte growth factor/scatter factor receptor c-MET and reduces migration and invasiveness of breast cancer cells. Clin Cancer Res 2001; 7:2555-62.
112. Jiang WG, Grimshaw D, Martin TA, Davies G, Parr C, Watkins G, et al. Reduction of stromal fibroblast-induced mammary tumor growth, by retroviral ribozyme transgenes to hepatocyte growth factor/scatter factor and its receptor, c-MET. Clin Cancer Res 2003; 9:4274-81.
113. Previdi S, Abbadessa G, Dalo F, France DS, Broggini M. Breast cancer-derived bone metastasis can be effectively reduced through specific c-MET Inhibitor tivantinib (ARQ 197) and shRNA c-MET knockdown. Mol Cancer Ther 2011; 11:214-23.
114. Yap TA, Olmos D, Brunetto AT, Tunariu N, Barriuso J, Riisnaes R, et al. Phase I trial of a selective c-MET inhibitor ARQ 197 incorporating proof of mechanism pharmacodynamic studies. J Clin Oncol 2011; 29:1271-9.
115. Xie Q, Bradley R, Kang L, Koeman J, Ascierto ML, Worschech A, et al. Hepatocyte growth factor (HGF) autocrine activation predicts sensitivity to MET inhibition in glioblastoma. Proc Natl Acad Sci U S A 2012; 109:570-5.
116. Perk LR, Stigter-van Walsum M, Visser GW, Kloet RW, Vosjan MJ, Leemans CR, et al. Quantitative PET imaging of Met-expressing human cancer xenografts with $^{89}$Zr-labelled monoclonal antibody DN30. Eur J Nucl Med Mol Imaging 2008; 35:1857-67.
117. Vosjan MJ, Vercammen J, Kolkman JA, Stigter-van Walsum M, Revets H, van Dongen GA. Nanobodies targeting the hepatocyte growth factor: potential new drugs for molecular cancer therapy. Mol Cancer Ther 2012; 11:1017-25.
118. Muller A, Homey B, Soto H, Ge N, Catron D, Buchanan ME, et al. Involvement of chemokine receptors in breast cancer metastasis. Nature 2001; 410:50-6.
119. Orimo A, Gupta PB, Sgroi DC, Arenzana-Seisdedos F, Delaunay T, Naeem R, et al. Stromal fibroblasts present in invasive human breast carcinomas promote tumor growth and angiogenesis through elevated SDF-1/CXCL12 secretion. Cell 2005; 121:335-48.
120. Teicher BA, Fricker SP. CXCL12 (SDF-1)/CXCR4 pathway in cancer. Clin Cancer Res 2010; 16:2927-31.
121. Kobayashi T, Tsuda H, Moriya T, Yamasaki T, Kikuchi R, Ueda S, et al. Expression pattern of stromal cell-derived factor-1 chemokine in invasive breast cancer is correlated with estrogen receptor status and patient prognosis. Breast Cancer Res Treat 2010; 123:733-45.
122. Hassan S, Ferrario C, Saragovi U, Quenneville L, Gaboury L, Baccarelli A, et al. The influence of tumor-host interactions in the stromal cell-derived factor-1/CXCR4 ligand/receptor axis in determining metastatic risk in breast cancer. Am J Pathol 2009; 175:66-73.
123. Mirisola V, Zuccarino A, Bachmeier BE, Sormani MP, Falter J, Nerlich A, et al. CXCL12/SDF1 expression by breast cancers is an independent prognostic marker of disease-free and overall survival. Eur J Cancer 2009; 45:2579-87.
124. Li YM, Pan Y, Wei Y, Cheng X, Zhou BP, Tan M, et al. Upregulation of CXCR4 is essential for HER2-mediated tumor metastasis. Cancer Cell 2004; 6:459-69.
125. Kato M, Kitayama J, Kazama S, Nagawa H. Expression pattern of CXC chemokine receptor-4 is correlated with lymph node metastasis in human invasive ductal carcinoma. Breast Cancer Res 2003; 5:R144-50.
126. Andre F, Xia W, Conforti R, Wei Y, Boulet T, Tomasic G, et al. CXCR4 expression in early breast cancer and risk of distant recurrence. Oncologist 2009; 14:1182-8.
127. Hassan S, Buchanan M, Jahan K, Aguilar-Mahecha A, Gaboury L, Muller WJ, et al. CXCR4 peptide antagonist inhibits primary breast tumor growth, metastasis and enhances the efficacy of anti-VEGF treatment or docetaxel in a transgenic mouse model. Int J Cancer 2011; 129:225-32.
128. Uy GL, Rettig MP, Motabi IH, McFarland K, Trinkaus KM, Hladnik LM, et al. A phase 1/2 study of chemosensitization with the CXCR4 antagonist plerixafor in relapsed or refractory acute myeloid leukemia. Blood 2012; 119:3917-24.

129. Woodard LE, Nimmagadda S. CXCR4-based imaging agents. J Nucl Med 2011; 52:1665-9.
130. Kuil J, Buckle T, van Leeuwen FW. Imaging agents for the chemokine receptor 4 (CXCR4). Chem Soc Rev 2012; 41:5239-61.
131. Jacobson O, Weiss ID, Szajek L, Farber JM, Kiesewetter DO. $^{64}$Cu-AMD3100-a novel imaging agent for targeting chemokine receptor CXCR4. Bioorg Med Chem 2009; 17:1486-93.
132. Nimmagadda S, Pullambhatla M, Stone K, Green G, Bhujwalla ZM, Pomper MG. Molecular imaging of CXCR4 receptor expression in human cancer xenografts with [$^{64}$Cu]AMD3100 positron emission tomography. Cancer Res 2010; 70:3935-44.
133. Weiss ID, Jacobson O, Kiesewetter DO, Jacobus JP, Szajek LP, Chen X, et al. Positron emission tomography imaging of tumors expressing the human chemokine receptor CXCR4 in mice with the use of $^{64}$Cu-AMD3100. Mol Imaging Biol 2012; 14:106-14.
134. Jacobson O, Weiss ID, Kiesewetter DO, Farber JM, Chen X. PET of tumor CXCR4 expression with 4-$^{18}$F-T140. J Nucl Med 2010; 51:1796-804.
135. Nimmagadda S, Pullambhatla M, Pomper MG. Immunoimaging of CXCR4 expression in brain tumor xenografts using SPECT/CT. J Nucl Med 2009; 50:1124-30.
136. Pages F, Galon J, Dieu-Nosjean MC, Tartour E, Sautes-Fridman C, Fridman WH. Immune infiltration in human tumors: a prognostic factor that should not be ignored. Oncogene 2010; 29:1093-102.
137. Loi S, Michiels S, Salgado R, Sirtaine N, Jose V, Fumagalli D, et al. Tumor infiltrating lymphocytes (TILs) indicate trastuzumab benefit in early-stage HER2-positive breast cancer (HER2+ BC). Cancer Res 2013; SABCS 2013:S1-05.
138. Denkert C, Loibl S, Salat C, Sinn BV, Schem C, Endris V, et al. Increased tumor-associated lymphocytes predict benefit from addition of carboplatin to neoadjuvant therapy for triple-negative and HER2-positive early breast cancer in the GeparSixto trial (GBG 66). Cancer Res 2013; SABCS 2013:S1-06.
139. Steding CE, Wu ST, Zhang Y, Jeng MH, Elzey BD, Kao C. The role of interleukin-12 on modulating myeloid-derived suppressor cells, increasing overall survival and reducing metastasis. Immunology 2011; 133:221-38.
140. Dong H, Strome SE, Salomao DR, Tamura H, Hirano F, Flies DB, et al. Tumor-associated B7-H1 promotes T-cell apoptosis: a potential mechanism of immune evasion. Nat Med 2002; 8:793-800.
141. Keir ME, Butte MJ, Freeman GJ, Sharpe AH. PD-1 and its ligands in tolerance and immunity. Annu Rev Immunol 2008; 26:677-704.
142. Stagg J, Loi S, Divisekera U, Ngiow SF, Duret H, Yagita H, et al. Anti-ErbB-2 mAb therapy requires type I and II interferons and synergizes with anti-PD-1 or anti-CD137 mAb therapy. Proc Natl Acad Sci U S A 2011; 108:7142-7.
143. Ghebeh H, Mohammed S, Al-Omair A, Qattan A, Lehe C, Al-Qudaihi G, et al. The B7-H1 (PD-L1) T lymphocyte-inhibitory molecule is expressed in breast cancer patients with infiltrating ductal carcinoma: correlation with important high-risk prognostic factors. Neoplasia 2006; 8:190-8.
144. Muenst S, Soysal SD, Gao F, Obermann EC, Oertli D, Gillanders WE. The presence of programmed death 1 (PD-1)-positive tumor-infiltrating lymphocytes is associated with poor prognosis in human breast cancer. Breast Cancer Res Treat 2013; 139:667-76.
145. Leach DR, Krummel F, Allison JP. Enhancement of antitumor immunity by CTLA-4 blockade. Science. 1996; 271:1734 -6.
146. Mao H, Zhang L, Yang Y, Zuo W, Bi Y, Gao W, et al. New Insights of CTLA-4 into Its Biological Function in Breast Cancer. Curr Cancer Drug Targets 2010; 10:728-36.
147. DeNardo DG, Brennan DJ, Rexhepaj E, Ruffell B, Shiao SL, Madden SF, et al. Leukocyte complexity predicts breast cancer survival and functionally regulates response to chemotherapy. Cancer Discov 2011; 1:54-67.
148. Bekaii-Saab TS, Roda JM, Guenterberg KD, Ramaswamy B, Young DC, Ferketich AK, et al. A phase I trial of paclitaxel and trastuzumab in combination with interleukin-12 in patients with HER2/neu-expressing malignancies. Mol Cancer Ther 2009; 8:2983-91.
149. Brahmer JR, Tykodi SS, Chow LQ, Hwu WJ, Topalian SL, Hwu P, et al. Safety and activity of anti-PD-L1 antibody in patients with advanced cancer. N Engl J Med 2012; 366:2455-65.
150. Grosso J, Horak CE, Inzunza D, Cardona DM, Simon JS, Kumar Gupta A, et al. Association of tumor PD-L1 expression and immune biomarkers with clinical activity in patients (pts) with advanced solid tumors treated with nivolumab (anti-PD-1; BMS-936558; ONO-4538). J Clin Oncol 2013; 31(suppl; abstr 3016).
151. Herbst RS, Gordon MS, Fine GD, Sosman JA, Soria J, Hamid O, et al. A study of MPDL3280A, an engineered PD-L1 antibody in patients with locally advanced or metastatic tumors. J Clin Oncol 2013; 31(suppl; abstr 3000).
152. Gianni L, Bianchini G, Valagussa P, Belousov A, Thomas M, Ross G, et al. Adaptive immune system and immune checkpoints are associated with response to pertuzumab (P) and trastuzumab (H) in the NeoSphere study. Cancer Res 2012; 72:Abstract nr S6-7.

153. Vonderheide RH, LoRusso PM, Khalil M, Gartner EM, Khaira D, Soulieres D, et al. Tremelimumab in combination with exemestane in patients with advanced breast cancer and treatment-associated modulation of inducible costimulator expression on patient T cells. Clin Cancer Res 2010; 16:3485-94.
154. Mao Y, Keller ET, Garfield DH, Shen K, Wang J. Stromal cells in tumor microenvironment and breast cancer. Cancer Metastasis Rev 2013; 32:303-15.
155. Folkman J. Angiogenesis: an organizing principle for drug discovery? Nat Rev Drug Discov 2007; 6:273-86.
156. Pollard JW. Macrophages define the invasive microenvironment in breast cancer. J Leukoc Biol 2008; 84:623-30.
157. Viacava P, Naccarato AG, Bocci G, Fanelli G, Aretini P, Lonobile A, et al. Angiogenesis and VEGF expression in pre-invasive lesions of the human breast. J Pathol 2004; 204:140-6.
158. Kim KJ, Li B, Winer J, Armanini M, Gillett N, Phillips HS, et al. Inhibition of vascular endothelial growth factor-induced angiogenesis suppresses tumour growth in vivo. Nature. 1993; 362:841-4.
159. Ferrara N, Hillan KJ, Gerber HP, Novotny W. Discovery and development of bevacizumab, an anti-VEGF antibody for treating cancer. Nat Rev Drug Discov 2004; 3:391-400.
160. Wagner AD, Thomssen C, Haerting J, Unverzagt S. Vascular-endothelial-growth-factor (VEGF) targeting therapies for endocrine refractory or resistant metastatic breast cancer. Cochrane Database Syst Rev 2012; 7:CD008941.
161. Brufsky AM, Hurvitz S, Perez E, Swamy R, Valero V, O'Neill V, et al. RIBBON-2: a randomized, double-blind, placebo-controlled, phase III trial evaluating the efficacy and safety of bevacizumab in combination with chemotherapy for second-line treatment of human epidermal growth factor receptor 2-negative metastatic breast cancer. J Clin Oncol 2011; 29:4286-93.
162. Brufsky A, Valero V, Tiangco B, Dakhil S, Brize A, Rugo HS, et al. Second-line bevacizumab-containing therapy in patients with triple-negative breast cancer: subgroup analysis of the RIBBON-2 trial. Breast Cancer Res Treat 2012; 133:1067-75.
163. Cameron D, Brown J, Dent R, Jackisch C, Mackey J, Pivot X, et al. Primary results of BEATRICE, a randomized phase III trial evaluating adjuvant bevacizumab-containing therapy in triple-negative breast cancer. Cancer Res 2012; 72:Abstract nr S6-5.
164. Martin M, Loibl S, von Minckwitz G, Morales S, Crespo C, Anton A, et al. Phase III trial evaluating the addition of bevacizumab to endocrine therapy as first-line treatment for advanced breast cancer – First efficacy results from the LEA study. Cancer Res 2012; 72:Abstract nr S1-7.
165. Gianni L, Romieu GH, Lichinitser M, Serrano SV, Mansutti M, Pivot X, et al. AVEREL: A randomized phase III trial evaluating bevacizumab in combination with docetaxel and trastuzumab as first-line therapy for HER2-positive locally recurrent/metastatic breast cancer. J Clin Oncol 2013; 31:1719-25.
166. Barrios CH, Liu MC, Lee SC, Vanlemmens L, Ferrero JM, Tabei T, et al. Phase III randomized trial of sunitinib versus capecitabine in patients with previously treated HER2-negative advanced breast cancer. Breast Cancer Res Treat 2010; 121:121-31.
167. Bergh J, Bondarenko IM, Lichinitser MR, Liljegren A, Greil R, Voytko NL, et al. First-line treatment of advanced breast cancer with sunitinib in combination with docetaxel versus docetaxel alone: results of a prospective, randomized phase III study. J Clin Oncol 2012; 30:921-9.
168. Burstein HJ, Chen YH, Parker LM, Savoie J, Younger J, Kuter I, et al. VEGF as a marker for outcome among advanced breast cancer patients receiving anti-VEGF therapy with bevacizumab and vinorelbine chemotherapy. Clin Cancer Res 2008; 14:7871-7.
169. Baar J, Silverman P, Lyons J, Fu P, Abdul-Karim F, Ziats N, et al. A vasculature-targeting regimen of preoperative docetaxel with or without bevacizumab for locally advanced breast cancer: impact on angiogenic biomarkers. Clin Cancer Res 2009; 15:3583-90.
170. Ramaswamy B, Elias AD, Kelbick NT, Dodley A, Morrow M, Hauger M, et al. Phase II trial of bevacizumab in combination with weekly docetaxel in metastatic breast cancer patients. Clin Cancer Res 2006; 12:3124-9.
171. Ferrara N. Binding to the extracellular matrix and proteolytic processing: two key mechanisms regulating vascular endothelial growth factor action. Mol Biol Cell 2010; 21:687-90.
172. Nagengast WB, de Korte MA, Oude Munnink TH, Timmer-Bosscha H, den Dunnen WF, Hollema H, et al. $^{89}$Zr-bevacizumab PET of early antiangiogenic tumor response to treatment with HSP90 inhibitor NVP-AUY922. J Nucl Med 2010; 51:761-7.
173. Nagengast WB, de Vries EG, Hospers GA, Mulder NH, de Jong JR, Hollema H, et al. In vivo VEGF imaging with radiolabeled bevacizumab in a human ovarian tumor xenograft. J Nucl Med 2007; 48:1313-9.
174. Gaykema SB, Brouwers AH, Lub-de Hooge MN, Pleijhuis RG, Timmer-Bosscha H, Pot L, et al. $^{89}$Zr-Bevacizumab PET Imaging in primary breast cancer. J Nucl Med 2013; 54:1014-8.
175. Oosting S, Brouwers AH, Van Es SC, Nagengast WB, Oude Munnink TH, Lub-de Hooge MN, et al. $^{89}$Zr-bevacizumab PET imaging in metastatic renal cell carcinoma patients before and during antiangiogenic treatment. J Clin Oncol 2012; 30:suppl; abstr 10581.

176. Hynes RO. Integrins: bidirectional, allosteric signaling machines. Cell 2002; 110:673-87.
177. Liotta LA, Tryggvason K, Garbisa S, Hart I, Foltz CM, Shafie S. Metastatic potential correlates with enzymatic degradation of basement membrane collagen. Nature. 1980; 284:67-8.
178. Stetler-Stevenson WG. Progelatinase A activation during tumor cell invasion. Invasion Metastasis. 1994; 14:259-68.
179. Chabottaux V, Noel A. Breast cancer progression: insights into multifaceted matrix metalloproteinases. Clin Exp Metastasis 2007; 24:647-56.
180. Manegold C, Vansteenkiste J, Cardenal F, Schuette W, Woll PJ, Ulsperger E, et al. Randomized phase II study of three doses of the integrin inhibitor cilengitide versus docetaxel as second-line treatment for patients with advanced non-small-cell lung cancer. Invest New Drugs 2013; 31:175-82.
181. Ricart AD, Tolcher AW, Liu G, Holen K, Schwartz G, Albertini M, et al. Volociximab, a chimeric monoclonal antibody that specifically binds α5β1 integrin: a phase I, pharmacokinetic, and biological correlative study. Clin Cancer Res 2008; 14:7924-9.
182. Zucker S, Cao J, Chen WT. Critical appraisal of the use of matrix metalloproteinase inhibitors in cancer treatment. Oncogene 2000; 19:6642-50.
183. Overall CM, Lopez-Otin C. Strategies for MMP inhibition in cancer: innovations for the post-trial era. Nat Rev Cancer 2002; 2:657-72.
184. Coussens LM, Fingleton B, Matrisian LM. Matrix metalloproteinase inhibitors and cancer: trials and tribulations. Science 2002; 295:2387-92.
185. Fingleton B. Matrix metalloproteinase inhibitors for cancer therapy:the current situation and future prospects. Expert Opin Ther Targets 2003; 7:385-97.
186. Barker HE, Cox TR, Erler JT. The rationale for targeting the LOX family in cancer. Nat Rev Cancer 2012; 12:540-52.
187. Curtis C, Shah SP, Chin SF, Turashvili G, Rueda OM, Dunning MJ, et al. The genomic and transcriptomic architecture of 2,000 breast tumours reveals novel subgroups. Nature 2012; 486:346-52.
188. van Kruchten M, de Vries EG, Brown M, de Vries EF, Glaudemans AW, Dierckx RA, et al. PET imaging of oestrogen receptors in patients with breast cancer. Lancet Oncol 2013; 14:e465-75.
189. Topalian SL, Hodi FS, Brahmer JR, Gettinger SN, Smith DC, McDermott DF, et al. Safety, activity, and immune correlates of anti-PD-1 antibody in cancer. N Engl J Med 2012; 366:2443-54.

# CHAPTER 5

# $^{111}$In-trastuzumab scintigraphy in HER2 positive metastatic breast cancer patients remains feasible during trastuzumab treatment

S.B.M. Gaykema[1]
J.R. de Jong[2]
P.J. Perik[1]
A.H. Brouwers[2]
C.P. Schröder[1]
T.H. Oude Munnink[1]
A.H.H. Bongaerts[3]
E.G.E. de Vries[1]
M.N. Lub-de Hooge[2,4]

Departments of Medical Oncology[1], Nuclear Medicine and Molecular Imaging[2], Radiology[3] and Hospital Pharmacy [4], University Medical Center Groningen, University of Groningen, The Netherlands

*Molecular Imaging and Biology 2014; 13: 1-6*

# Abstract

**Purpose:** Human epidermal growth factor receptor (HER)2 imaging with radiolabeled trastuzumab might support HER2 targeted therapy. It is however frequently questioned whether HER2 imaging is also possible during trastuzumab treatment as the receptor might be saturated. Here, we studied the effect of trastuzumab treatment on $^{111}$In-trastuzumab uptake.

**Procedures:** Patients received trastuzumab weekly and paclitaxel 3-weekly. $^{111}$In-trastuzumab was injected on day 1 of cycle 1 and day 15 of cycle 4. Whole-body planar scintigraphy was acquired on different time points post injection. Tumor uptake and organ distribution between first and repeated scan series were calculated via residence times.

**Results:** 25 tumor lesions in 12 patients were visualized on both scintigraphy series. Tumor uptake decreased (19.6%; $P = 0.03$). Residence times of normal organs remained similar, except the cardiac blood pool (+16.3%; $P = 0.014$).

**Conclusion:** Trastuzumab treatment decreases tumor $^{111}$In-trastuzumab uptake around 20%, leaving enough uptake for HER2 imaging during trastuzumab treatment.

# Introduction

Tumor overexpression or amplification of the human epidermal growth factor receptor (HER)2 occurs in 25% to 30% of patients with breast cancer and is involved in tumor cell survival, proliferation, maturation, dissemination and angiogenesis, and has anti-apoptotic effects[1,2]. Trastuzumab is a humanized monoclonal antibody approved for treatment in the (neo)adjuvant and metastatic setting of patients with HER2 positive breast cancer. Addition of trastuzumab to chemotherapy results in an increased time to disease progression, higher objective response rates, and longer overall survival[3,4]. Accurate characterization of HER2 expression is essential for optimal therapy. Therefore, the HER2 status should be assessed in all patients with breast cancer to identify HER2 positive tumors. Ex vivo methods to determine the HER2 status of the primary tumor are immunohistochemistry (IHC) and fluorescence in-situ hybridization (FISH). These methods require biopsies which are not always feasible. Furthermore, sampling error cannot be ruled out with repeated biopsies. This is particularly relevant in view of possible heterogeneous HER2 expression. Heterogeneity can exist between the primary tumor and the metastases[5], between different metastases and within a metastasis. Discordance of HER2 expression between primary tumors and metastases, as measured by IHC and/or FISH, varies between 10-24%[6,7]. Loss or gain of HER2 expression can have clear therapeutic consequences, as patients with HER2 positive lesions benefit from anti-HER2 therapy[3,8]. This underlines the necessity to accurately assess HER2 status during the course of metastatic breast cancer. Non-invasive determination of HER2 expression can potentially be performed with molecular imaging. This might facilitate selection of patients for HER2 targeted therapy and assess the immediate response to therapeutic interventions. In the clinical setting HER2 imaging may be performed with trastuzumab radiolabelled with the γ-emitter indium-111 ($^{111}$In) and with the positron emission tomography (PET) isotope zirconium-89 ($^{89}$Zr)[9,10]. Experience with HER2 imaging increases, however this comes with the frequently asked question whether and how trastuzumab treatment affects the HER2 scan as the receptor may be already occupied. We previously reported about $^{111}$In-trastuzumab scintigraphy in 17 patients with HER2 over-expressing metastatic breast cancer after the first loading dose of trastuzumab[9]. Part of these patients underwent a second scintigraphy procedure during treatment. This gives us the unique opportunity to assess the feasibility of HER2 imaging in patients while on trastuzumab treatment.

Therefore, the aim of this study is to quantitatively describe the biodistribution and uptake of $^{111}$In-trastuzumab over time during 14 weeks of trastuzumab treatment.

# Methods

## Patients and Treatment

Eligibility criteria were described earlier[9]. In short, included patients were women with histological confirmed HER2 positive metastatic breast cancer eligible for treatment with paclitaxel and trastuzumab. After the loading dose of 4 mg/kg, trastuzumab was administered as a weekly intravenous infusion of 2 mg/kg. Paclitaxel (175 mg/m$^2$) was administered intravenously in 4 hours as an intravenous infusion, once every 3 weeks for 6 cycles. The study was approved by the local medical ethical committee. All patients provided written informed consent.

## $^{111}$In-trastuzumab Scintigraphy

Trastuzumab was radiolabelled with indium-111 ($^{111}$In), using as described previously[11]. A total of 100 - 150 MBq 5 mg $^{111}$In-trastuzumab was injected intravenously, within 24 hours after the infusion of the trastuzumab loading dose at baseline. $^{111}$In-trastuzumab injection was repeated after the trastuzumab dose on day 15 of the fourth cycle (14 weeks later). Whole body planar scintigraphy was performed at 4 different time points at 15 minutes, 24, 72 - 96 and 168 hours post injection (Figure 1). A dual-head Multispect-2 camera or dual-head E.Cam camera was used (Siemens, CTI, Knoxville, TN) as previous described[9]. Scintigraphy series for each patient series were performed on the same camera. Only patients with a first and repeated scintigraphy series were analyzed. For quality control of dosimetry calculations an aliquot of dose containing a known fraction of the injected radioactivity was positioned adjacent to the patient during scanning.

## $^{111}$In-trastuzumab Tumor Uptake, Organ Distribution and Radiation Dosimetry

The uptake of $^{111}$In-trastuzumab was determined by calculating residence times for tumors and organs. Residence time was defined as the area under the curve of radioactivity versus time (time-activity curve) and was calculated using the SPRIND software package[12]. The set of organs for which the residence times were calculated was limited to those organs that were clearly distinguishable on the planar scintigraphy. The residence time was in addition used for internal radiation dose assessment according to the medical internal radiation dose (MIRD) scheme[13]. The radiation absorbed dose for all organs of interest as well as the effective dose was determined in accordance with the International Commission on Radiological Protection publication 60 (ICRP-60)[14]. The estimated dose (ED) was calculated as a weighted mean of the absorbed radiation dose over organs defined within the ICRP framework. Organ level internal radiation dose calculations using the MIRD and ICRP-60 are implemented in the OLINDA/EXM software package[15]. OLINDA/EXM incorporates a set of phantoms (adult male, adult female etc) that define the size of organs and the geometric relation between them. This determines the contribution from radioactivity in one organ to the absorbed dose in another organ. The quantitative results of the scintigraphy series were statistically tested for difference between the first and repeated scintigraphy series.

**Figure 1.** $^{111}$In-trastuzumab scintigraphy at first and repeated scintigraphy series during treatment.

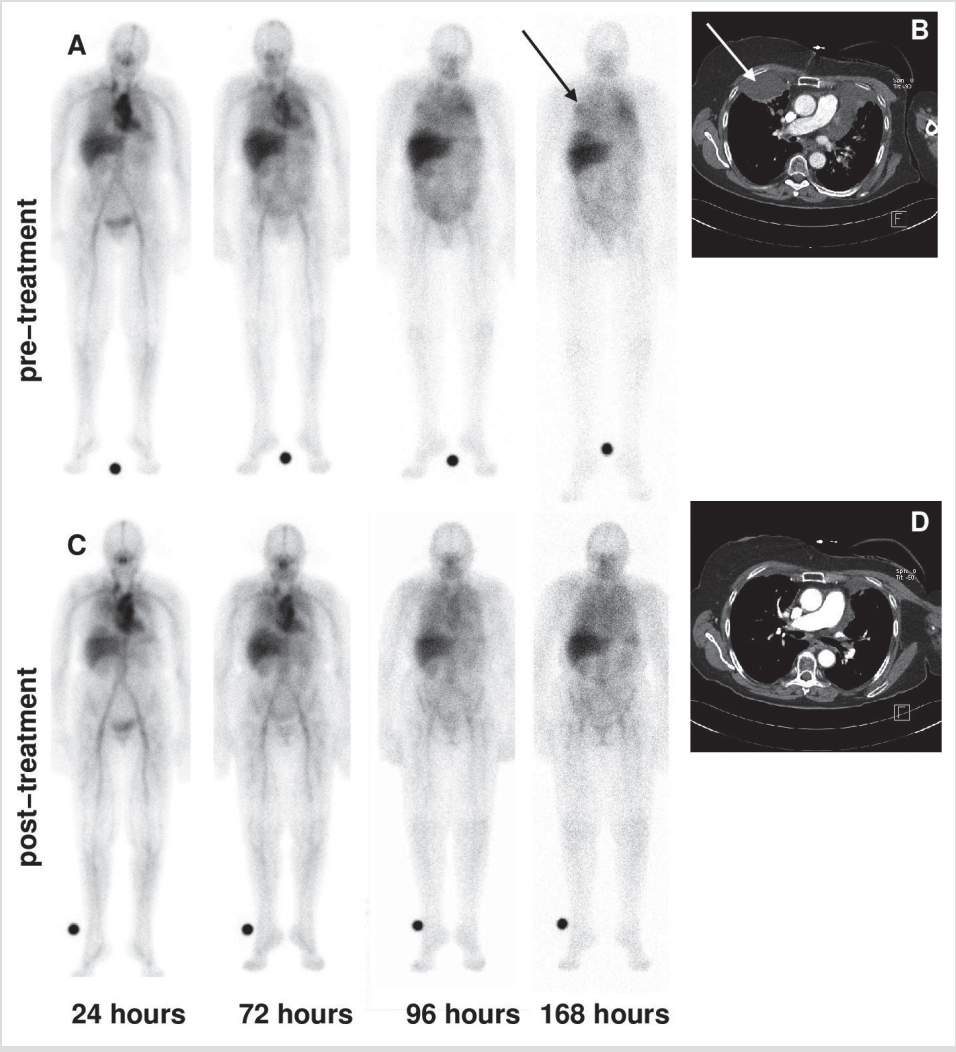


$^{111}$In-trastuzumab scintigraphy at 24, 72, 96, and 168 hours postinjection in the first (A) and repeated (C) scan series. The pleural lesion on computed tomography (indicated with an *arrow*) pretreatment (B) is almost completely disappeared after treatment (D).

## Statistical Analysis

Data are presented as mean ± standard deviation (SD). Statistical analysis was performed using the Wilcoxon test for paired non-parametric data (SPSS, version 19, IBM). A double sided *P*-value < 0.05 was considered significant.

# Results

## Patient Characteristics

Seventeen patients were included between January 2002 and June 2004. In 12 patients, serial analyses of tumor uptake, organ absorbed dose and radiation dosimetry, determined from $^{111}$In-trastuzumab scintigraphy on first and second scintigraphy series could be assessed. In the remaining five patients, three were withdrawn from the study prematurely due to clinical deterioration and/or disease progression, and in two patients the scintigraphy series were incomplete.

## $^{111}$In-trastuzumab Tumor Uptake

In these 12 patients, all in total 25 tumor lesions were detected on $^{111}$In-trastuzumab scintigraphy at first and repeated scintigraphy series during treatment (See Figure 2 for an example). In 20 of the 25 tumor lesions the $^{111}$In-trastuzumab uptake was decreased at the repeated compared to first scintigraphy series. Mean residence time in tumor lesions was 0.22 ± 0.30 (0.04-1.26) at baseline, and 0.14 ± 0.17 (0.02-0.79) after 12 weekly therapeutic trastuzumab doses. Between first and repeated scintigraphy series, there was a mean reduction in $^{111}$In-trastuzumab uptake per lesion of 19.6% ± 53.8 (range increase of 72.9 to decrease of 188.5%; $P = 0.003$). The mean reduction per patient was 17.0% ± 35.0 ($P = 0.07$).

## $^{111}$In-trastuzumab Organ Distribution and Radiation Dosimetry

The residence times of healthy organs remained the same between first and repeated scintigraphy series, except for an increase in the cardiac blood pool ($P = 0.014$) (Table 1). The absorbed dose for the organs and the effective dose thus also remained similar. The effective dose of $^{111}$In-trastuzumab was 0.19 ± 0.02 mSv/MBq. The three organs with the highest absorbed dose were liver (0.60 ± 0.18 mGy/MBq), spleen (0.36 ± 0.08 mGy/MBq) and heart wall (0.34 ± 0.05 mGy/MBq). The three organs with the highest contribution to the effective dose were liver (0.030 ± 0.009 mSv/MBq), lungs (0.035 ± 0.007/mSv MBq) and ovaries (0.032 ± 0.004 mSv/MBq) (Table 2).

**Table 1.** Residence times and standard deviations of measured organs.

| Organ | Residence time (hours) *t* = first | Residence time (hours) *t* = second/repeated |
|---|---|---|
| Blood pool | 2.39 ± 0.71 | 2.78 ± 0.71 |
| Kidney | 0.86 ± 0.30 | 0.86 ± 0.31 |
| Liver | 12.96 ± 5.15 | 11.13 ± 4.29 |
| Lung | 3.26 ± 1.09 | 3.36 ± 1.25 |
| Spleen | 0.91 ± 0.33 | 0.92 ± 0.27 |
| Red marrow | 0.78 ± 0.19 | 0.90 ± 0.22 |

**Figure 2.** $^{111}$In-trastuzumab scintigraphy at first and repeated scintigraphy series during treatment.

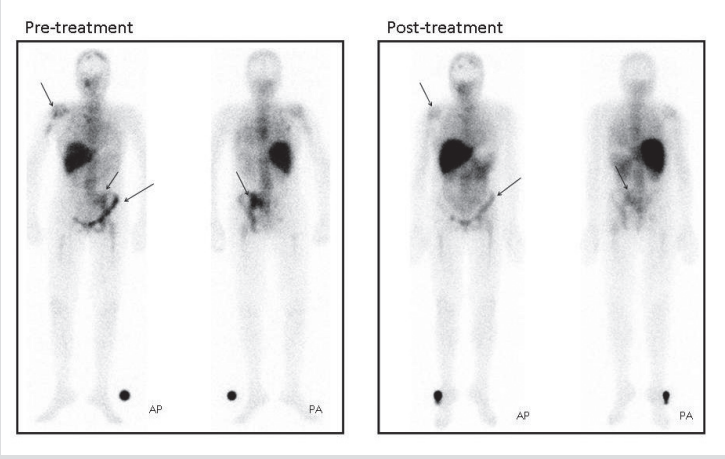


$^{111}$In-trastuzumab scintigraphy in a patient with multiple bone lesions at the first and repeated scan series.



**Table 2.** Radiation absorbed dose estimates for organs and effective dose contribution of ICRP 60 target organs on the first scan series.

| Organ | Radiation absorbed dose (μGy/MBq) ± SD | ICRP 60 Effective dose contribution (μSv/MBq) ± SD |
|---|---|---|
| Adrenal gland | 230 ± 17 | 1.1 ± 0.2 |
| Brain | 106 ± 16 | 0.5 ± 0.1 |
| Breast | 115 ± 12 | 5.7 ± 0.6 |
| Gallbladder wall | 277 ± 37 | * |
| Lower colon wall | 152 ± 21 | 18.3 ± 2.6 |
| Small intestine | 156 ± 16 | 0.7 ± 0.1 |
| Stomach wall | 181 ± 16 | 21.8 ± 1.9 |
| Upper colon wall | 180 ± 15 | 0.9 ± 0.2 |
| Heart wall | 339 ± 49 | * |
| Kidney | 268 ± 42 | 1.3 ± 0.3 |
| Liver | 598 ± 183 | 29.9 ± 9.1 |
| Lung | 291 ± 54 | 34.9 ± 6.5 |
| Muscle | 131 ± 14 | 0.6 ± 0.1 |
| Ovary | 158 ± 21 | 31.7 ± 4.1 |
| Pancreas | 238 ± 17 | 1.1 ± 0.2 |
| Red marrow | 132 ± 15 | 15.8 ± 1.8 |
| Skin | 84 ± 10 | 0.8 ± 0.1 |
| Spleen | 360 ± 78 | 2.8 ± 3.2 |
| Thymus | 167 ± 21 | 0.8 ± 0.2 |
| Thyroid | 117 ± 17 | 5.8 ± 0.8 |
| Urinary bladder wall | 140 ± 20 | 7.0 ± 1.0 |
| Uterus | 156 ± 21 | 0.7 ± 0.1 |
| Total Body | 151 ± 13 | * |
| Effective dose | * | 185 ± 16 |

* Not defined

# Discussion and Conclusions

This is the first study with serial $^{111}$In-trastuzumab scintigraphy at the start and during trastuzumab treatment in patients with HER2 positive metastatic breast cancer. It showed persistent $^{111}$In-trastuzumab uptake in all tumor lesions during trastuzumab treatment, with only a 20% lower absolute uptake after 12 weeks of trastuzumab treatment. This indicates that sufficient HER2 is constantly available at the tumor cell membrane to bind trastuzumab and that it is impossible to completely saturate the receptor. Furthermore this is the first study to present radiation dosimetry data for $^{111}$In-trastuzumab.

There are several potential explanations contributing for the 19.6 % lower $^{111}$In-trastuzumab uptake during trastuzumab treatment. It may be the consequence of the antitumor effect of paclitaxel and trastuzumab on the size of the tumor lesion or on HER2 expression itself. Unfortunately, rigorous evaluation of size effects of all tumor lesions was not possible. Specific for breast cancer is the fact that most metastases are located in the bones which are not included in RECIST. Also no serial biopsies were taken so down regulation of HER2 expression could not be assessed. Last important explanation for the lower $^{111}$In-trastuzumab uptake during treatment might be that therapeutic trastuzumab circulating in the blood competes with $^{111}$In-trastuzumab for binding to HER2. Of the normal organs, only the cardiac blood pool showed a 16% higher uptake of $^{111}$In-trastuzumab after the second injection during treatment. This can be explained by the fact that trastuzumab elimination half-life is dose-dependent, after multiple trastuzumab doses half-life time increases[16]. However, we showed that tumor lesions could still be clearly visualized under trastuzumab treatment. Thus, we conclude that there is no complete down regulation or saturation of the HER2. Preferably this would be confirmed with HER2 staining of tumor tissue in future clinical studies. There are however preclinical data available. Preclinical evaluation of change of HER2 status on trastuzumab therapy with molecular imaging was performed previously in two studies with a human breast cancer xenograft. Micro-SPECT with $^{111}$In-pertuzumab and $^{18}$F-FBEM-$_{HER2:243}$ were performed pre-and post trastuzumab treatment in mice bearing human tumor xenografts. Uptake of the tracers was decreased, but not completely blocked, after 3 weeks of treatment, which corresponded with changes in tumor size[17-18]. Distinct from our study, there was no competition between the tracer and the therapeutic agent in these studies, because both tracers bind to another domain of HER2 than trastuzumab. Thus, extrapolating to our study results, we conclude that during trastuzumab treatment visualization of tumor lesions with $^{111}$In-trastuzumab is feasible and not completely blocked or saturated, despite this competition of the (subtherapeutic amount of) radiolabelled trastuzumab with therapeutic trastuzumab.

In a human HER2 overexpressing SKOV-3 ovarian tumor xenograft there was higher uptake of $^{111}$In-trastuzumab compared to a HER2 negative tumor xenograft[11] indicating tumor specific uptake.

As no significant differences in organ distribution were found radiation absorbed dose of organs between the two scintigraphy series is comparable. Radiation dose estimates with $^{111}$In-trastuzumab were comparable to those calculated by others[19]. Trastuzumab can also be radiolabelled with a positron emission tomography (PET) isotope copper-64 (NCT01093612) or zirconium-89 ($^{89}$Zr) for clinical purposes. PET provides a higher spatial resolution a better signal to noise ratio and better quantification. No dosimetric results for $^{89}$Zr-trastuzumab have been published so far. However, as the physical half-lives of $^{111}$In and $^{89}$Zr are comparable, the data for $^{111}$In-trastuzumab can be used to estimate the ED for $^{89}$Zr-trastuzumab, resulting in an ED of 0.5 mSv/MBq $^{89}$Zr. For a typical administration of 37 MBq of $^{89}$Zr-trastuzumab, the radiation dose amounts to 18 mSv, which is comparable to the radiation dose of 100 MBq $^{111}$In.



We realize that this study has several shortcomings, mainly because it was originally not intended and powered to look at tumor size and HER2 expression over time. However while experience with molecular HER2 imaging is expanding, we wondered whether trastuzumab treatment affects imaging. The fact that this study showed that all tumor lesions remained visible during treatment, means that HER2 imaging is feasible even during trastuzumab treatment.

# References


1. Slamon DJ, Clark GM, Wong SG, Levin WJ, Ullrich A, McGuire WL. Human breast cancer: correlation of relapse and survival with amplification of the HER-2/neu oncogene. Science 1987; 235:177-182.
2. Masood S, Bui MM. Prognostic and predictive value of HER2/neu oncogene in breast cancer. Microsc.Res.Tech 2002; 59:102-108.
3. Slamon DJ, Leyland-Jones B, Shak S et al. Use of chemotherapy plus a monoclonal antibody against HER2 for metastatic breast cancer that overexpresses HER2. N.Engl.J.Med 2001; 344:783-792.
4. Cobleigh MA, Vogel CL, Tripathy D et al. Multinational study of the efficacy and safety of humanized anti-HER2 monoclonal antibody in women who have HER2-overexpressing metastatic breast cancer that has progressed after chemotherapy for metastatic disease. J.Clin.Oncol 1991; 17:2639-2648.
5. Tanchiu E, Kaufman PA, Paik S et al. registHER: A prospective, longitudinal cohort study of women with HER2 positive metastatic breast cancer. J Clin Oncol 2005; (Meeting Abstracts) 23:670.
6. Niikura N, Liu J, Hayashi N et al. Loss of human epidermal growth factor receptor 2 (HER2) expression in metastatic sites of HER2-overexpressing primary breast tumors. J.Clin.Oncol 2012; 30:593-599.
7. Amir E, Miller N, Geddie W et al. Prospective study evaluating the impact of tissue confirmation of metastatic disease in patients with breast cancer. J.Clin.Oncol; 2012. 30:587-592.
8. Piccart-Gebhart MJ, Procter M, Leyland-Jones B et al. Trastuzumab after adjuvant chemotherapy in HER2-positive breast cancer. N.Engl.J.Med; 2005. 353:1659-1672.
9. Perik PJ, Lub-De Hooge MN, Gietema JA et al. Indium-111-labeled trastuzumab scintigraphy in patients with human epidermal growth factor receptor 2-positive metastatic breast cancer. J.Clin.Oncol; 2006 24:2276-2282.
10. Dijkers EC, Oude Munnink TH, Kosterink JG et al. Biodistribution of $^{89}$Zr-trastuzumab and PET imaging of HER2-positive lesions in patients with metastatic breast cancer. Clin.Pharmacol.Ther; 2010. 87:586-592
11. Lub-de Hooge MN, Kosterink JG, Perik PJ et al. Preclinical characterisation of $^{111}$In-DTPA-trastuzumab. Br.J.Pharmacol; 2004. 143:99-106.
12. Visser E, Postema E, Boerman O, Visschers J, Oyen W, Corstens F. Software package for integrated data processing for internal dose assessment in nuclear medicine (SPRIND). Eur.J.Nucl.Med.Mol.Imaging 2006; 34:413-421.
13. Howell RW, Wessels BW, Loevinger R et al. The MIRD perspective 1999. Medical Internal Radiation Dose Committee. J.Nucl.Med 1999; 40:3S-10S.
14. Anonymous 1990 Recommendations of the International Commission on Radiological Protection. Ann.ICRP 1991; 21:1-201.
15. Stabin MG, Sparks RB, Crowe E. OLINDA/EXM: the second-generation personal computer software for internal dose assessment in nuclear medicine. J.Nucl.Med 2005; 46:1023-1027.
16. Bruno R, Washington CB, Lu JF, Lieberman G, Banken L, Klein P (2005) Population pharmacokinetics of trastuzumab in patients with HER2+ metastatic breast cancer. Cancer Chemother.Pharmacol. 56:361-369.
17. McLarty K, Cornelissen B, Cai Z et al. Micro-SPECT/CT with 111In-DTPA-pertuzumab sensitively detects trastuzumab-mediated HER2 downregulation and tumor response in athymic mice bearing MDA-MB-361 human breast cancer xenografts. J.Nucl.Med 2009; 50:1340-1348.
18. Kramer-Marek G, Gijsen M, Kiesewetter DO et al. Potential of PET to predict the response to trastuzumab treatment in an ErbB2-positive human xenograft tumor model. J.Nucl.Med 2012; 53:629-637.
19. Wong JY, Raubitschek A, Yamauchi D et al. A pretherapy biodistribution and dosimetry study of indium-111-radiolabeled trastuzumab in patients with human epidermal growth factor receptor 2-overexpressing breast cancer. Cancer Biother.Radiopharm 2010; 25:387-394.

# CHAPTER 5B

# $^{89}$Zr-trastuzumab PET as a tool to solve a clinical dilemma in a breast cancer patient

S.B.M. Gaykema[1]
A.H. Brouwers[2]
S. Hovenga[3]
M.N. Lub-de Hooge[2,4]
E.G.E. de Vries[1]
C.P. Schröder[1]

Departments of Medical Oncology[1], Nuclear Medicine and Molecular Imaging[2] and Hospital Pharmacy[4], University Medical Center Groningen, University of Groningen, The Netherlands and [3]Department of Internal Medicine, Nij Smellinghe Hospital Drachten, The Netherlands

*Journal of Clinical Oncology 2012; 30:e74-5*

# Case Report

A 34 year old woman was diagnosed with two right-sided primary breast cancers. One tumor was 10 cm in diameter, histological grade 3 and negative for estrogen receptor (ER), progesterone receptor (PgR) and human epidermal growth factor receptor 2 (HER2), while the other tumor was 6.5 cm in diameter, grade 3 and ER positive, PgR negative and HER2 positive. Standard work-up revealed no metastases. Her primary treatment consisted of right sided mastectomy with axillary lymph node dissection. This dissection showed tumor involvement in 11 out of 14 lymph nodes. Adjuvant treatment consisted of doxorubicin and cyclophosphamide followed by trastuzumab combined with paclitaxel. Thereafter trastuzumab monotherapy was continued for one year. Chemotherapy was followed by tamoxifen and leuprorelin.

Two years since diagnosis, during routine check-up, serum CA15.3 level was elevated (70 kU/L). Physical exam was unremarkable. Dissemination analysis showed on computed tomography (CT) scan a large mediastinal mass and a small liver lesion, while no lesions were present on the bone scan. To determine which primary tumor had metastasized, a biopsy of the liver lesion was performed, which showed no tumor cells on histological examination. In order to obtain tissue of the mediastinal lesion, a mediastinoscopy would be required. Therefore the patient was referred to our hospital, to assess the HER2 status of the tumor non-invasively by means of Zirconium-89-trastuzumab ($^{89}$Zr-trastuzumab) positron emitting tomography (PET) imaging. The procedure was carried out as described earlier, with acquisition of the PET images 4 days after intravenous administration of 37 MBq $^{89}$Zr-trastuzumab (protein dose 50 mg)[1]. The PET scan showed uptake in the mediastinal mass, lymph nodes in the neck region level 4 on both sides and level 3 right sided, and sacral spine (Fig 1). No liver lesions were detected.

It was concluded from the $^{89}$Zr-trastuzumab PET, that the metastatic process was HER2 positive. Given the progression during hormonal treatment and the large mediastinal mass tamoxifen treatment was temporarily discontinued and chemotherapy was initiated. The patient received 3 cycles of 5-fluorouracil, epirubicin and cyclophosphamide, followed by 3 cycles paclitaxel and trastuzumab. Thereafter the CT scan showed a partial tumor response and the trastuzumab was continued in combination with the aromatase inhibitor anastrozole.

**Figure 1.**

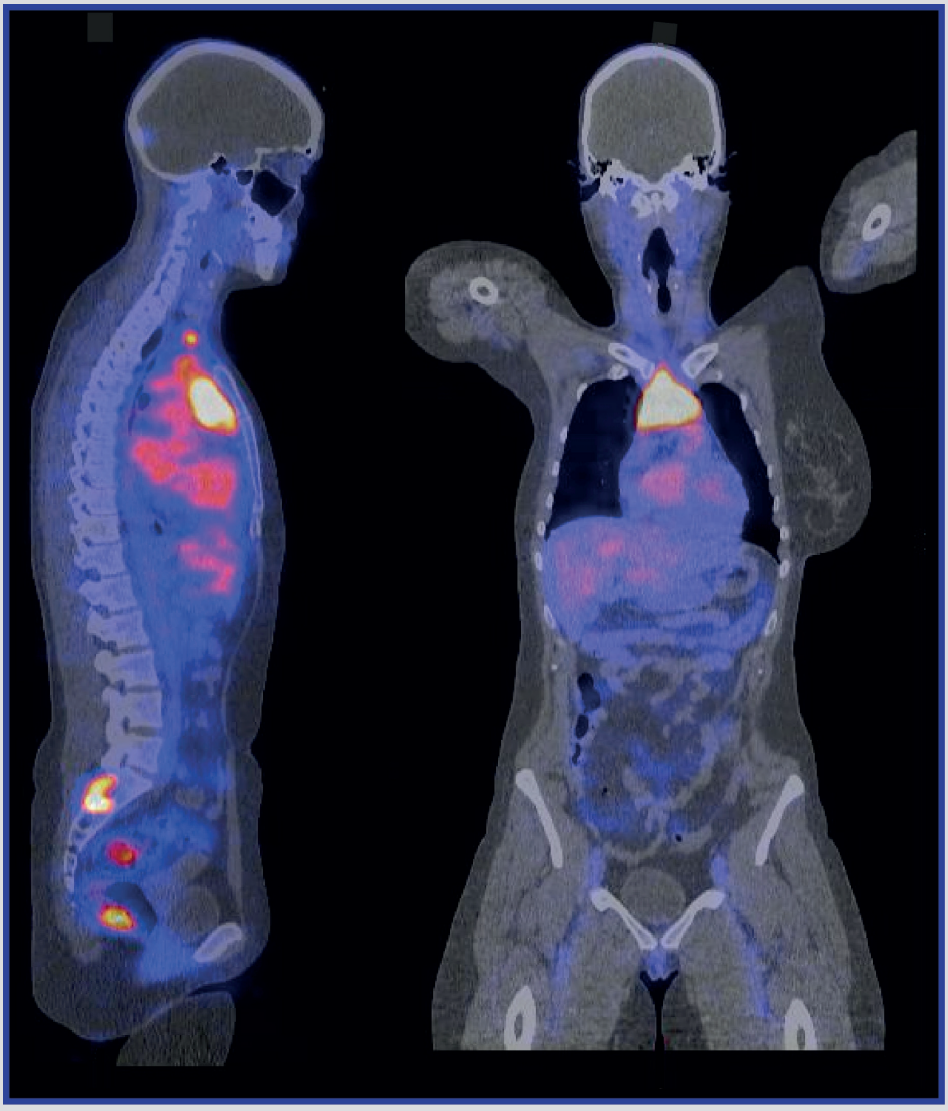

# Discussion

When metastases of breast cancer are suspected, standard work-up consists of a CT scan of the chest and abdomen and a bone scan. In clinical situations in which other staging is equivocal or conflicting, an $^{18}$F-fluordeoxyglucose PET (FDG-PET) should be considered[2,3]. In addition to this regular work-up for a first tumor recurrence, biopsies are recommended to confirm the malignant nature of the lesion, and the presence of ER, PgR and HER2. Although clinical guidelines encourage the use of repeated biopsies during the course of the disease[2,3], in practice, this is not always feasible. Furthermore, sampling error cannot be ruled out with repeated biopsies, which is particularly relevant in view of possible heterogeneous HER2 expression between the primary tumor and the metastases[4], between different metastases and within a metastasis. Discordance of HER2 expression between primary tumors and metastases, as measured by immunohistochemistry (IHC) and/or FISH, varies between 0-33.2%[5-16]. The largest report included 382 paired primary tumors and metastases, which were evaluated by IHC. In this study, a discordant HER2 status was found in 33.2% of paired samples: 23.6% changed from positive to negative while 9.6% changed from negative to positive[16]. Between synchronous tumors, there appears to be a larger degree of concordance than in metachronous tumors. However, even in synchronous tumors a discordant HER2 expression was found in 7 out of 29 patients (24%)[17].

Loss or gain of HER2 expression can have clear therapeutic consequences, as patients with HER2 positive lesions benefit from anti-HER2 therapy[18,19]. Therefore it is of interest to accurately assess HER2 status during the course of metastatic breast cancer, which is possible with a biopsy, but in case of an inaccessible lesion an $^{89}$Zr-trastuzumab PET is of potential interest.

$^{89}$Zr-trastuzumab PET was developed, as a noninvasive whole body visualization strategy to determine HER2 expression and localization of HER2-overexpressing tumor lesions. This includes assessment of the HER2 expression in distant metastases that may not be accessible for biopsy and excludes sampling error. Initially, HER2 imaging was performed with single photon emission computed tomography (SPECT)-tracer Indium-111-trastuzumab in HER2-overexpressing metastatic breast cancer. With this technique, 45% of single tumor lesions, detected with conventional imaging, could be shown. In addition, this approach revealed new tumor lesions not previously identified with conventional staging in 13 out of 15 patients[20]. Since PET imaging provides a higher spatial resolution and a better signal-to-noise ratio than SPECT, and availability of the long-lived positron emitter Zirconium-89 ($^{89}$Zr) with ideal physical characteristics for immuno-PET, allowed to develop the $^{89}$Zr-trastuzumab tracer. We showed that PET scanning using $^{89}$Zr-trastuzumab in addition permitted quantification of HER2 positive tumor lesions in breast cancer patients[1] In a feasibility study, we found that 50 mg $^{89}$Zr-trastuzumab, consisting of 1.5 mg $^{89}$Zr-trastuzumab (37 MBq) replenished with nonradioactive trastuzumab, is a dose for optimal HER2 visualization in trastuzumab-naive patients. Lower trastuzumab doses resulted in rapid excretion by the liver[1].

In the present case, $^{89}$Zr-trastuzumab PET was instrumental for non-invasive assessment of the HER2 status of metastatic breast cancer. The patient was treated for HER2 positive metastatic breast cancer with trastuzumab and paclitaxel, which resulted in a partial response.

The addition of trastuzumab to chemotherapy in HER2 positive metastatic breast cancer patients resulted in an increased time to disease progression, higher objective response rates, and longer overall survival[21,22]. Accurate real-time assessment of HER2 status of metastatic breast cancer can have clear clinical implication for tailored treatment. The present case illustrates that $^{89}$Zr-trastuzumab PET can be helpful when standard work up fails to establish the HER2 status of the metastatic lesions. Therefore, we are currently proceeding to assess the role of $^{89}$Zr-trastuzumab PET in decision making in a prospective multicenter study.

# References


1. Dijkers EC, Oude Munnink TH, Kosterink JG, et al. Biodistribution of 89Zr-trastuzumab and PET imaging of HER2-positive lesions in patients with metastatic breast cancer. Clin Pharmacol Ther 2010; 87:586-592.
2. Cardoso F, Senkus-Konefka E, Fallowfield L, et al. Locally recurrent or metastatic breast cancer: ESMO clinical practice guidelines for diagnosis, treatment and follow-up. Ann Oncol 2010; 21 Suppl 5:v15-9.
3. NCCN clinical practice guidelines in clinical oncology.
4. Tanchiu E, Kaufman PA, Paik S, et al. registHER: A prospective, longitudinal cohort study of women with HER2 positive metastatic breast cancer. J Clin Oncol (Meeting Abstracts) 2005; 23:670.
5. Masood S, Bui MM. Assessment of her-2/neu overexpression in primary breast cancers and their metastatic lesions: An immunohistochemical study. Ann Clin Lab Sci 2000; 30:259-265.
6. Shimizu C, Fukutomi T, Tsuda H, et al. c-erbB-2 protein overexpression and p53 immunoreaction in primary and recurrent breast cancer tissues. J Surg Oncol 2000; 73:17-20.
7. Tanner M, Jarvinen P, Isola J. Amplification of HER-2/neu and topoisomerase IIalpha in primary and metastatic breast cancer. Cancer Res 2001; 61:5345-5348.
8. Gancberg D, Di Leo A, Cardoso F, et al. Comparison of HER-2 status between primary breast cancer and corresponding distant metastatic sites. Ann Oncol 2002; 13:1036-1043.
9. Vincent-Salomon A, Jouve M, Genin P, et al. HER2 status in patients with breast carcinoma is not modified selectively by preoperative chemotherapy and is stable during the metastatic process. Cancer 2002; 94:2169-2173.
10. Edgerton SM, Moore D,2nd, Merkel D, et al. erbB-2 (HER-2) and breast cancer progression. Appl Immunohistochem Mol Morphol 2003; 11:214-221.
11. Regitnig P, Schippinger W, Lindbauer M, et al. Change of HER-2/neu status in a subset of distant metastases from breast carcinomas. J Pathol 2004; 203:918-926.
12. Zidan J, Dashkovsky I, Stayerman C, et al. Comparison of HER-2 overexpression in primary breast cancer and metastatic sites and its effect on biological targeting therapy of metastatic disease. Br J Cancer 2005; 93:552-556.
13. Gong Y, Booser DJ, Sneige N. Comparison of HER-2 status determined by fluorescence in situ hybridization in primary and metastatic breast carcinoma. Cancer 2005; 103:1763-1769.
14. Vincent-Salomon A, Pierga JY, Couturier J, et al. HER2 status of bone marrow micrometastasis and their corresponding primary tumours in a pilot study of 27 cases: A possible tool for anti-HER2 therapy management? Br J Cancer 2007; 96:654-659.
15. Santinelli A, Pisa E, Stramazzotti D, et al. HER-2 status discrepancy between primary breast cancer and metastatic sites. impact on target therapy. Int J Cancer 2008; 122:999-1004.
16. Lower EE, Glass E, Blau R, et al. HER-2/neu expression in primary and metastatic breast cancer. Breast Cancer Res Treat 2009; 113:301-306.
17. Kollias J, Pinder SE, Denley HE, et al. Phenotypic similarities in bilateral breast cancer. Breast Cancer Res Treat 2004; 85:255-261.
18. Slamon DJ, Leyland-Jones B, Shak S, et al. Use of chemotherapy plus a monoclonal antibody against HER2 for metastatic breast cancer that overexpresses HER2. N Engl J Med 2001; 344:783-792.
19. Piccart-Gebhart MJ, Procter M, Leyland-Jones B, et al. Trastuzumab after adjuvant chemotherapy in HER2-positive breast cancer. N Engl J Med 2005; 353:1659-1672.
20. Perik PJ, Lub-De Hooge MN, Gietema JA, et al. Indium-111-labeled trastuzumab scintigraphy in patients with human epidermal growth factor receptor 2-positive metastatic breast cancer. J Clin Oncol 2006; 24:2276-2282.
21. Pietras RJ, Fendly BM, Chazin VR, et al. Antibody to HER-2/neu receptor blocks DNA repair after cisplatin in human breast and ovarian cancer cells. Oncogene 1994; 9:1829-1838.
22. Hudziak RM, Lewis GD, Winget M, et al. p185HER2 monoclonal antibody has antiproliferative effects in vitro and sensitizes human breast tumor cells to tumor necrosis factor. Mol Cell Biol 1989; 9:1165-1172.

# CHAPTER 6

# $^{89}$Zr-bevacizumab PET Imaging in Primary Breast Cancer

S.B.M. Gaykema[1]
A.H. Brouwers[2]
M.N. Lub-de Hooge[2,3]
R.G. Pleijhuis[4]
H. Timmer-Bosscha[1]
L. Pot[1]
G.M. van Dam[4]
S.B. van der Meulen[5]
J.R. de Jong[2]
J. Bart[5]
J. de Vries[4]
L. Jansen[4]
E.G.E. de Vries[1]
C.P. Schröder[1]

Departments of Medical Oncology[1], Nuclear Medicine and Molecular Imaging[2], Hospital and Clinical Pharmacy[3], Surgical Oncology[4], Radiology[5] and Pathology[6] University of Groningen, University Medical Center Groningen, The Netherlands.

*Journal of nuclear medicine 2013; 54: 1014-8*

# Abstract

Vascular endothelial growth factor (VEGF)-A is overexpressed in most (pre)malignant breast lesions. VEGF-A can be visualized non-invasively with positron emission tomography (PET) imaging and using the tracer Zirconium-89 ($^{89}$Zr) labeled bevacizumab. In this clinical feasibility study, we assessed whether VEGF-A in primary breast cancer can be visualized by $^{89}$Zr-bevacizumab PET.

**Methods:** Prior to surgery, breast cancer patients underwent a PET/CT scan of breasts and axillary regions, four days after 37 MBq/5 mg $^{89}$Zr-bevacizumab intravenous administration. PET images were compared with standard imaging modalities. $^{89}$Zr-bevacizumab uptake was quantified as the maximum standard uptake value ($SUV_{max}$). VEGF-A levels in tumor and normal breast tissues were assessed with Enzyme-Linked Immuno Sorbent Assay. Data are presented as mean ± SD.

**Results:** Twenty-five of 26 breast tumors (size: 25.1 mm ± 19.8, range 4-80) in 23 patients were visualized. $SUV_{max}$ was higher in tumors (1.85 ± 1.22, range 0.52-5.64) than in normal breasts (0.59 ± 0.37; range, 0.27-1.69; $P < .001$). The only non-PET-detected tumor was 10 mm in diameter. Lymph node metastases were present in 10 axillary regions; 4 could be detected with PET ($SUV_{max:}$ 2.66 ± 2.03; range, 1.32-5.68). VEGF-A levels in the 17 assessable tumors were higher compared to normal breast tissue in all cases (VEGF-A/mg protein 184 ± 169 pg *v* 10 ± 21 pg; $P = .001$), whereas $^{89}$Zr-bevacizumab tumor uptake correlated with VEGF-A tumor levels (r = 0.49).

**Conclusion:** VEGF-A in primary breast cancer can be visualized by means of $^{89}$Zr-bevacizumab PET

# Introduction

Breast cancer is the most common cause of cancer related deaths among women[1]. The application of molecular imaging can visualize, and potentially quantifies functional differences between tumor and normal cells. A molecular target of interest in this respect is vascular endothelial growth factor (VEGF)-A. VEGF-A is involved in the development and maintenance of tumorangiogenesis and already involved early during tumorigenesis. Various studies have reported overexpression of VEGF-A in breast cancer microenvironment compared to normal breast tissue[2-5]. All VEGF-A splice variants are bound by the clinically used monoclonal antibody bevacizumab. When labeled with the PET-isotope zirconium-89 ($^{89}$Zr), bevacizumab preserves its VEGF-A binding properties. Thus, tracer dosages of radiolabeled bevacizumab can be used for tumor specific, whole body imaging of VEGF-A. In preclinical studies[6,7] and in a study in renal cell cancer patients[8], we have already shown an excellent tumor-to-background ratio with an optimum at 4 days after tracer injection when using $^{89}$Zr-bevacizumab. In the present clinical feasibility study, we used $^{89}$Zr-bevacizumab PET to provide proof-of-principle whether VEGF-A imaging can be used for detection of primary breast tumors.

# Materials and methods

## Patients

Eligible patients had a histologically or cytologically confirmed adenocarcinoma of the breast and were scheduled for mastectomy or lumpectomy. Additional eligibility criteria included a minimum age of 18 years and World Health Organisation (WHO) performance status of ≤2. In all patients, standard diagnostics consisted of mammography and ultrasonography. When needed to better define tumor extent, MRI was also performed. Exclusion criteria included pregnancy or lactation, prior radiotherapy in the involved area, major surgery within 28 days before initiation of the study, clinically significant cardiovascular disease or prior allergic reactions to immunoglobulins. In premenopausal patients, a pregnancy test was performed to exclude pregnancy.

The study was approved by the Medical Ethics Committee of the University Medical Center of Groningen. This local committee was supervised by the Central Committee on Research Involving Human Subjects which acts as the competent authority. All patients gave written informed consent. The trial is registered under clinicaltrial.gov number NCT00991978.

## $^{89}$Zr-bevacizumab PET Imaging

Patients received 37 MBq/5 mg protein $^{89}$Zr-bevacizumab as an intravenous bolus injection 4 days prior to PET scanning and observed for allergic reactions for 1 hour. The dose of 5 mg bevacizumab was chosen as this was the lowest dose possible which was reproducible during the labeling procedure. The same dose was used in a study with indium-111 labeled bevacizumab, which visualized all known melanoma lesions[9]. $^{89}$Zr has a decay half-life of 78,4 hours, the mean beta energy is 395.5 keV, the positron branching fraction is 22.74% and the main gamma emissions: 511 keV 45.5% and 909 keV 99.04%. Clinical $^{89}$Zr-bevacizumab was produced as follows: reconstituted bevacizumab (Avastin®, Roche) was conjugated with tetrafluorophenol-N-succinyldesferal-Fe (VU University Medical Center, Amsterdam, The Netherlands), purificated, and stored at -80°C. Good manufacturing practice-produced $^{89}$Zr-oxalate (BV Cyclotron, Amsterdam. The Netherlands) was used for radiolabeling the conjugate. Quality control was performed to ensure (radio) chemical purity (>95%), antigen binding and stability. PET/CT acquisition was performed with a Siemens Biograph mCT 64 slice (PET/CT) camera (Siemens, Knoxville, TN). Scanning of both breasts and the axillary regions was performed in 2 bed positions with 5 minutes of imaging per bed position. In addition a low dose CT scan was performed which was used for attenuation and scatter correction. The patient was positioned in prone position with hanging breasts. PET data was reconstructed with Siemens iterative reconstruction, involving ordinary poison (OP) OSEM 3D reconstruction without time-of-flight and point-spread-function methods. The settings used for reconstruction were 2 iterations and 8 subsets, a matrix size of 200 and a post-processing filter of 10 mm, resulting in an effective resolution of 11 mm. For sentinel lymph node detection and SPECT imaging as standard

of care, 100 MBq Technetium-99m ($^{99m}$Tc) labeled nanocolloid was administered one day prior to surgery. To avoid interference of SPECT imaging a minimal interval of 3 half-life episodes of $^{89}$Zr-bevacizumab (11 days) was taken into account between the administration of $^{89}$Zr-bevacizumab and $^{99m}$Tc-nanocolloid to allow for sufficient $^{89}$Zr isotope decay.

### $^{89}$Zr-bevacizumab PET Analysis

Final images analysis was done by a nuclear medicine physician (AHB). Separate analysis of the mammography and ultrasonographic images was executed by a radiologist (SBM) and compared with the PET images in collaboration with the nuclear medicine physician to confirm that the tumor location on both imaging modalities was identical. The uptake of $^{89}$Zr-bevacizumab in the tumor was quantified using AMIDE Medical Image Data Examiner software (version 0.9.3, Stanford University, Stanford, CA)[10]. For the quantification of radioactivity within the tumor, 3D regions of interest (ROIs) were manually drawn around the tumor and axillary lymph node metastasis (if present) (SBMG). For determining the background also the uptake in the cardiac blood pool, normal breast (ipsi-and contralateral) and nipple were quantified. The data is presented as the maximum standardized uptake value ($SUV_{max}$). Furthermore, the images were analyzed for uptake of $^{89}$Zr-bevacizumab uptake along the cytology or biopsy channel.



### Enzyme-Linked Immuno Sorbent Assay (ELISA) to Detect VEGF-A

For quantification of VEGF-A expression in the surgical specimen, an ELISA was performed according to the manufacturer instructions (Quantikine®, R&D Systems, Bristol, UK). Three random samples were collected from the surgical specimen of the primary tumor, ipsilateral normal tissue and nipple tissue. Tissue was lyzed manually using mammalian protein extraction reagent (M-PER, Pierce, Rockford, IL). Thereafter, mixtures were centrifuged at 20,000 g for 15 minutes and subsequently stored at -20 °C until analysis. Results of VEGF-A measurement were normalized for the protein concentration of the same samples determined by the Bradford assay[11].

### Tumor Histology and Immunohistochemistry

Tumor tissue of the surgical specimen was typed and graded according to the WHO and modified Bloom en Richardson guidelines, respectively. Immunohistochemistry for VEGF-A and Ki-67 was performed on tumors, ductal carcinoma in situ (DCIS) (if present) and normal breast tissue using paraffin-embedded slides. Slides were deparaffinized in xylene and rehydrated in ethanol. Endogenous peroxidase was blocked by incubation with 0.3% hydrogen peroxidase for 30 minutes. Primary antibodies rabbit anti-VEGF-A (A20-c152, 1:50, Santa Cruz Biotechnology, Santa Cruz, CA), mouse anti-Ki-67 (1:300, clone MIB-1, DAKO) and mouse anti-CD31 (BD Pharmingen, San Diego CA) were applied for 60 minutes, followed by suitable secondary antibodies and immunostaining was visualized with 3′ 3-diaminobenzidine tetrahydrochloride. Counterstaining was performed with hematoxylin. All stainings were scored by two independent observers (SBMG and JB).

*VEGF-A* was scored (negative/positive) at 400× magnification. The proliferation index was calculated by counting of *Ki-67* positive versus negative cells in at least 5 high power fields (400×). Micro vessel density (MVD) was scored in 5 areas defined as hotspots areas with maximum number of microvessels.

Breast cancer molecular subtypes according to immunohistochemical profile were categorized as follows: luminal A (ER positive or PR positive and Ki-67 < 14%;) luminal B (ER positive or PR positive and Ki-67 ≥ 14%), HER2 enriched (ER negative, PR negative, and HER2 positive), and basal-like (ER negative, PR negative, HER2 negative). Luminal B also included tumors that were ER positive and/or PR positive and HER2 positive[12].

## Phantom Study

In order to define the detection limit of the PET/CT camera system, a breast simulation phantom study was carried out. Breast-shaped phantoms were produced as described earlier[13,14]. For tumor-like agarose inclusions, 2% agarose (Hispanagar, Burgos, Spain) was suspended in tris-buffered saline and heated to 70 °C. Subsequently, $^{89}$Zr-oxalate was dissolved to a final concentration of 7,700 Bq/mL. Silicone molds were filled with the agarose mixture to create tumor-like inclusions ranging from 5 to 20 mm in diameter.

Breast phantoms were constructed with two tumor-like inclusions. PET imaging was performed on day 1 and every 3 to 4 days until visual disappearance of the lesions on the scan. Final image analysis was performed as stated above. The recovery coefficient was determined by calculating the ratio between the measured amount of $^{89}$Zr on the PET and the inserted dose measured by a dose calibrator, corrected for decay.

## Statistical Analyses

Data are presented as a mean ± standard deviation (SD). Statistical analysis was performed using the paired *t*-test test or Wilcoxon signed rank test for paired data and the unpaired t-test for unpaired data. Associations between parameters were evaluated using Pearson's correlation test (SPSS version 19.0, IBM, New York, NY). A double sided *P*-value < .05 was considered significant.

# Results

## Patient Characteristics

A total of 23 patients with 26 breast tumors were included. Patients had no history of prior malignancies. Two women had bilateral breast cancer and one patient had two ipsilateral tumors. Patient and tumor characteristics are shown in Table 1. Breast tumors were detected with mammography (n = 22), ultrasound (n = 25) or MRI (n = 1). Histological analyses showed invasive ductal carcinoma (n = 23), invasive lobular carcinoma (n = 2) and invasive tubular carcinoma (n = 1). Of the 25 available invasive cancers, 9 tumors were classified as luminal A and 14 as luminal B breast cancer. There was one basal like- and one HER2 enriched tumor. Six patients had pathologically proven axillary lymph node metastases prior to surgery. In three additional patients, tumor cells were detected in the sentinel lymph node after surgery. In a patient with bilateral breast cancer, axillary lymph node involvement on one side was already known prior to surgery and was also detected in a sentinel lymph node of the opposite axilla.



**Table 1.** Patient-and tumor characteristics

| | Patients (n = 23) |
|---|---|
| Tumors (n) | 26 |
| Median age patient, years (range) | 54.9 ± 10.2 (32-73) |
| Tumor size mm (range) | 25.1 ± 19.8 (4-80) |
| Tumor type (n) | |
| - Invasive ductal carcinoma | 23 |
| - Invasive lobular carcinoma | 2 |
| - Invasive tubular carcinoma | 1 |
| Tumor stage (n): | |
| - T1 | 15 |
| - T2 | 5 |
| - T3 | 5 |
| - T4 | 1 |
| Nodal stage (n): | |
| - N0 | 15 |
| - N1 | 4 |
| - N2 | 2 |
| - N3 | 4 |

## $^{89}$Zr-bevacizumab PET

In this study, no adverse events were seen. $^{89}$Zr-bevacizumab PET imaging showed uptake in 25 of the 26 breast tumors (96.1%). Figure 1 shows a representative example. Uptake of $^{89}$Zr-bevacizumab was higher in breast tumors than in normal breast tissue (of both the ipsi- and contralateral breast); $SUV_{max}$ in breast tumors was 1.85 ± 1.22 (range, 0.52-5.64) *v* 0.59 ± 0.37 (range, 0.27-1.69) in ipsilateral normal breast tissue and 0.51 ± 0.26 (range, 0.20-1.12) in contralateral normal breast tissue; (both $P < .001$) (Figure 2A). There was a similar $^{89}$Zr-bevacizumab uptake in normal tissue of both breasts ($P = .88$). $SUV_{max}$ of luminal A tumors was 1.28 ± 0.58 compared to 2.04 ± 1.08 in luminal B tumors ($P = .06$). In the patients with a basal like and HER2 overexpressing breast tumor, $SUV_{max}$ was 0.52

**Figure 1.**

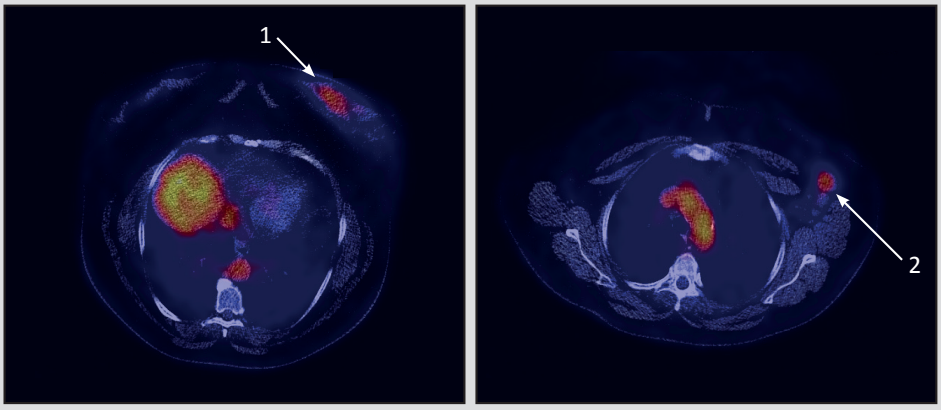


Axial slices of $^{89}$Zr-bevacizumab PET from a patient with a primary breast tumor (1) and lymph node metastasis (2).

**Figure 2.**

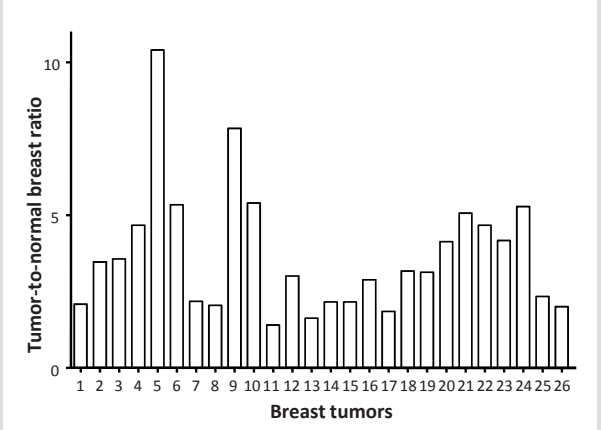


Analysis per patient (X-axis). The ratio between $^{89}$Zr-bevacizumab uptake expressed as SUVmax in breast tumors versus normal breast tissue .

and 5.64, respectively. The only breast tumor which did not show preferential $^{89}$Zr-bevacizumab uptake was an invasive ductal carcinoma with a diameter of 10 mm. Lymph node metastases (size ranging 3-42 mm), were present in 10 axillary regions (of 9 patients); 4 of these lymph node positive axillary regions were detected by PET ($SUV_{max}$ 2.66 ± 2.03, range 1.32 - 5.68). All four positive axillary regions were already known prior to surgery based on ultrasound and cytology. $^{89}$Zr-bevacizumab PET detected none of 4 positive axillary regions with 1-3 lymph node metastases (pN1), and 4 out of 6 positive axillary regions with 4 or more lymph node metastases (≥ pN2). There were no false positive readings and there was no $^{89}$Zr-bevacizumab uptake along the cytology or biopsy tract.

Next to tumor visualization there was slightly higher uptake in the nipples of both breasts compared to background in 20 of the 23 patients. $SUV_{max}$ of nipple tissue was 1.13 ± 0.59 (range 0.47 - 3.02). This is lower than the $SUV_{max}$ in tumor tissue ($P$ = .01). $SUV_{max}$ in the blood pool on day 4 was 4.17 ± 1.07 (range 2.97 - 7.05), which is 2.3 and 3.7 fold higher than in the tumors and nipples respectively.



## VEGF-A ELISA

For VEGF-A ELISA measurements, surgical specimens of 17 breast tumors and 24 specimens of normal ipsilateral breast tissue were available. Pathologic examination of the tissue confirmed tumor in all macroscopic tumors. Mean tumor VEGF-A/mg protein was higher (184 pg ± 169) than in normal breast tissue (10 pg ± 21, $P$ = .001) (Figure 2). In the tumor of 10 mm which was not detected by $^{89}$Zr-bevacizumab PET, 371 pg/mg protein VEGF-A was measured. $^{89}$Zr-bevacizumab tumor uptake of the $^{89}$Zr-bevacizumab detected tumors correlated with the VEGF-A protein level (Pearson r = 0.49, $P$ = .04) (Figure 3).

In the 11 available nipple specimens (from one patient with bilateral breast cancer both nipples) VEGF-A level was 10 pg ± 13 per mg protein, which was not different from normal breast tissue ($P$ = .96).

**Figure 3.**

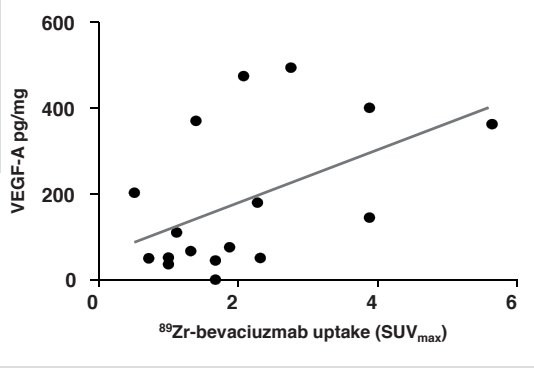


Correlation between $^{89}$Zr-bevacizumab tumor uptake (X-axis) and tumor VEGF-A (Y-axis) levels as measured by ELISA (Pearson r = 0.49, $P$ = 0.04).

**Figure 4.**

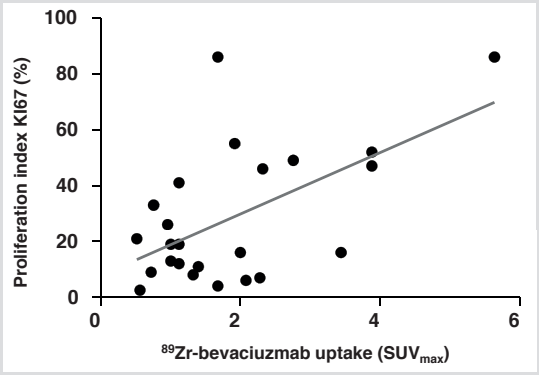


Correlation between $^{89}$Zr-bevacizumab tumor uptake (X-axis) and proliferation index (Y-axis) as measured with KI-67 expression by tumor (Pearson r = 0.55, *P* = 0.005).

## Immunohistochemistry

All available tumors (n = 25) showed positive staining for VEGF-A expression. VEGF-A expression in normal tissue was absent in two and present in 23 of the 25 operated breasts. DCIS was present in 10 patients and stained positive for VEGF-A in all cases. $^{89}$Zr-bevacizumab tumor uptake correlated positively with a mean proliferation index of 32.1 ± 24.3 (range 6.0-86.0) (Pearson r = 0.55, *P* = .005) (Figure 4). The MVD was not correlated with $^{89}$Zr-bevacizumab uptake (r = 0.10, *P* = 0.64).

## Phantom Study

All tumor-like inclusions were visible on day 1. The recovery coefficient was 73% for the smallest inclusion and 96% for the largest one. The last time point before visual disappearance was day 1 (5 mm inclusion), day 10 (10 mm inclusion), day 14 (15 mm inclusion) and day 17 (20 mm inclusion).

# Discussion

This is the first clinical feasibility study with $^{89}$Zr-bevacizumab PET in breast cancer patients. Uptake of $^{89}$Zr-bevacizumab was visualized in 96.1% of the primary tumor lesions and there was a relation with the level of VEGF-A in the tumor. This provides proof that $^{89}$Zr-bevacizumab might be potentially valuable for biological characterization of tumors as well as prediction and evaluation of the effect of VEGF-A targeting therapeutics.

VEGF-A is reported in several studies to be overexpressed in malignant breast tumors as well as in DCIS[5,15], thus covering the full spectrum of early stage breast cancer to more advanced stages. More frequent VEGF-A staining was found to be related to aggressiveness as assessed by VEGF-A staining in a study with 1,788 breast tumors[5]. $^{89}$Zr-bevacizumab PET proved to be able to detect a broad range of VEGF-A expression levels. Quantitative tumor analyses showed a more than 10-fold difference between individual $SUV_{max}$ suggesting large differences in VEGF-A tumor levels between patients, which was confirmed by the broad difference in VEGF-A measured by ELISA. Although there was a high visualization rate, the $SUV_{max}$ of tumors and normal tissues do overlap in this study. Importantly in individual patients, $SUV_{max}$ was always higher in tumor than in normal breast tissues. The higher VEGF-A ratio between tumor and normal breast measured by ELISA compared to PET, might be explained by the fact that (in contrast to $^{89}$Zr-bevacizumab PET) the ELISA also measures intracellular VEGF-A[16]. Moreover, the resolution of the PET camera is 10 mm while ELISA and immunohistochemistry measure on cellular level.

$^{89}$Zr-bevacizumab uptake in the primary breast tumors was relatively low, compared to uptake in a series of 22 metastatic renal cell cancers in our institution (mean $SUV_{max}$ 1.85 *v* 10.1)[15]. Anti-angiogenic treatment has monotherapy activity in renal cell cancers which is not the case in tumor types such as breast cancer[17,18]. The difference in $^{89}$Zr-bevacizumab uptake, and therefore VEGF-A levels, is possibly related to this varying efficacy. $^{89}$Zr-bevacizumab might be potentially valuable for biological characterization of tumors as well as prediction and evaluation of the effect of VEGF-A targeting therapeutics.

The failure to detect one tumor lesion with the size of 10 mm in diameter out of 26 lesions, despite sufficient VEGF-A expression, can be explained by the findings in our phantom study. Small lesions visually disappear much earlier on $^{89}$Zr-PET compared to larger lesions. This effect might influence the tumor uptake of $^{89}$Zr-bevacizumab measured by $SUV_{max}$. The observed effect of tumor size on PET detection is shared by FDG-PET[19,20], but is larger in case of $^{89}$Zr-PET. Due to the higher radiation dose per MBq of $^{89}$Zr, a lower amount of activity was injected compared to FDG. $^{89}$Zr has a smaller yield of positron compared to $^{18}$F which results in increased noise and therefore $^{89}$Zr-bevacizumab PET images require more smoothing. This degrades resolution and increases size effects. Importantly, imaging with $^{89}$Zr-bevacizumab PET delivered no false-positive lesions.

Most patients had uptake of $^{89}$Zr-bevacizumab in the region of the nipple, while the VEGF-A level as measured with ELISA was low and equal to normal tissue. $^{89}$Zr has a long

half life of 78.4 h. When labeled to bevacizumab, a considerably amount of the tracer remains in the circulation. Therefore, the uptake of $^{89}$Zr-bevacizumab in the nipple is likely due to high vascularization of the nipple compared to normal breast tissue[21]. In the tumor, the contribution of perfusion to increased $^{89}$Zr-bevacizumab uptake in the tumor is less likely to play a role, based on preclinical and clinical data. In a xenograft mouse model, we have shown that tumor accumulation of $^{89}$Zr-bevacizumab increases in time, while uptake in normal organs decreases[6]. This increase in $^{89}$Zr-bevacizumab tumor accumulation over time was also shown in melanoma patients who underwent $^{111}$In-bevacizumab SPECT[9]. In a human SKOV-3 ovarian tumor xenograft there was higher uptake of $^{89}$Zr-bevacizumab compared to $^{89}$Zr-IgG[6] indicating tumor specific uptake. $^{89}$Zr-IgG PET in the patient setting is not possible due to radiation exposure concerns. This is also the limiting factor in using $^{89}$Zr-bevacizumab PET in healthy subjects as a negative control. However, the MVD did not influenced $^{89}$Zr-bevacizumab uptake. Moreover, the relation between VEGF-A measured by ELISA and $^{89}$Zr-bevacizumab uptake in tumors and not in nipple tissue, is in line with the preclinical findings that the tracer uptake is in fact tumor specific.

The limiting factor for more general application of imaging with radionuclides is the radiation burden. In a study comparing the risks of radiation-induced cancer from mammography, molecular breast imaging (MBI) and positron emitting mammography (PEM), the cumulative cancer incidence is 15-30 times higher for PEM and MBI compared to mammography[22]. The estimated radiation burden of $^{89}$Zr-bevacizumab-PET is 19 milliSieverts (mSv) per tracer injection, based on extrapolation from $^{111}$In-bevacizumab data and a dosimetry study on $^{89}$Zr-U36, compared to 5.3 mSv for FDG-PET[23-25].

To make optimal use of the tumor specificity of molecular imaging of VEGF-A while overcoming radiation issues, bevacizumab was also linked to the near-infrared fluorescent dye IRDye 800CW in our institution. This technique has already been tested in human xenograft-bearing athymic mice, detecting tumor lesions *in vivo* with high sensitivity and specificity. IRdye 800CW labeled bevacizumab revealed submilimeter lesions with a clinical intraoperative fluorescence camera[26]. Recently, we started a study with IRDye 800CW labeled bevacizumab in early breast cancer (NCT01508572). The aim of this study is to determine the uptake of the VEGF-A targeting fluorescent tracer in breast tumors, both during preoperative diffuse optical tomography as well as during surgery. This approach can potentially contribute to the development of a tumor specific tracer.

## Conclusion

In this first clinical feasibility study with $^{89}$Zr-bevacizumab PET in breast cancer patients, we have shown that uptake of $^{89}$Zr-bevacizumab was visible in most primary breast tumors and correlated with the protein level of VEGF-A in the tumor. These findings support use of VEGF-A imaging in breast cancer for future imaging purposes.

## Acknowledgements

The authors thank Arieke Prozée, Kees Meijer and Marian Beernink for their assistance in patient inclusion in the trial and Tineke van der Sluis and Esther M.E. van Straten for their technical assistance.

# References


1. Ferlay J, Shin HR, Bray F, Forman D, Mathers C, Parkin DM. Estimates of worldwide burden of cancer in 2008: GLOBOCAN 2008. Int J Cancer 2010;127:2893-2917.
2. Vogl G, Bartel H, Dietze O, Hauser-Kronberger C. HER2 is unlikely to be involved in directly regulating angiogenesis in human breast cancer. Appl Immunohistochem Mol Morphol 2006;14:138-145.
3. Kostopoulos I, Arapantoni-Dadioti P, Gogas H, et al. Evaluation of the prognostic value of HER-2 and VEGF in breast cancer patients participating in a randomized study with dose-dense sequential adjuvant chemotherapy. Breast Cancer Res Treat 2006;96:251-261.
4. Fuckar D, Dekanic A, Stifter S, et al. VEGF expression is associated with negative estrogen receptor status in patients with breast cancer. Int J Surg Pathol 2006;14:49-55.
5. Liu Y, Tamimi RM, Collins LC, et al. The association between vascular endothelial growth factor expression in invasive breast cancer and survival varies with intrinsic subtypes and use of adjuvant systemic therapy: Results from the nurses' health study. Breast Cancer Res Treat 2011;129:157-184.
6. Nagengast WB, de Vries EG, Hospers GA, et al. In vivo VEGF imaging with radiolabeled bevacizumab in a human ovarian tumor xenograft. J Nucl Med 2007;48:1313-1319.
7. Nagengast WB, de Korte MA, Oude Munnink TH, et al. 89Zr-bevacizumab PET of early antiangiogenic tumor response to treatment with HSP90 inhibitor NVP-AUY922. J Nucl Med 2010;51:761-767.
8. Oosting SF, Brouwers AH, Van Es SC, et al. $^{89}$Zr-bevacizumab PET imaging in metastatic renal cell carcinoma patients before and during antiangiogenic treatment. J Clin Oncol 2012;30(suppl abstr 10581).
9. Nagengast WB, Hooge MN, van Straten EM, et al. VEGF-SPECT with $^{111}$In-bevacizumab in stage III/IV melanoma patients. Eur J Cancer 2011;47:1595-1602.
10. Loening AM, Gambhir SS. AMIDE: A free software tool for multimodality medical image analysis. Mol Imaging 2003;2:131-137.
11. Bradford MM. A rapid and sensitive method for the quantitation of microgram quantities of protein utilizing the principle of protein-dye binding. Anal Biochem. 1976;72:248-254.
12. Goldhirsch A, Wood WC, Coates AS, et al. Strategies for subtypes--dealing with the diversity of breast cancer: Highlights of the st. gallen international expert consensus on the primary therapy of early breast cancer 2011. Ann Oncol 2011;22:1736-1747.
13. De Grand AM, Lomnes SJ, Lee DS, et al. Tissue-like phantoms for near-infrared fluorescence imaging system assessment and the training of surgeons. J Biomed Opt 2006;11:014007.
14. Pleijhuis RG, Langhout GC, Helfrich W, et al. Near-infrared fluorescence (NIRF) imaging in breast-conserving surgery: Assessing intraoperative techniques in tissue-simulating breast phantoms. Eur J Surg Oncol 2011;37:32-39.
15. Bluff JE, Menakuru SR, Cross SS, et al. Angiogenesis is associated with the onset of hyperplasia in human ductal breast disease. Br J Cancer 2009;101:666-672.
16. Toi M, Kondo S, Suzuki H, et al. Quantitative analysis of vascular endothelial growth factor in primary breast cancer. Cancer. 1996;77:1101-1106.
17. Brufsky AM, Hurvitz S, Perez E, et al. RIBBON-2: A randomized, double-blind, placebo-controlled, phase III trial evaluating the efficacy and safety of bevacizumab in combination with chemotherapy for second-line treatment of human epidermal growth factor receptor 2-negative metastatic breast cancer. J Clin Oncol 2011;29:4286-4293.
18. Yang JC, Haworth L, Sherry RM, et al. A randomized trial of bevacizumab, an anti-vascular endothelial growth factor antibody, for metastatic renal cancer. N Engl J Med 2003;349:427-434.
19. Avril N, Rose CA, Schelling M, et al. Breast imaging with positron emission tomography and fluorine-18 fluorodeoxyglucose: Use and limitations. J Clin Oncol 2000;18:3495-3502.
20. Veronesi U, De Cicco C, Galimberti VE, et al. A comparative study on the value of FDG-PET and sentinel node biopsy to identify occult axillary metastases. Ann Oncol 2007;18:473-478.
21. O'Dey D, Prescher A, Pallua N. Vascular reliability of nipple-areola complex-bearing pedicles: An anatomical microdissection study. Plast Reconstr Surg 2007;119:1167-1177.
22. O'Connor MK, Li H, Rhodes DJ, Hruska CB, Clancy CB, Vetter RJ. Comparison of radiation exposure and associated radiation-induced cancer risks from mammography and molecular imaging of the breast. Med Phys 2010;37:6187-6198.
23 de Jong JR, Warnders FJ, Nagengast WB et al. Radiation dosimetry of $^{111}$In-bevacizumab for VEGF-SPECT in melanoma patients. Eur J Nucl Med Mol Imaging 2010;37:S477-S477.
24 Börjesson PK, Jauw YW, de Bree R et al. Radiation dosimetry of $^{89}$Zr-labeled chimeric monoclonal antibody U36 as used for immuno-PET in head and neck cancer patients. J Nucl Med 2009;50:1828-1836.

25. Murano T, Minamimoto R, Senda M, et al. Radiation exposure and risk-benefit analysis in cancer screening using FDG-PET: Results of a japanese nationwide survey. Ann Nucl Med 2011;25:657-666.
26. Terwisscha van Scheltinga AG, van Dam GM, Nagengast WB, et al. Intraoperative near-infrared fluorescence tumor imaging with vascular endothelial growth factor and human epidermal growth factor receptor 2 targeting antibodies. J Nucl Med 2011;52:1778-1785.

# CHAPTER 7

# $^{89}$Zr-trastuzumab and $^{89}$Zr-bevacizumab PET to Evaluate the Effect of the Heat Shock Protein 90 Inhibitor NVP-AUY922 in Metastatic Breast Cancer Patients

S.B.M. Gaykema[1]
C.P. Schröder[1]
J. Vitfell-Rasmussen[2]
S. Chua[2]
T.H. Oude Munnink[1]
A.H. Brouwers[3]
A.H.H. Bongaerts[4]
M. Akimov[5]
C. Fernandez-Ibarra[5]
M.N. Lub-de Hooge[3,6]
E.G.E. de Vries[1]
C. Swanton[2]
U. Banerji[2]

Departments of Medical Oncology[1], Nuclear Medicine and Molecular Imaging[3], Radiology[4] and Hospital and Clinical Pharmacy[6], University of Groningen, University Medical Center Groningen, Groningen, The Netherlands
Section of Medicine[2], The Institute of Cancer Research, Sutton, UK and Drug Development Unit, The Royal Marsden Hospital, Sutton, United KingdomNovartis Pharma AG[5], Basel, Switzerland; Novartis Pharmaceuticals, Cambridge, MA

*Clinical cancer research 2014; 20:3945-54*

## Translational relevance

Metastatic breast cancer is rarely cured and finding treatment for this disease is an unmet clinical need. Heat shock protein 90 (HSP90) is a target of interest in cancer treatment, as a molecular chaperone which plays a critical role in protein folding and thereby functioning of a broad range of cancer related client proteins. Gaining insight of *in vivo* degradation of client proteins caused by HSP90 inhibition is challenging. In this clinical trial, the effect of HSP90 inhibitor NVP-AUY922 on client proteins human epidermal receptor 2 (HER2) or vascular endothelial growth factor (VEGF; with hypoxia inducible transcription factor (HIF)-1α as the actual client protein) was studied with $^{89}$Zr-trastuzumab PET or $^{89}$Zr-bevacizumab PET, in patients with advanced HER2 or estrogen receptor (ER) positive metastatic breast cancer. The results of PET imaging were correlated with conventional CT scanning. $^{89}$Zr-trastuzumab uptake on PET at 3 weeks correlated with CT responses in individual lesions at 8 weeks and revealed areas of heterogeneous response in patients with HER2 amplified metastatic breast cancer. Thus novel PET probes such as $^{89}$Zr-trastuzumab can be used to provide insights into responses to novel agents active in HER2 amplified breast cancer such as NVP-AUY922.

# Abstract

**Purpose:** Heat shock protein 90 (HSP90) chaperones have key client proteins that are involved in all hallmarks of breast cancer growth and progression. The primary aim of this clinical trial was to evaluate the feasibility of using $^{89}$Zr-trastuzumab PET (for human epidermal receptor 2 (HER2) positive breast cancer) or $^{89}$Zr-bevacizumab PET (for estrogen receptor (ER) positive breast cancer) to determine in vivo degradation of client proteins caused by the novel HSP90 inhibitor NVP-AUY922.

**Experimental design:** 70 mg/m$^2$ NVP-AUY922 was administered intravenously in a weekly schedule to patients with advanced HER2 or ER positive breast cancer. Biomarker analysis consisted of serial PET imaging with $^{18}$F-fluordeoxyglucose (FDG), $^{89}$Zr-trastuzumab or $^{89}$Zr-bevacizumab. Response evaluation was performed according to RECIST1.0. FDG, $^{89}$Zr-trastuzumab and $^{89}$Zr-bevacizumab distribution were scored visually and quantitatively by calculating the maximum standardized uptake values ($SUV_{max}$). In blood samples, serial HSP70 levels, extracellular form of HER2 (HER2-ECD) and pharmacokinetic and pharmacodynamic parameters were measured.

**Results:** Sixteen patients (10 HER2 positive, 6 ER positive tumors), were included. One partial response was observed; 7 patients showed stable disease. $SUV_{max}$ change in individual tumor lesions on baseline versus 3 week $^{89}$Zr-trastuzumab PET was heterogeneous and related to size change on CT after 8 weeks treatment ($r^2 = 0.69$; $P = 0.006$). Tumor response on $^{89}$Zr-bevacizumab PET and FDG-PET was not correlated with CT response. Conclusions: NVP-AUY922 showed proof of concept clinical response in HER2 amplified metastatic breast cancer. Early change on $^{89}$Zr-trastuzumab PET was positively associated with change in size of individual lesions assessed by CT.

# Introduction

Metastatic breast cancer remains an incurable disease in the majority of cases, despite advances in systemic treatment that have improved median survival[1,2]. The development of novel agents for this disease is an area of unmet need. Heat shock protein 90 (HSP90) is a molecular chaperone which plays a critical role in protein folding and function of a broad range of client proteins[3]. HSP90 client proteins playing a role in metastatic breast cancer include human epidermal growth factor receptor 2 (HER2), the hypoxia inducible transcription factor (HIF)-1α and the estrogen receptor (ER)[4-6]. HER2 is a sensitive client protein of HSP90, which can be depleted by HSP90 inhibition with NVP-AUY922 in many different preclinical experiments including breast cancer models[7,8]. HIF-1α is the key factor involved in upregulating the transcription of vascular endothelial growth factor (VEGF)-A in hypoxic cells[9]. HSP90 is overexpressed in metastatic breast cancer. In addition, HSP90 in tumor cells preferentially binds to HSP90 inhibitors compared to normal cells, which further validates HSP90 as a cancer target[10,11]. Thus there are many different reasons for evaluating HSP90 inhibitors in breast cancer. Several HSP90 inhibitors are currently in clinical development. Of the resorcinyclic pyrazole/isoaxazole amide analogues, HSP90 inhibitor NVP-AUY922 is the most potent[8]. NVP-AUY922 is active against HER2 positive as well as HER2 negative human breast cancer cells in vitro and in vivo[8,12,13]. Clinical responses to HSP90 inhibitors have been shown in multiple early phase studies[14-16]. Furthermore, HSP90 inhibition has shown efficacy when used in conjunction with other HER2 targeting agents such as trastuzumab[17]. Nonetheless, gaining insight into the *in vivo* degradation of client proteins caused by HSP90 inhibition is challenging.

In this setting, *in vivo* visualization of HSP90 inhibition effect might be helpful. $^{18}$F-fluordeoxyglucose (FDG)-positron emission tomography (PET) for assessing tumor glucose metabolism, is used to monitor early drug response to anticancer agents[18-21]. More target based imaging of HSP90 inhibition effect was performed in preclinical studies, in which critical client proteins VEGF and HER2 could be visualized with zirconium-89 ($^{89}$Zr)-bevacizumab PET, gallium-68-(Fab'2)trastuzumab PET and $^{89}$Zr-trastuzumab PET imaging[22-24]. In human breast cancer xenograft mouse model models, tumor uptake of $^{18}$F-FDG was unaffected by treatment with the HSP90 inhibitor 17AAG, while radiolabeled trastuzumab tumor uptake was on average reduced by 50%. This indicates that target based imaging may be more useful as an early biomarker for HSP90 inhibition than metabolic $^{18}$F-FDG imaging[24]. $^{89}$Zr-trastuzumab PET and $^{89}$Zr-bevacizumab PET has been used in several clinical trials, including in breast cancer specific studies[25-27].

To evaluate HSP90 inhibition effect on the *in vivo* degradation of client proteins, blood-based assays have been used. Serial circulating HER2 extracellular domain (HER2-ECD) measurements predicted response to trastuzumab-based therapy in a study of 55 patients[28]. In a phase 1 study with NVP-AUY922, plasma NVP-AUY922 levels and pharmacodynamic

biomarkers such as HSP70 induction in peripheral blood mononuclear cells (PBMC) were assessed, in addition to establishment of the toxicity profile[29].

Thus, the primary aim of this clinical trial with HSP90 inhibitor NVP-AUY922 in HER2 or ER positive metastatic breast cancer patients, was to evaluate the feasibility of using serial FDG-PET and novel [89]Zr-trastuzumab PET or [89]Zr-bevacizumab PET to determine the *in vivo* degradation of client proteins caused by the HSP90 inhibitor NVP-AUY922. Furthermore, we aimed to evaluate whether these assessments were related to CT response (according to RECIST) and serum shed HER2 levels (if applicable), and to underpin these assessments with evidence of pharmacokinetic and pharmacodynamic parameters which have already been defined in detail in the previous phase I study[29].

# Patients and Methods

## Patients

Eligible patients for treatment with NVP-AUY922, had a diagnosis of histologically confirmed, measurable progressive metastatic or locally advanced breast cancer, and had received up to two prior lines of cytotoxic therapy for advanced disease. In addition, patients with HER2 positive breast cancer were required to have a history of trastuzumab resistance and up to a maximum of 3 anti-HER2 based regimens for advanced disease. Patients with ER positive breast cancer had progressive disease on at least one and up to a maximum of three lines of standard endocrine therapy. Further eligibility criteria included: age ≥ 18 years, World Health Organisation (WHO) performance status ≤ 2, at least one measurable lesion evaluable with RECIST1.0[30], HER2 positive ((immunohistochemistry (IHC) 3+ or fluorescent in situ hybridization (FISH) ratio ≥2, or ER positive breast cancer (archival primary tumor tissue), and resolution of toxicities from other therapies to National Cancer Institute common terminology criteria for adverse events (NCI CTCAE version 3.0) grade ≤ 2. Patients should have adequate hematological, hepatic and renal function which was defined by laboratory values, adequate cardiac function defined by electrocardiogram (ECG) and MUGA scan or ultrasound. Patients eligible for treatment with NVP-AUY922 in this trial (Trial Registration ID: NCT00526045), were also eligible for assessment of treatment effect with $^{89}$Zr-trastuzumab PET (Trial Registration ID: NCT01081600) for HER2 positive breast cancer or $^{89}$Zr-bevacizumab PET (Trial Registration ID: NCT01081613) for ER positive breast cancer.

This clinical trial was performed at the University Medical Center of Groningen (Groningen, The Netherlands) and the Royal Marsden Hospital (London, United Kingdom). Medical ethical committee approval was obtained in both institutions. All patients signed written informed consent. Consent for the $^{89}$Zr-trastuzumab PET or $^{89}$Zr-bevacizumab side studies was obtained separately from consent for the clinical trial with NVP-AUY922 treatment.

## Treatment

NVP-AUY922 was administered once a week intravenously at a starting dose of 70 mg/m$^2$ which was the recommended phase II dose in the first-in-human phase I trial with monotherapy NVP-AUY922[29]. As per protocol doses were reduced to 54 mg/m$^2$ for significant adverse events which were defined as ≥ grade 3 toxicity or grade 2 toxicity for at least 7 days. NVP-AUY922 was discontinued for any grade 4 toxicity.

## Toxicity Assessments

Patients were examined and assessed for adverse events weekly, and toxic effects were graded with the NCI CTCAE version 3.0. A complete blood and platelet count and serum chemistry panel measurement were repeated every week in the first 2 cycles, thereafter once every 2 weeks. After reports of visual symptoms in the phase I study, this trial required

complete ophthalmologic assessment including testing for visual acuity, intraocular pressure, slit-lamp, dilated fundus and color-vision. Additional an electro retinogram was conducted. All opthalmologic examinations were performed at baseline, when visual symptoms became present and at the end of cycle 2. 12-lead electrocardiograms were obtained at baseline and before and after every NVP-AUY922 infusion. The electrocardiograms were assessed for changes in QT duration. Patients were instructed to use loperamide as needed for diarrhea.

### $^{89}$Zr-trastuzumab and $^{89}$Zr-bevacizumab PET imaging

Patients with HER2 positive breast cancer, who consented to the $^{89}$Zr-trastuzumab PET imaging side study, received 37 MBq/50 mg $^{89}$Zr-trastuzumab intravenously. Production of clinical grade $^{89}$Zr-trastuzumab as described previously[31]. Each patient underwent a PET scan on day 2 and 4 postinjection. Two scan sequences were performed, with $^{89}$Zr-trastuzumab injections at baseline and at day 15 of cycle 1. For patients with ER positive breast cancer, who consented to the $^{89}$Zr-bevacizumab PET imaging side study, a similar time frame was used after injection of 37 MBq/ 5 mg $^{89}$Zr-bevacizumab. Clinical grade $^{89}$Zr-bevacizumab was produced as described earlier[26]. $^{89}$Zr-trastuzumab and $^{89}$Zr-bevacizumab distribution were scored visually and quantitatively by calculating the mean and maximum standardized uptake values ($SUV_{mean/max}$) at baseline and following NVP-AUY922 treatment (SBG, AHB). If > 10 tumor lesions were visualized in one organ, then 10 were quantified. A high correlation was found between $SUV_{mean}$ and $SUV_{max}$ for healthy organs and tumor lesions (Pearson $r^2 = 0.99$ and $r^2 = 0.97$ respectively, $P < 0.0001$). Since it is less operator dependent, we present data as $SUV_{max}$. Response on $^{89}$Zr-trastuzumab and $^{89}$Zr-bevacizumab PET was compared with the response on CT after 8 weeks, only lesions of at least 1.0 cm were used to compare.

### Pharmacodynamic markers

HSP70 and HER2-ECD were quantified by enzyme linked immunosorbent assays (ELISA) in PBMC and serum samples, respectively. PBMC samples were collected pre-treatment and 5, 24 and 48 hours post dose and prior to infusion on day 8. Serum samples were collected at baseline, pre-treatment at cycle 1 and 2 day 1, day 3, day 8, day 15 and every odd cycle.

### Assessment of tumor response by CT and FDG-PET

Imaging included a CT-scan of the chest, abdomen and pelvis, performed pre-treatment and at the end of every even cycle. CT-scans were assessed for tumor response by two independent radiologists according to RECIST1.0 criteria[30]. All patients with a partial response (PR) or complete response (CR) were required to have confirmation of response performed ≥ 4 weeks after the criteria for response were first met. In case of stable disease (SD), follow-up measurements must have met SD criteria at least once after study entry at a minimum interval of 6 weeks. The best overall response was defined as the best response recorded from the start of the treatment until disease progression or withdrawal from the

study. Clinical benefit rate was defined as CR+PR+SD. In a waterfall plot, best change in longitudinal tumor size will be presented. Whole body FDG-PET scans were performed at baseline and after 4 and 8 weeks. The acquisition protocol was standardized across sites. Patient needed to fast for approximately 6 hours prior to FDG-PET scanning. The patient was encouraged to maintain good hydration. Glucose levels were measured prior to the administration of FDG. The patient needed a blood glucose value of ≤200 mg/dL in order for the patient to have the FDG-PET. These scans were assessed per center by two independent nuclear medicine specialists blinded for clinical information. FDG-PET scans were assessed for new tumor lesions. In addition, up to five lesions with the highest uptake were identified on the baseline scans as index lesions. The index lesions were scored quantitatively by calculating the maximal standardized uptake value ($SUV_{max}$). The percentage of change was subsequently calculated. The definitions for metabolic response were defined according to the EORTC, into a group with CR or PR (< –25%), a group with SD (–25% to +25%), and a group with PD (> +25% and/or new tumor lesions)[32]. Response on FDG-PET was compared with the response on CT after 8 weeks, only lesions in the field of view of the CT and a size of at least 1.0 cm were used to compare.

## Drug concentration measurements and pharmacokinetic (PK) assessment

Blood sampling to characterize PK was performed on cycle 1 day 1, immediately prior to NVP-AUY922 infusion, 5 minutes, 15 minutes, 30 minutes during NVP-AUY922 infusion, immediately prior to the end of the infusion, at 5 minutes, 30 minutes, 1, 2, 4, 5, 8, 24, 48 and 72 hours post infusion and prior to infusion on day 8. The sample was centrifuged at a minimum of 1500 *g* for 15 minutes and all plasma was transferred in tubes. An additional 2 mL of whole blood was obtained for plasma assay of NVP-AUY922 and its pharmacologically inactive metabolite BJP762 at the following time points: on cycle 1 day 1 at the end of the infusion, and then 1, 5 and 24 hours post infusion. Due to the light sensitivity of NVP-AUY922 and its lack of stability in handling, all blood samples were protected from light during collection, handling, and processing and then stored at -70°C.

The blood and plasma samples collected were assayed for NVP-AUY922 and BJP762 concentrations by Novartis using a validated liquid chromatography-tandem mass spectrometry assay (LC-MS/MS). Values below the lower limit of quantification of 0.8 ng/mL were reported as 0.00 ng/mL. PK parameters were determined by non-compartimental method using WinNonlin Pro (Version 5.2).

## Statistical analysis

All clinical data were collected by electronic data capture (Timaeus). Data are presented as mean ± standard deviation and range. Statistical analysis was performed using a paired sampled T-test for paired data. For correlation of the companion biomarker with RECIST 1.0 the Pearson's test was used. The Kaplan-Meier method was used to estimate rates of progression over time and median times to progression (SPSS, version 19). All testing was two-sided at 5% level of significance.

# Results

## Patient characteristics

Sixteen patients were enrolled between February 2010 and July 2011. Baseline characteristics are summarized in Table 1. All patients have discontinued treatment (range 1-11 months), 13 (81%) because of radiological disease progression and two patients because of clinical progression (13%). One patient (6%) stopped treatment because of grade 2 nausea which did not resolve after dose reduction.

**Table 1.** Patient characteristics at study entry.

| | Patients with HER2 positive BC *n* = 10 (%) | Patients with ER positive BC *n* = 6 (%) | All patients *n* = 16 (%) |
|---|---|---|---|
| Age-years (SD) | 54.6 (10.5) | 56.2 (9.0) | 55.2 (9.7) |
| Predominant race-n (%) | | | |
| Caucasian | 8 (80.0) | 6 (100.0) | 14 (87.5) |
| Black | 1 (10.0) | 0 | 1 (6.3) |
| Other | 1 (10.0) | 0 | 1 (6.3) |
| Body surface area-m$^2$ (SD) | 1.9 (0.3) | 1.8 (0.3) | 1.8 (0.3) |
| LVEF* (%) (SD) | 64.7 (11.1) | 62.3 (6.8) | 63.8 (9.5) |
| WHO Performance Status | | | |
| 0 | 7 (70.0) | 5 (83.3) | 12 (75.0) |
| 1 | 3 (30.0) | 1 (16.7) | 4 (25.0) |
| Tumor stage | | | |
| III | 1 (10) | 1 (16.7) | 2 (12.7) |
| IV | 9 (90) | 5 (83.3) | 14 (87.5) |
| Number of earlier regimens | | | |
| 1 | 1 | 0 | 1 |
| 2 | 0 | 1 | 1 |
| 3 | 3 | 0 | 3 |
| 4 | 3 | 4 | 7 |
| >4 | 3 | 1 | 4 |
| Other | 1 | 0 | 1 |

*Left ventricular ejection fraction

## Toxicity

The actual cumulative administered doses of NVP-AUY922 were lower than planned: 951.2 mg/m$^2$ versus 1175.4 mg/m$^2$. Eight patients required a dose reduction to 54 mg/m$^2$. Median time to reduction was 2.5 weeks (range 2-6). The most frequent adverse events (all grades, regardless of causality) were summarized in Table S1. Nine serious adverse events occurred in 6 (37.5%) of the patients, none of which were suspected to be related to study drug. Scan procedures were uneventful, except in one case, in which the patient developed

shivering, rigors, and bronchospasm after $^{89}$Zr-trastuzumab administration. This was completely reversed within 10 minutes by hydrocortisone and chlorpheniramine administration, in line with a mild allergic reaction to trastuzumab. No more scan procedures with $^{89}$Zr-trastuzumab were performed in this patient.

## PET imaging

Repeated FDG-PET could be performed in 8 of 10 patients with HER2 positive breast cancer, and in all of 6 patients with ER positive breast cancer. Best percentage change from baseline for FDG-PET $SUV_{max}$ is shown graphically in Figure 1. Partial metabolic response was seen in 5 patients, four with HER2 positive breast cancer and 1 with ER positive breast cancer. Mean decrease in $SUV_{max}$ on FDG-PET after 4 and 8 weeks, was 12% ± 22% and 7% ± 30% respectively ($P$ = 0.09). Response on FDG-PET was not correlated with response on CT after 8 weeks ($r^2$ = 0.18; $P$ = 0.12 at 4 weeks and $r^2$ = 0.17; $P$ = 0.13 at 8 weeks).

**Figure 1.**

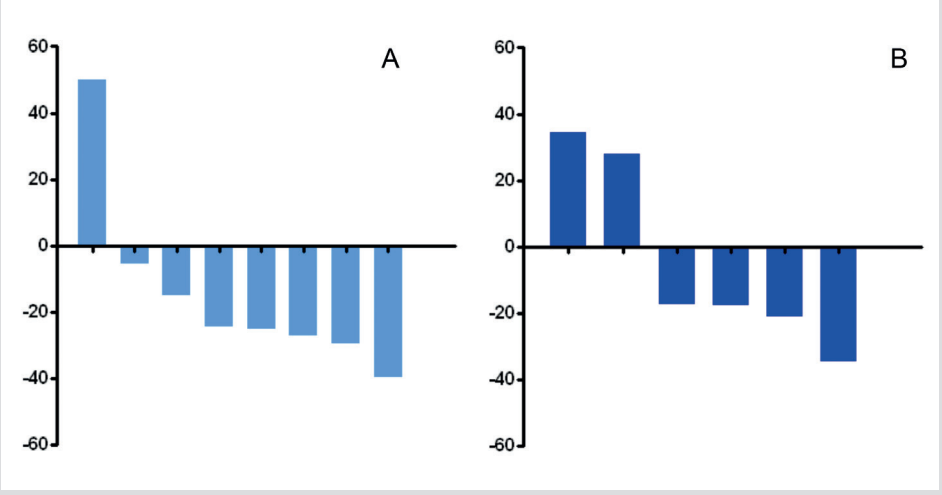


Maximal percentage change in $SUV_{max}$ of target lesions on FDG-PET between baseline and after 3 weeks of treatment, in patients with HER2 positive (A) and ER positive (B) breast cancer. Repeated FDG-PET could be performed in 8 of 10 patients with HER2 positive breast cancer, and in all of 6 patients with ER positive breast cancer.

Repeated $^{89}$Zr-trastuzumab PET could be performed in 5 patients with HER2 positive disease, one patient only received the baseline scan. Twenty-nine lesions were visible on $^{89}$Zr-trastuzmab PET. Visual analysis of PET imaging showed a time dependent accumulation of $^{89}$Zr-trastuzumab within the tumors at day 2 and 4 after $^{89}$Zr-trastuzumab injection. The following analyses therefore reflect day 4 data from $^{89}$Zr-trastuzumab PET at baseline and during treatment (the latter is now referred to as 3 week scan). Figure 2 shows a representative $^{89}$Zr-trastuzumab PET. The mean $SUV_{max}$ of $^{89}$Zr-trastuzumab uptake at baseline was 9.0 ± 7.6 (0.9-26.9), decreasing during treatment to 7.8 ± 6.3 (range 0.7-24.2, $P$ = 0.047). Heterogeneous treatment effect on $SUV_{max}$ in the 29 individual tumor lesions was observed, both within and between patients (Figure 2; Table S3). There was a correlation between the mean decrease in SUV on $^{89}$Zr-trastuzumab PET scans after 3 weeks compared to baseline, and the change of size of tumor lesions on CT after 8 weeks of treatment compared to baseline ($r^2$ = 0.69, $P$ = 0.006) (Figure 3).

**Figure 2.**

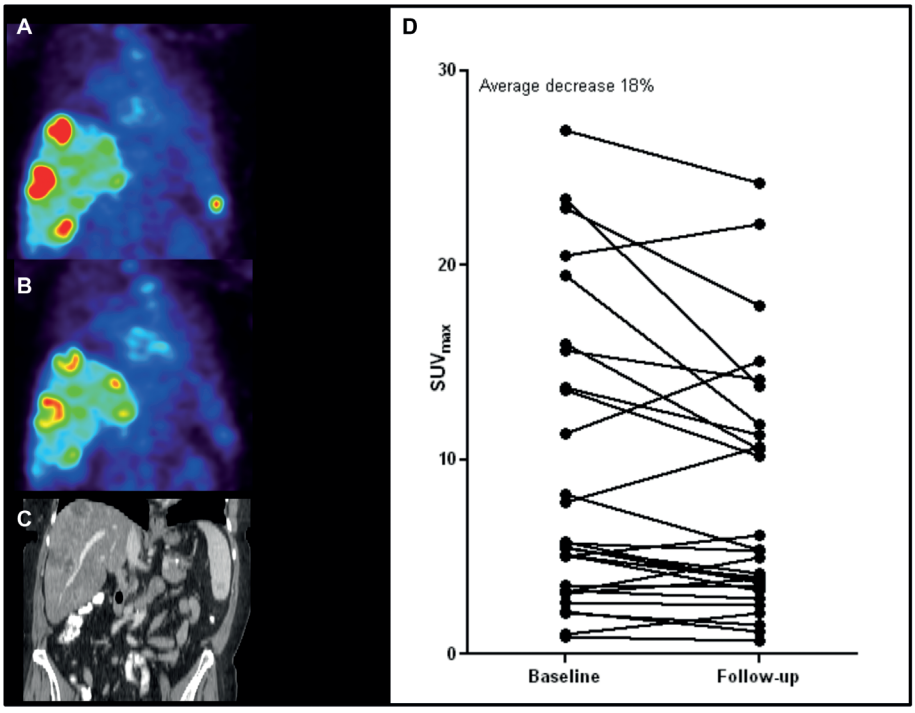


Representative coronal $^{89}$Zr-trastuzuzmab PET images of a patient scanned before (A) and after (B) 3 weeks of treatment. Multiple liver lesions and one splenic lesion are shown. $^{89}$Zr-trastuzumab PET could be performed in 6 of 10 HER2 positive patients of which 5 underwent repeated scan procedures. The CT-scan pre-treatment is shown in panel C. Panel D shows a heterogeneous response in individual tumor lesions (n = 29) between baseline and follow-up, with an average decrease in $SUV_{max}$ of 18%.

**Figure 3.**

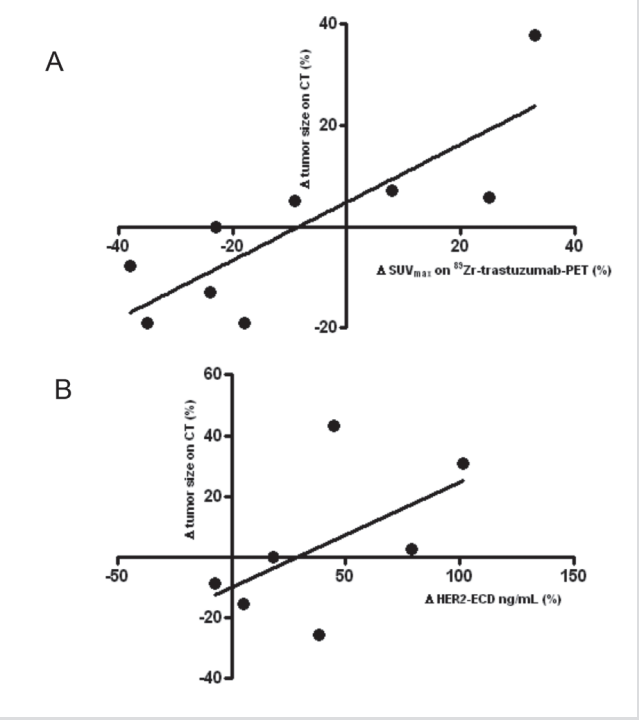


Panel A shows correlation of percentage change in $SUV_{max}$ of $^{89}$Zr-trastuzumab (x-axis) per lesion (n = 9) between baseline $^{89}$Zr-trastuzumab-PET of 5 patients and after 3 weeks NVP-AUY922 treatment, and change in size of corresponding lesions on CT (y-axis) between baseline and after 8 weeks treatment with NVP-AUY922 (y-axis) ($r^2$ = 0.69, *P* = 0.0057). Panel B shows correlation of maximal increase of HER2-ECD (n = 6) compared to baseline (x-axis), and change in size of CT in all target lesions of an individual patient (y-axis) ($r^2$ = 0.69, *P* = 0.02).

Of patients with ER positive breast cancer, 5 underwent a repeated $^{89}$Zr-bevacizumab PET scan, one patient only received the baseline scan. Visual analysis of PET imaging at day 2 and 4 post tracer injection showed a time dependent accumulation of $^{89}$Zr-bevacizumab within the tumor lesions, with on day 4 a 1.12 fold higher $^{89}$Zr-bevacizumab tumor uptake compared to day 2. The following analyses therefore reflect day 4 data from $^{89}$Zr-bevacizumab PET at baseline and during treatment. Figure 4 shows a representative $^{89}$Zr-bevacizumab-PET. $SUV_{max}$ on the day 4 scan at baseline was 2.3 ± 1.1 (range 0.9-5.2) which was unaffected during treatment with 2.4 ± 1.4 (range 0.6-6.6) (*P* = 0.56). Because of a high physiologic liver uptake of $^{89}$Zr-bevacizumab, liver lesions could not be visualized, except for two patients in whom the liver metastases were not accumulating $^{89}$Zr-bevacizumab, therefore leaving a 'cold' spot that could be visualized. Twenty-three lesions at baseline were detected in five patients, 20 of them were bone lesions which were also detected on FDG-PET, but not measurable on CT (Table S4).

**Figure 4.**

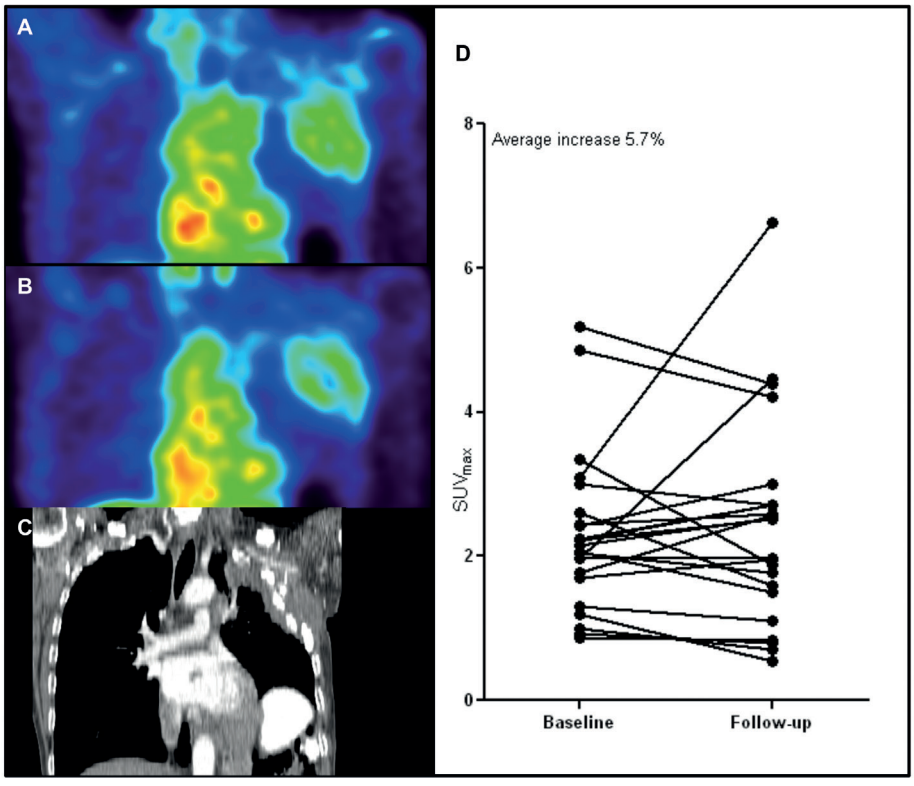


Representative coronal [89]Zr-bevacizumab PET images of a patient scanned before (A) and after (B) 3 weeks of treatment. The patient had a large tumor mass in the chest wall. [89]Zr-bevacizumab PET could be performed in 6 of 10 patients of which 5 underwent repeated scan procedures. The CT-scan pre-treatment is shown in panel C. Panel D shows a heterogeneous response in individual tumor lesions (n = 23) between baseline and follow-up, with an average increase of $SUV_{max}$ of 5.7%.

## Biomarkers

At baseline, measurement of HSP70 levels in PMBCs was performed in 15 patients. Median HSP70 levels were 29.0 ng/mg (range 10.0-69.1). Between baseline and follow up measurements, the medium of all maximal HSP70 increases in PBMCs in these patients was 359.4% ± 350.5. The induction in HSP70 confirmed target inhibition defined in a previous phase 1 study[29]. A higher baseline level of HER2-ECD was correlated with a larger tumor size decrease on CT, (Pearson $r^2 = 0.60$; $P = 0.025$). The median of maximal HER2-ECD increase was 13.6% ± 33.4%, which was also positively correlated with tumor size decrease after 8 weeks of treatment (Pearson $r^2 = 0.69$; $P = 0.020$).

**Figure 5.**

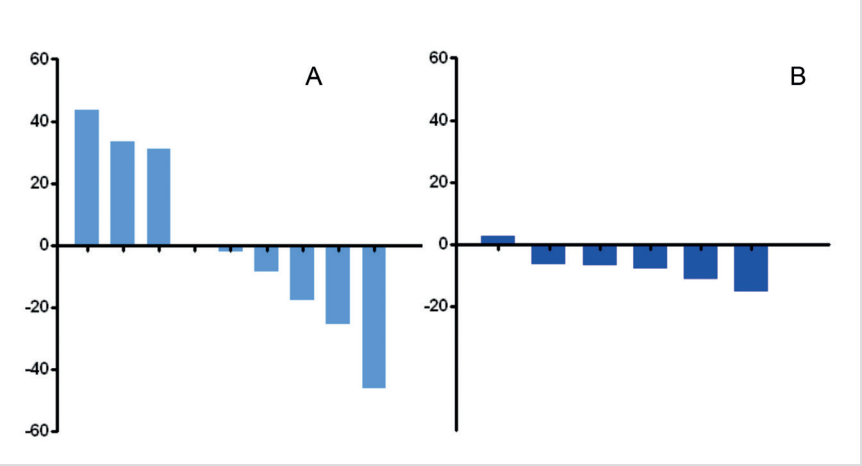


Maximal percentage change in sum of longitudinal axis of target lesions on CT, between baseline and 8 weeks of treatment in patients with HER2 positive (A) and ER positive (B) breast cancer. Repeated CT was performed in 9 of 10 patients with HER2 positive breast cancer and in all 6 patients with ER positive breast cancer.

## Efficacy

One patient with HER2 positive breast cancer experienced a confirmed PR after 8 weeks. An additional seven patients (3 with HER2 positive breast cancer and 4 with ER positive breast cancer) experienced confirmed SD (Table 2), resulting in a disease control rate of 50% (95% confidence interval 24.7%-75.3%). Median time to progression was 3 months (range 1-10). Five patients experienced time to progression >6 months. A waterfall plot of best responses on CT showed a decrease of mean tumor size in most patients (Figure 5).

## Pharmacokinetics

Supplementary Figure 1 shows mean blood concentration-time profiles for NVP-AUY922 (A) and its metabolite BJP762 (B). Following the initial rapid decline in concentration levels after the infusion, NVP-AUY922 was eliminated slowly with a flat terminal phase half life of 120 hours (range 54-404). Area under de curve (AUC) from time zero until the last measurable samples were $7.7*10^3 \pm 2.5*10^3$ and $4.5*10^3 \pm 2.0*10^3$ for respectively AUY922 and BJP762 in the HER2 group and $9.9*10^3 \pm 2.6*10^3$ and $1.3*10^4 \pm 2.1*10^4$ for respectively AUY922 and BJP762 in the ER group. Peak concentrations were observed at the end of infusion for both NVP-AUY922 and BJP762, suggesting the rapid biotransformation from NVP-AUY922 to BJP762 *in vivo*. It should be noted that whole blood AUY922 is measured, including the fraction encapsulated in red blood cells (which is not available for metabolization): this makes the apparent half-life longer for parent AUY922 as compared to its metabolite BJP762. These results were in line with the findings in the first in human phase I and ongoing phase II studies[29,33].

# Discussion

This study provides early evidence that the change between tumor uptake on baseline and early $^{89}$Zr-trastuzumab PET after 3 weeks of treatment with HSP90 inhibitor NVP-AUY922, had a moderate positive correlation with change in tumor size on CT after 8 weeks of treatment. In contrast, early FDG-PET, performed after 4 weeks of treatment, did not correlate with change in tumor size on the 8 week CT.

In a preclinical model, $^{18}$F-FDG uptake was minimally affected by NVP-AUY922 administered to a spheroid model with BT474 breast cancer cells[34]. Previously, 17AAG effect could be visualized *in vivo* by reduced radiolabeled trastuzumab uptake, but not by means of FDG-PET[24]. These results all support that more specific imaging of targets is more useful to assess the effects of HSP90 inhibition. In human tumor-bearing mice, we showed that HER2 and VEGF downregulation could be visualized after treatment with an HSP90 inhibitor[22,23]. Now also in the clinical setting, we observed that novel PET probes such as $^{89}$Zr-trastuzumab can potentially be used to provide whole body insights into response of HER2 amplified breast cancer to NVP-AUY922. Interestingly, we found a heterogeneous effect on the $SUV_{max}$, within tumor lesions, both within and between patients. This effect was in line with both heterogeneous intra- and inter patient tumor responses on CT. A further application of $^{89}$Zr-trastuzumab PET could be predefining areas of tumor that are not responding to targeted treatment with HSP90 inhibitors such as NVP-AUY922. Biopsying such areas would provide valuable insights in the biology of HSP90 resistance in the tumor. Also interlesional heterogeneity of gene expression is increasingly recognized as a relevant factor which is likely to affect treatment response[35,36]. The precise clinical implications of *in vivo* heterogeneity of HER2 expression are currently further investigated in the Dutch multicenter IMPACT breast trial (Trial Registration ID: NCT01832051). With regard to the use of $^{89}$Zr-trastuzumab- or $^{89}$Zr-bevacizumab PET it should be taken into account that not much is known about reproducibility of the scans in cancer patients. However, a test-retest set up for this type of scan requires an interval of at least two weeks because of the particularly long half-life of $^{89}$Zr-tracers. Such an interval would require otherwise stable conditions, which is not typically the case in metastatic cancer patients. As a result, variation in measurements can also be induced by a factor such as tumor growth. In addition, the often necessary start of systemic treatment in (rapidly) progressive disease, would induce further variability. In a preclinical study there was no significant difference in uptake of $^{89}$Zr-trastuzumab-F(ab')$_2$ in SKBR3 tumor bearing mice without treatment (interval between two scans 7 days)[37].

We did not find a correlation between uptake change on $^{89}$Zr-bevacizumab PET and CT. This could be due to the fact that most lesions found on $^{89}$Zr-bevacizumab PET were bone lesions which were not measurable on CT. Another potentially contributing factor is that HIF-1$\alpha$ is likely a less prominent client protein of HSP90 than HER2[38]. HSP90 can influence

angiogenesis in multiple ways, including degradation of HIF-1α which drives production of VEGF or degradation of VEGF receptor. Although angiogenesis is a hallmark of cancer[39], inhibition of angiogenesis is less critical to response to treatment of breast cancer as evidenced by an increasing number of studies showing no clinical benefit of bevacizumab in breast cancer[40,41]. Moreover in breast tumors, $^{89}$Zr-bevacizumab uptake was consistently lower than in renal cell cancer[25,27]. In view of this, the fact that ER itself is influenced by HSP90 inhibition, and that it is now possible to visualize ER on tumor lesions by means of whole body $^{18}$Fluorestradiol (FES) PET, it would be of great interest to use FES-PET in patients with ER positive breast cancer receiving HSP90 inhibition. However, at time of design of this study FES was not clinically available in our clinic. So, while $^{89}$Zr-bevacizumab PET cannot be used to assess treatment response, a recent clinical study in breast cancer patients indicated that it may be of use in the setting of primary tumor detection[27]. In addition, in patients with HER2 positive metastatic breast cancer, HER2-ECD at baseline and decrease during treatment, positively correlated with tumor response. This is in line with a previous trial, in which HER2-ECD also correlated to trastuzumab and paclitaxel response[28]. Pharmacodynamic markers such as HSP70 induction and PK parameters confirmed pharmacokinetic and pharmacodynamic findings observed in a previous phase I study[29].

In the present trial, we found an encouraging clinical benefit rate of 50% in heavily pre-treated breast cancer patients with progressive disease at start of treatment. Studies with first generation HSP90 inhibitors only demonstrated modest clinical benefit in HER2 amplified breast cancer[30], however in this trial the clinical benefit was also seen in ER positive breast cancer. NVP-AUY922 is currently further evaluated in combination with trastuzumab and has shown encouraging results in a phase II study[17]. In light of our results, it would also be of interest to further evaluate HSP90 inhibition for the treatment of ER positive metastatic breast cancer, particularly because the ER itself is a client protein of HSP90.

Concluding, in this clinical trial in patients with advanced HER2 or ER positive metastatic breast cancer, effect of treatment with HSP90 inhibitor NVP-AUY922, on *in vivo* degradation of HER2 and VEGF was assessed with $^{89}$Zr-trastuzumab PET or $^{89}$Zr-bevacizumab PET. $^{89}$Zr-trastuzumab PET results at 3 weeks positively correlated with CT responses in individual lesions. Thus novel PET probes such as $^{89}$Zr-trastuzumab might provide insights into responses to novel agents active in HER2 amplified breast cancer, such as NVP-AUY922. This finding should be assessed in further, larger studies.

## Acknowledgments

The authors would like to thank J.R. de Jong, H.H. Nienhuis, G. Sieling and L. Pot for assistance. This clinical trial was in part designed at the 2007 ECCO-AACR-ASCO 9th Workshop: Methods in Clinical Cancer Research (Flims, Switzerland by C.P. Schröder).

# References


1. Chia SK, Speers CH, D'yachkova, et al. The impact of new chemotherapeutic and hormone agents on survival in a population-based cohort of women with metastatic breast cancer. Cancer 2007; 110:973-9.
2. Gennari A, Conte P, Rosso R, et al. Survival of metastatic breast carcinoma patients over a 20-year period: A retrospective analysis based on individual patient data from six consecutive studies. Cancer 2005; 1041742-50.
3. Banerji U. Heat shock protein 90 as a drug target: Some like it hot. Clin Cancer Res 2009; 15:9-14.
4. Banerji U, Walton M, Raynaud F, et al. Pharmacokinetic-pharmacodynamic relationships for the heat shock protein 90 molecular chaperone inhibitor 17-allylamino, 17-demethoxygeldanamycin in human ovarian cancer xenograft models. Clin Cancer Res 2005; 11:7023-32.
5. Bagatell R, Khan O, Paine-Murrieta G, et al. Destabilization of steroid receptors by heat shock protein 90-binding drugs: A ligand-independent approach to hormonal therapy of breast cancer. Clin Cancer Res 2001; 7:2076-84.
6. Lee MO, Kim EO, Kwon HJ, et al. Radicicol represses the transcriptional function of the estrogen receptor by suppressing the stabilization of the receptor by heat shock protein 90. Mol Cell Endocrinol 2002; 188:47-54.
7. Wainberg ZA, Anghel A, Rogers AM, et al. Inhibition of HSP90 with AUY922 induces synergy in HER2-amplified trastuzumab-resistant breast and gastric cancer. Mol Cancer Ther 2013; 12:509-19.
8. Eccles SA, Massey A, Raynaud FI, et al. NVP-AUY922: A novel heat shock protein 90 inhibitor active against xenograft tumor growth, angiogenesis, and metastasis. Cancer Res 2008; 68:2850-60.
9. Forsythe JA, Jiang BH, Iyer NV, et al. Activation of vascular endothelial growth factor gene transcription by hypoxia-inducible factor 1. Mol Cell Biol 1996; 16:4604-13.
10. Ferrarini M, Heltai S, Zocchi MR, et al. Unusual expression and localization of heat-shock proteins in human tumor cells. Int J Cancer 1992; 51:613-9.
11. Kamal A, Thao L, Sensintaffar, et al. A high-affinity conformation of Hsp90 confers tumour selectivity on Hsp90 inhibitors. Nature 2003; 425:407-10.
12. Brough PA, Aherne W, Barril X, et al. 4,5-diarylisoxazole Hsp90 chaperone inhibitors: Potential therapeutic agents for the treatment of cancer. J Med Chem 2008; 51:196-218.
13. Jensen MR, Schoepfer J, Radimerski T, et al. NVP-AUY922: A small molecule HSP90 inhibitor with potent antitumor activity in preclinical breast cancer models. Breast Cancer Res 2008; 10:R33.
14. Sequist LV, Gettinger S, Senzer NN, et al. Activity of IPI-504, a novel heat-shock protein 90 inhibitor, in patients with molecularly defined non-small-cell lung cancer. J Clin Oncol 2010; 28:4953-60.
15. Pacey S, Wilson RH, Walton M, et al. A phase I study of the heat shock protein 90 inhibitor alvespimycin (17-DMAG) given intravenously to patients with advanced solid tumors. Clin Cancer Res 2011; 17:1561-70.
16. Modi S, Stopeck AT, Linden HM, et al. HSP90 inhibition is effective in breast cancer: A phase 2 trial of tanespimycin (17AAG) plus trastuzumab in patients with HER2-positive metastatic breast cancer progressing on trastuzumab. Clin Cancer Res 2011; 7:5132-9.
17. Kong A. Phase IB/II study of the HSP90 inhibitor AUY922, in combination with trastuzumab, in patients with HER2+ advanced breast cancer. J Clin Oncol (Meeting Abstracts) May 2012 vol 30 no 15_suppl 530.
18. Friedberg JW, Chengazi V. PET scans in the staging of lymphoma: Current status. Oncologist 2003; 8:438-47.
19. Torizuka T, Nakamura F, Kanno T, et al. Early therapy monitoring with FDG-PET in aggressive non-Hodgkin's lymphoma and Hodgkin's lymphoma. Eur J Nucl Med Mol Imaging 2004; 31:22-8.
20. Weber WA. Use of PET for monitoring cancer therapy and for predicting outcome. J Nucl Med 2005; 46:983-95.
21. Kelloff GJ, Hoffman JM, Johnson B, et al. Progress and promise of FDG-PET imaging for cancer patient management and oncologic drug development. Clin Cancer Res 2005; 11:2785-808.
22. Oude Munnink TH, Korte MA, Nagengast WB, et al. 89Zr-trastuzumab PET visualises HER2 downregulation by the HSP90 inhibitor NVP-AUY922 in a human tumour xenograft. Eur J Cancer 2010; 46:678-84.
23. Nagengast WB, de Korte MA, Oude Munnink TH, et al. 89Zr-bevacizumab PET of early antiangiogenic tumor response to treatment with HSP90 inhibitor NVP-AUY922. J Nucl Med 2010; 51:761-7.
24. Smith-Jones PM, Solit D, Afroze F, et al. Early tumor response to Hsp90 therapy using HER2 PET: Comparison with 18F-FDG PET. J Nucl Med 2006; 47:793-6.
25. Oosting SF, Brouwers AH, Van Es SC, et al. 89Zr-bevacizumab PET imaging in metastatic renal cell carcinoma patients before and during antiangiogenic treatment. J Clin Oncol (Meeting Abstracts) 2012; suppl abstr 10581.
26. Dijkers EC, Oude Munnink TH, Kosterink JG, et al. Biodistribution of 89Zr-trastuzumab and PET imaging of HER2-positive lesions in patients with metastatic breast cancer. Clin Pharmacol Ther 2010; 87:586-92.
27. Gaykema SB, Brouwers AH, Lub-de Hooge MN, et al. 89Zr-bevacizumab PET imaging in primary breast cancer. J Nucl Med 2013; 54:1014-8.

28. Fornier MN, Seidman AD, Schwartz MK, et al. Serum HER2 extracellular domain in metastatic breast cancer patients treated with weekly trastuzumab and paclitaxel: Association with HER2 status by immunohistochemistry and fluorescence in situ hybridization and with response rate. Ann Oncol 2005; 16:234-9.
29. Sessa C, Shapiro GI, Bhalla KN, et al. First-in-human phase I dose-escalation study of the HSP90 inhibitor AUY922 in patients with advanced solid tumors. Clin Cancer Res 2013; 19:3671-80.
30. Therasse P, Arbuck SG, Eisenhauer EA, et al. New guidelines to evaluate the response to treatment in solid tumors. European Organization for Research and Treatment of Cancer, National Cancer Institute of The United States, National Cancer Institute of Canada. J Natl Cancer Inst 2000; 92:205-16.
31. Dijkers EC, Kosterink JG, Rademaker AP, et al. Development and characterization of clinical-grade 89Zr-trastuzumab for HER2/neu immunoPET imaging. J Nucl Med 2009; 50:974-81.
32. Young H, Baum R, Cremerius U, et al. Measurement of clinical and subclinical tumour response using [18F]-fluorodeoxyglucose and positron emission tomography: Review and 1999 EORTC recommendations. European Organization for Research and Treatment of Cancer (EORTC) PET study group. Eur J Cancer 1999; 35:1773-82.
33. Schröder CP, Pedersen JV, Chua S, et al. Use of biomarkers and imaging to evaluate the treatment effect of AUY922, an HSP90 inhibitor, in patients with HER2+ or ER+ metastatic breast cancer. J Clin Oncol (Meeting Abstracts) 2011; suppl abstr e11024.
34. Bergstrom M, Monazzam A, Razifar P, et al. Modeling spheroid growth, PET tracer uptake, and treatment effects of the Hsp90 inhibitor NVP-AUY922. J Nucl Med 2008; 49:1204-10.
35. Hanna WM, Ruschoff J, Bilous M, et al. HER2 in situ hybridization in breast cancer: Clinical implications of polysomy 17 and genetic heterogeneity. Mod Pathol 2014; 27:4-18.
36. Gerlinger M, Rowan AJ, Horswell S, et al. Intratumor heterogeneity and branched evolution revealed by multiregion sequencing. N Engl J Med 2012; 366:883-92.
37. Oude Munnink TH, de Vries EG, Vedelaar SR, et al. Lapatinib and 17AAG reduce 89Zr-trastuzumab-F(ab')2 uptake in SKBR3 tumor xenografts. Mol Pharm 2012; 9:2995-3002.
38. Sain N, Krishnan B, Ormerod MG, et al. Potentiation of paclitaxel activity by the HSP90 inhibitor 17-allylamino-17-demethoxygeldanamycin in human ovarian carcinoma cell lines with high levels of activated AKT. Mol Cancer Ther 2006; 5:1197-208.
39. Hanahan D, Weinberg RA. Hallmarks of cancer: The next generation. Cell 2011; 144:646-74.
40. Brufsky AM, Hurvitz S, Perez E, et al. RIBBON-2: A randomized, double-blind, placebo-controlled, phase III trial evaluating the efficacy and safety of bevacizumab in combination with chemotherapy for second-line treatment of human epidermal growth factor receptor 2-negative metastatic breast cancer. J Clin Oncol 2011; 29:4286-93.
41. Robert NJ, Dieras V, Glaspy J, et al. RIBBON-1: Randomized, double-blind, placebo-controlled, phase III trial of chemotherapy with or without bevacizumab for first-line treatment of human epidermal growth factor receptor 2-negative, locally recurrent or metastatic breast cancer. J Clin Oncol 2011; 29:1252-60.

# Supplementary files

**Figure 1.**

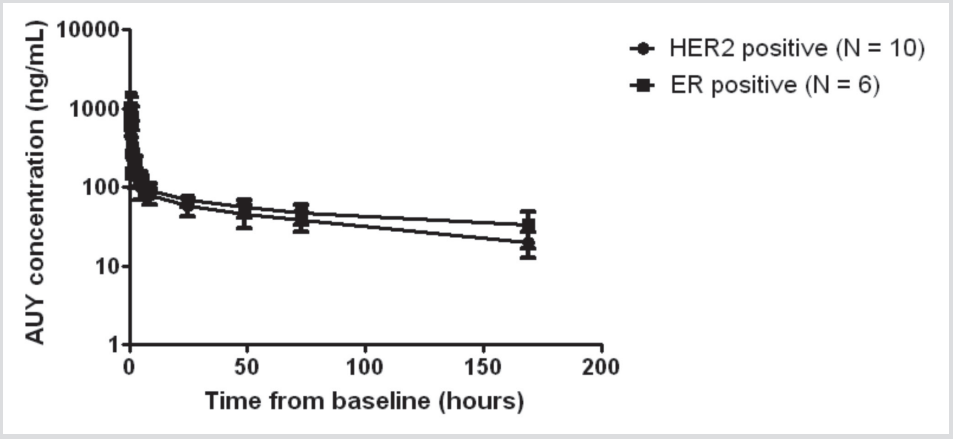


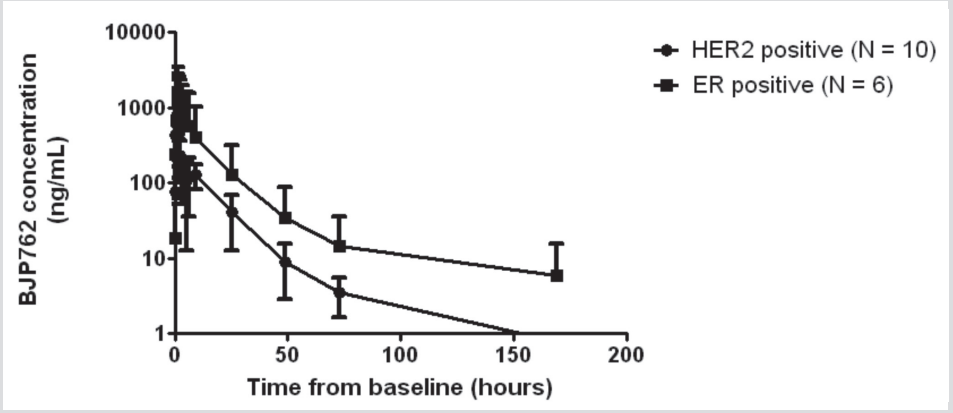


Arithmetic mean concentration-time profiles for AUY922 (A) and BJP762 (B) blood levels in hours post NVP-AUY922 infusion.

**Table 1.** Most common adverse events (occurring in at least 10 % of patients).

| | All patients n = 16 n (%) |
|---|---|
| Patients with at least one AE | 16 (100.0) |
| Diarrhea | 16 (100.0) |
| Fatigue | 13 (81.3) |
| Night blindness | 11 (68.8) |
| Nausea | 10 (62.5) |
| Vision blurred | 8 (50.0) |
| Headache | 7 (43.3) |
| Photopsia | 7 (43.8) |
| Decreased appetite | 5 (31.3) |
| Vomiting | 5 (31.3) |
| Back pain | 4 (25.0) |
| Rash | 4 (25.0) |
| Abdominal pain | 3 (18.8) |
| Anemia | 3 (18.8) |
| Dry mouth | 3 (18.8) |
| Non-cardiac chest pain | 3 (18.8) |
| Pain in extremity | 3 (18.8) |
| ALAT increased | 2 (12.5) |
| Constipation | 2 (12.5) |
| Cough | 2 (12.5) |
| Halo vision | 2 (12.5) |
| Muscle spasms | 2 (12.5) |
| Pain of skin | 2 (12.5) |
| Photophobia | 2 (12.5) |
| Retinogram abnormal | 2 (12.5) |
| Urinary tract infection | 2 (12.5) |
| Weight decrease | 2 (12.5) |

**Table 2.** Adverse events with CTCAE grades 3 and 4 regardless of causality.

| | All patients n = 16 n (%) |
|---|---|
| Patients with at least one grade 3 or 4 AE | 7 (43.8) |
| ALAT increased | 2 (12.5) |
| Dyspnea | 1 (6.3) |
| Flank pain | 1 (6.3) |
| Hyperbilirubinemia | 1 (6.3) |
| Hypercalcemia | 1 (6.3) |
| Malignant pleural effusion | 1 (6.3) |
| Night blindness | 1 (6.3) |
| Pleural effusion | 1 (6.3) |
| Urosepticemia | 1 (6.3) |
| Vomiting | 1 (6.3) |

**Table 3.** $^{89}$Zr-trastuzumab uptake per lesion and per patient ($SUV_{max}$) before and during treatment with AUY-922.

| Patient | Uptake baseline scan ($SUV_{max}$) | Uptake 3week scan ($SUV_{max}$) |
|---|---|---|
| 202 | 22.9 | 17.9 |
| | 23.4 | 13.8 |
| | 26.9 | 24.2 |
| | 16.0 | 10.5 |
| | 13.5 | 10.2 |
| | 8.2 | 5.3 |
| | 2.1 | 1.5 |
| | 5.7 | 5.3 |
| | 5.5 | 3.7 |
| | 7.8 | 10.7 |
| 203 | 11.3 | 15.1 |
| | 3.3 | 2.8 |
| | 5.0 | 6.1 |
| | 20.5 | 22.1 |
| | 15.6 | 14.1 |
| | 5.1 | 3.9 |
| 204 | 5.8 | 3.7 |
| | 5.1 | 3.3 |
| | 5.1 | 3.8 |
| | 2.2 | 1.1 |
| | 0.9 | 0.7 |
| | 2.7 | 2.5 |
| | 19.4 | 11.8 |
| 205 | 13.7 | 11.3 |
| 207 | 1.4 | 4.1 |
| | 2.8 | 3.9 |
| | 3.5 | 4.0 |
| | 3.1 | 4.9 |
| | 2.8 | 4.9 |

**Table 4.** $^{89}$Zr-bevacizumab uptake per lesion and per patient ($SUV_{max}$) before and during treatment with AUY-922.

| Patient | Uptake baseline scan ($SUV_{max}$) | Uptake 3week scan ($SUV_{max}$) |
|---|---|---|
| 302 | 1.7 | 1.9 |
| | 2.5 | 2.6 |
| | 2.4 | 3.0 |
| | 2.0 | 2.0 |
| | 2.2 | 2.7 |
| | 2.2 | 2.5 |
| | 2.2 | 2.5 |
| 303 | 3.1 | 6.6 |
| 304 | 1.8 | 2.6 |
| | 2.6 | 1.6 |
| | 2.0 | 4.5 |
| | 2.2 | 2.7 |
| | 3.3 | 1.9 |
| 305 | 5.2 | 4.4 |
| | 2.1 | 2.1 |
| | 4.9 | 4.2 |
| 306 | 3.0 | 4.7 |
| | 2.1 | 1.8 |
| | 1.2 | 0.5 |
| | 1.3 | 1.1 |
| | 1.0 | 0.7 |
| | 0.9 | 0.8 |
| | 0.9 | 0.8 |

# CHAPTER 8

## Summary and future perspectives

# Summary

Cancer is treated with surgery, radiotherapy and/or systemic treatment including chemotherapy, targeted and immunotherapeutic anticancer drugs. Chemotherapeutic drugs have proven efficacy in several tumor types and their regimens differ in side effects. Therefore ongoing research is performed to find the most effective treatment with the fewest side effects. Targeted drugs aim at particular molecular tumor characteristics. Assessment of these characteristics prior to and early during treatment, can support treatment response prediction and treatment decisions at an early stage. This would clearly benefit the patient. In case of successful response prediction, patients who likely will not respond to a certain therapy do not have to suffer from the side-effects and can move on to another therapy sooner. Molecular tumor characterization is usually performed on the primary tumor, or on a metastasis biopsy. However, such a biopsy is not always feasible, and it can only provide static information disregarding possible conversion and heterogeneity of molecular characteristics[1,2]. In this setting, molecular imaging with for example positron emission tomography (PET) is of interest. It can be easily serially performed by developing a monocloncal antibody tracer against a tumor membrane receptor or a ligand. Examples are radiolabeled trastuzumab and bevacizumab, antibody directed against human epidermal growth factor receptor-2 (HER2) and vascular endothelial growth factor-A (VEGF-A).

This thesis aimed at improving cancer treatment and allocation, by assessing optimal treatment duration, detection and monitoring of treatment. Optimal chemotherapeutic regimen duration was evaluated in patients with gestational trophoblastic neoplasia. Detection of targets in tumor lesions as well as monitoring treatment response was evaluated in breast cancer patients by means of radio-labeled monoclonal antibody imaging of HER2 and VEGF-A.

**Chapter 1** provides a concise background and outline of this thesis.

In **chapter 2** treatment of gestational trophoblastic neoplasia is described. Therapy of low risk gestational trophoblastic neoplasia not responding to monotherapy and primary high risk gestational trophoblastic neoplasia consists of polychemotherapy. Currently standard treatment consists of actinomycin D (0.5 mg days 1-2), etoposide (100 mg/m$^2$ days 1-2), methotrexate (300 mg/m$^2$), folinic acid (15 mg), vincristine (0.8 mg/m$^2$ day 8), cyclophosphamide (600 mg/m$^2$ day 8) (EMA/CO). EMACP, a regimen consisting of etoposide (100 mg/m$^2$ days 1-5), methotrexate (300 mg/m$^2$ day 1), cyclophosphamide (600 mg/m$^2$ day 1), actinomycin D (0.5 mg/m$^2$ day 2) and cisplatin (50 mg/m$^2$ day 4) has also proven efficacy. Etoposide (100 mg/m$^2$ days 1-5) and cisplatin (20 mg/m$^2$ days 1-5) (EP) may be an alternative regimen with comparable efficacy and a shorter treatment time. After normalization of the βhCG serum levels, patients treated with EMACP received 2 additional consolidation cycles, which is not the case for EP. We evaluated the safety,

efficacy, and treatment time of EP. All patients with high risk gestational trophoblastic neoplasia who were treated since 2001 with EP at our institution were included in this cohort analysis and compared with the results of patients treated between 1984-2001 with EMACP. Thirteen patients started treatment with EP and and 16 patients with EMACP. With a median follow up duration of 173 months (range 11-344) overall survival rates are comparable for both regimens (EP 92.3%, EMACP 93.8%; $P = 0.88$). Median treatment time was shorter with EP (EP 78 days, range 63-84 days; EMACP 110 days, range 84-168 days; ($P = 0.006$). In this retrospective single institution analysis of the treatment of high risk gestational trophoblastic neoplasia, the EP regimen has survival rates in the same range as EMACP with comparable toxicity and a shorter treatment time.

In **chapter 3**, the role of molecular imaging in drug development is described where imaging of HER2 and VEGF serve as role models. Molecular imaging with radiolabeled monoclonal antibodies can give information about antibody tumor uptake and about presence of the target of the antibody in all tumor lesions across the patient's body. PET can be used to evaluate changes in targets as a consequence of treatment with monoclonal antibody and non-monoclonal antibody targeted drugs. It can also potentially contribute to optimal patient selection for targeted therapy.

Increasingly, the microenvironment of the primary tumor and its metastases is awarded a central role in the process of tumor progression and metastatic dissemination. Therefore, targeting factors in the microenvironment that support the process of tumor progression and metastases, can be a rational way to improve therapy of cancer patients. In **chapter 4**, we focus on the current knowledge of processes in the microenvironment involved in breast cancer. The number of drugs targeting key factors in these processes is expanding, and the available clinical data is increasing. Therefore current strategies for intervention and prediction of treatment response are outlined. At present, targeting the bone metastatic niche and obesity induced metabolic stimulation, have already shown to be clinically effective. Targeting the immune system is a field of great research interest in cancer treatment, currently showing very promising results in clinical trials. In earlier stages of development are compounds targeting tumor cell migration. However, targeting angiogenesis or matrix remodeling appears to be of limited clinical relevance in breast cancer treatment so far.



In **chapter 5**, the focus is HER2 again. We reported earlier on indium-111 ($^{111}$In)-trastuzumab scintigraphy in 17 patients with human epidermal growth factor receptor-2 (HER2) overexpressing metastatic breast cancer after the first loading dose of trastuzumab. In the present study, we present the analyses of the patients who underwent a baseline- and second scintigraphy procedure during trastuzumab treatment. This provided unique data to assess the presence of HER2 measured by $^{111}$In-trastuzumab uptake during treatment with trastuzumab. A loading-dose trastuzumab of 4 mg/kg, and thereafter once-a-week trastuzumab doses of 2 mg/kg for 11 weeks, and concomitant paclitaxel once every 3 weeks (175 mg/m$^2$) was administered. $^{111}$In-trastuzumab was injected on day 1 ($t = 0$) and after 11 weeks. Whole-body planar scintigraphy was acquired on 4 time points between 15

minutes- 7 days postinjection. Differences in tumor and organ uptake were determined from radiation dosimetric data and expressed as residence time (defined as area under the curve of radioactivity versus time). In total 25 tumor lesions in 12 patients were visualized, all on both scintigraphy procedures. The tumor residence time decreased by 19.6 ± 53.8% at $t = 1$ *v* $t = 0$, while $^{111}$In-trastuzumab uptake in most normal organs did not differ. $^{111}$In-trastuzumab levels in the cardiac blood pool were higher at *t = 1*. Change in residence time was not related with tumor response as measured by conventional imaging. So, trastuzumab treatment did not mask visualization of HER2 positive tumor lesions by $^{111}$In-trastuzumab scintigraphy.

In **chapter 5B,** the findings with Zirconium-89 ($^{89}$Zr)-trastuzumab PET in an exceptional patient are described. The patient described in this chapter had a history of two different breast tumors; one was HER2 negative, the other HER2 positive. Two years after diagnosis, metastases were found on CT. The tumor lesions were difficult to reach for a biopsy. On $^{89}$Zr-trastuzumab PET, there was uptake in the metastatic lesions, indicating the presence of HER2 as target for treatment. In line with the scan results, this patient was treated for HER2 positive metastatic breast cancer with paclitaxel and trastuzumab, with a partial tumor response.

The clinical feasibility of VEGF-A imaging by means of $^{89}$Zr-bevacizumab PET in primary breast cancer is shown in the study described in **chapter 6.** This study was performed to evaluate $^{89}$Zr-bevacizumab uptake in primary breast cancer. Prior to surgery, breast cancer patients underwent a PET/CT scan of breast and axillary regions, 4 days after 37 MBq $^{89}$Zr-bevacizumab administration. $^{89}$Zr-bevacizumab uptake was quantified as the maximum standardized uptake value ($SUV_{max}$) and correlated with VEGF-A expression measured by Enzyme-linked Immuno Sorbent Assay (ELISA) of tumor tissue. In 25 of the 26 tumor lesions we could visualize the tumor. $SUV_{max}$ was higher in tumors (1.85 ± 1.22, range 0.52-5.64) than in normal breast (0.59 ± 0.37; range, 0.27-1.69; $P < 0.001$) of individual patients. The only non-PET detected tumor was 10 mm in diameter, which was presumably below the detection limit of the camera. VEGF-A levels in 17 assessable tumors were higher compared to normal breast tissue in all cases (VEGF-A/mg protein 184 ± 169 pg *v* 10 ± 21 pg; $P = 0.001$), whereas $^{89}$Zr-bevacizumab uptake correlated with VEGF-A tumor levels (r = 0.49) measured by ELISA. Tumor specific imaging of VEGF-A is feasible in the vast majority of primary breast tumors.

One of the therapies for which molecular imaging could serve as an early biomarker is HSP90 inhibition. In preclinical models the HSP90 inhibitor NVP-AUY922 downregulates the expression of many oncogenic HSP90 client proteins (including HER2), and inhibits angiogenesis by downregulating hypoxia inducible factor 1α (HIF-1α) resulting in decreased VEGF-A excretion. In **chapter 7**, a phase 2 study with NVP-AUY922 in metastatic breast cancer patients is described. 70 mg/m$^2$ NVP-AUY922 was administered intravenously in a weekly schedule to patients with advanced HER2 or ER positive breast cancer. Biomarker analysis consisted of serial PET imaging with $^{18}$F-fluordeoxyglucose (FDG), $^{89}$Zr-trastuzumab or $^{89}$Zr-bevacizumab. Response evaluation was performed according to

RECIST1.0. FDG, $^{89}$Zr-trastuzumab and $^{89}$Zr-bevacizumab distribution were scored by calculating the maximum $SUV_{max}$. In blood samples, serial HSP70 levels, extracellular form of HER2 (HER2-ECD) were measured. NVP-AUY922 was administered to 16 patients (10 patients with HER2 positive and 6 with ER positive breast cancer). One partial response was observed (HER2 positive tumor); seven patients showed stable disease (3 HER2 positive, 4 ER positive tumors). $SUV_{max}$ change in individual tumor lesions on baseline versus 3 weeks $^{89}$Zr-trastuzumab PET was heterogeneous and related to size change on CT after 8 weeks treatment ($r^2 = 0.69$; $P = 0.006$). $^{89}$Zr-bevacizumab PET and FDG PET did not correlate with CT. Thus novel PET probes such as $^{89}$Zr-trastuzumab can be used to provide insights into responses to novel agents active in HER2 amplified breast cancer such as NVP-AUY922.

# Discussion and future perspectives

## Improving therapy for gestational trophoblastic neoplasia

In the exploratory study in chapter 2 we showed that it seems feasible to decrease the intensity of the treatment of high-risk gestational trophoblastic neoplasia and put 3 or 4 cycles of EP as initial treatment. Clearly, a randomized control trial is needed to confirm the findings in chapter 2 prospectively. Such a trial should also encompass long-term side effects.

## Further establishment of HER2 and VEGF-A imaging for clinical use

In chapters 5 and 7, HER2 status of metastatic lesions could be visualized by means of $^{89}$Zr-trastuzumab PET. In view of the proven benefit of anti-HER2 therapy in HER2 expressing breast cancer, when standard workup fails to establish the HER2 status of metastatic lesions, $^{89}$Zr-trastuzumab PET could be of potential value. Therefore, we are currently performing a prospective multicenter study to assess the role of $^{89}$Zr-trastuzumab PET in individualizing therapy (NCT 01957332). To evaluate the clinical utility of $^{89}$Zr-trastuzumab PET at first presentation of metastatic breast cancer a trial is ongoing (NCT 01832051).

## Molecular imaging of HER2 as biomarker for response to multiple treatments

The value of $^{89}$Zr-trastuzumab PET upfront to select lesions not responding to treatment with trastuzumab-DM1 (T-DM1) is currently studied (NCT 0565200). T-DM1 is an anti-HER2 antibody-drug conjugate. DM1 is a highly potent derivate of the antimicrotubule agent maytansine and its trastuzumab derived form combines the HER2-targeting with the intracellular delivery of DM1[3]. Whether this will imply that heterogeneic metastatic disease needs a heterogeneic treatment, in which non-responding lesions may be more suitable for local treatment, will have to be examined in future studies.

## Molecular imaging as screening tool

Tumor specific imaging, making use of molecular characteristics of the tumor, might potentially be of value as screening tool for early breast cancer. In this setting, a technique without radiation burden is preferable. The current estimated radiation burden of $^{89}$Zr-bevacizumab and $^{89}$Zr-trastuzumab PET is 19 milliSieverts (mSv) per tracer injection. To make optimal use of the tumor specificity of molecular imaging of VEGF-A while overcoming radiation issues, bevacizumab was also linked to the near-infrared fluorescent dye IRDye 800CW. This technique was tested in human xenograft-bearing athymic mice and detected tumor lesions in vivo. 800CW-bevacizumab detected lesions in the submillimeter range with a clinical intraoperative camera[4], which is more specific than $^{89}$Zr-bevacizumab PET and X-ray. Currently, a study with 800CW-bevacizumab in early breast cancer patients (NCT01508572) is almost finalized. The aim of this study is to determine the uptake of the VEGF-A targeting fluorescent tracer in breast cancer tissue, with diffuse optical tomography before and during surgery. With diffuse optical tomography,

we expect to visualize the tumor *in vivo*. When the tracer turns out to be tumor specific this may support further translation of this tracer for use during screening of breast cancer and other tumor types. Other antibodies such as trastuzumab can also be labeled with 800CW[4]. It is expected that major progress will be made in the clinical translation of optical imaging with fluorescent labeled antibodies as not only during surgery but also use during endoscopies is currently explored.

### Molecular imaging in other tumor types

As HER2 and especially VEGF-A play also a role in other tumor types, experience with molecular imaging can be translated to these tumors, for example in gestational trophoblastic neoplasia. Placental site trophoblastic tumor exhibited strong staining for VEGF, and gestational choriocarcinoma showed strong staining for VEGF receptor-3. Therefore, detection of metastases and even treatment in these subtypes might potentially be performed by means of molecular imaging. Further research in this rare disease is needed.

In conclusion, this thesis describes various aspects of optimizing patient- and treatment selection, which may ultimately contribute to improve outcome.

# References

1. Lower EE, Glass E, Blau R, et al. HER-2/neu expression in primary and metastatic breast cancer. Breast Cancer Res Treat 2009; 113:301-306.
2. Niikura N, Liu J, Hayashi N, et al. Loss of human epidermal growth factor receptor 2 (HER2) expression in metastatic sites of HER2-overexpressing primary breast tumors. J Clin Oncol 2012; 30:593-599.
3. Burris HA,3rd, Rugo HS, Vukelja SJ, et al. Phase II study of the antibody drug conjugate trastuzumab-DM1 for the treatment of human epidermal growth factor receptor 2 (HER2)-positive breast cancer after prior HER2-directed therapy. J Clin Oncol 2011; 29:398-405.
4. Terwisscha van Scheltinga AG, van Dam GM, Nagengast WB, et al. Intraoperative near-infrared fluorescence tumor imaging with vascular endothelial growth factor and human epidermal growth factor receptor 2 targeting antibodies. J Nucl Med 2011; 52:1778-1785.

# CHAPTER 9

## Nederlandse samenvatting

# Samenvatting

Ondanks vele nieuwe behandelingen is kanker is nog steeds één van de belangrijkste doodsoorzaken in de Westerse wereld. Kanker wordt behandeld met chirurgie, radiotherapie en/of systemische behandeling. Als systeemtherapie worden naast chemotherapie ook, doelgerichte medicijnen gegeven. Sinds kort is immunotherapie in opkomst. De bijwerkingen van anti-kanker behandelingen hangen samen met het soort medicijn, de dosering van het medicijn en de duur van de behandeling. Er wordt veel onderzoek verricht naar wat de meest optimale behandeling is voor patiënten.

Doelgerichte medicijnen zijn gericht tegen specifieke moleculaire kenmerken van de tumor. Het evalueren van deze kenmerken voorafgaande en vroeg tijdens de behandeling, kan mogelijk de respons op behandeling voorspellen, of in een vroeg stadium de beslissing om een behandeling te staken of te continueren ondersteunen. De patiënt hoeft dan niet nodeloos bijwerkingen te ervaren en er kan eerder worden overgegaan op een andere behandeling. We weten dat bijvoorbeeld het bepalen van de oestrogeenreceptor (ER) en de humane epidermale groeifactor receptor 2 (HER2) bij borstkanker zin heeft. Moleculaire typering van de tumor wordt meestal uitgevoerd op de primaire tumor of op een biopt van een uitzaaiing. Het nemen van biopten is echter niet altijd mogelijk, en het nadeel van een biopt is daarnaast dat het alleen een momentopname van de tumor biedt[1,2]. Het in beeld brengen van de moleculaire kenmerken met een radioactieve speurdosis gericht tegen een eigenschap met positron emissie tomografie (PET) is niet invasief, het kan een overzicht geven van het gehele lichaam en het kan bij herhaling worden uitgevoerd.

Een voorbeeld van een moleculair kenmerk voor moleculaire beeldvorming is HER2. HER2 is een belangrijke groeifactorreceptor en fosforylatie van HER2 leidt tot tumorcelgroei en differentiatie. In 20-25% van de borstkankers is er sprake van overexpressie van HER2. Het doelgericht behandelen gericht op deze receptor met trastuzumab geeft overlevingswinst in de adjuvante setting en bij vrouwen met uitgezaaide borstkanker[3,4]. Een ander voorbeeld is de vasculaire groeifactor (VEGF-A), die een sleutelfactor is in de omgeving van de tumorcellen, het micromilieu, waar het vaatnieuwvorming veroorzaakt. VEGF-A wordt door vele verschillende soorten kanker tot overexpressie gebracht. Radioactief gelabelde monoklonale antilichamen, gericht tegen HER2 en VEGF-A, kunnen als PET tracer deze eigenschappen afbeelden.

In dit proefschrift wordt onderzoek beschreven dat gericht is op het verbeteren van de behandeling van kanker door het evalueren van de optimale behandelduur, de detectie van tumoren en het monitoren van de behandeling. Het optimale chemotherapeutisch regime werd geëvalueerd bij patiënten met een persisterende trofoblast. Detectie van moleculaire kenmerken van tumorlaesies en tumorrespons op behandeling werd geëvalueerd bij patiënten met borstkanker door middel van beeldvorming met radioactief gelabelde monoklonale antilichamen gericht tegen HER2 en VEGF-A.

In **hoofdstuk 1** wordt een korte inleiding gegeven en worden de verschillende hoofdstukken geïntroduceerd. In **hoofdstuk 2** wordt de behandeling van een persisterende trofoblast

beschreven. Behandeling van laag risico persisterende trofoblast die niet reageert op monotherapie evenals primair hoog risico persisterende trofoblast bestaat uit polychemotherapie. De standaardbehandeling bevat chemokuren met actinomycine D (0,5 mg dag 1-2), etoposide (100 mg/m$^2$ dag 1-2), methotrexaat (300 mg/m$^2$), folinezuur (15 mg), vincristine (0,8 mg/m$^2$ dag 8) en cyclofosfamide (600 mg/m$^2$ dag 8) (EMA / CO). EMACP, een regiem bestaande uit etoposide (100 mg/m$^2$ dag 1-5), methotrexaat (300 mg/m$^2$ dag 1), cyclofosfamide (600 mg/m$^2$ dag 1), actinomycine D (0,5 mg/m$^2$ dag 2) en cisplatine (50 mg/m$^2$ dag 4) is ook bewezen werkzaam. Etoposide (100 mg/m$^2$ dag 1-5) en cisplatine (20 mg/m$^2$ dag 1-5) (EP) kan een alternatief zijn met dezelfde werkzaamheid en een kortere behandeltijd. Na normalisatie van het βhCG kregen patiënten behandeld met EMACP nog 2 consolidatiekuren, wat niet het geval is bij EP. In dit hoofdstuk evalueerden we de veiligheid, effectiviteit en behandelduur van EP en EMACP. Alle patiënten met een hoog risico, of een laag risico persisterende trofoblast die niet reageerde op monotherapie en werden behandeld sinds 2001 met EP in het Universiteits Medisch Centrum Groningen zijn vergeleken met de patiënten die tussen 1984-2001 werden behandeld met EMACP. Dertien patiënten kregen EP en 16 patiënten EMACP. Met een mediane follow-up duur van 173 maanden (range 11-344) was de overleving vergelijkbaar voor beide regimes (EP 92,3%, 93,8% EMACP, $P$ = 0,88). De mediane behandelingsduur was korter met EP (EP 78 dagen, range 63-84 dagen; EMACP 110 dagen, range 84-168 dagen; ($P$ = 0,006)). Concluderend kan gesteld worden dat in deze retrospectieve analyse EP dezelfde overleving had als EMACP met vergelijkbare toxiciteit en een kortere behandelduur.

In **hoofdstuk 3** wordt de rol van moleculaire beeldvorming in de ontwikkeling van doelgerichte anti-kankertherapie beschreven met de beeldvorming van HER2 en VEGF als voorbeelden. Moleculaire beeldvorming met radioactief gelabelde monoklonale antilichamen kan informatie geven over de aanwezigheid van de doelwitten voor deze doelgerichte behandelingen, bij alle tumorlaesies van de patiënt. PET kan gebruikt worden om veranderingen van de eigenschappen van de tumor door behandeling met een radioactief antilichaam te evalueren. Deze techniek kan mogelijk ook bijdragen om patiënten optimaal te selecteren voor doelgerichte anti-kanker therapie.

Steeds vaker wordt het micromilieu van de tumor, namelijk de directe omgeving waarin de tumorcellen zitten, een belangrijke rol toegedicht in het proces van tumorgroei en uitzaaiing. Factoren die deze processen ondersteunen zouden een doelwit kunnen zijn voor behandeling. In **hoofdstuk 4** wordt een uitgebreide literatuurbeschrijving gegeven van deze doelwitten in het micromilieu, die mogelijk gebruikt kunnen worden om zo kanker te behandelen. Ook worden de beschikbare methodes beschreven die het effect van behandeling kunnen monitoren en voorspellen. Een behandeling gericht op bot, met bisfosfonaten, kan een gunstig effect hebben op zowel de borstkanker zelf als eventuele uitzaaiingen in bot. Overgewicht beïnvloedt de energiehuishouding van (borst)kanker op een ongunstige manier, en tegengaan van overgewicht wordt een steeds belangrijker aspect bij behandeling van kanker. Naar het beïnvloeden van het immuunsysteem, om uitzaaiingen op te ruimen, wordt op dit moment veel onderzoek gedaan. Het beïnvloeden van de bloedvatvoorziening en de tumormatrix van uitzaaiingen lijkt nauwelijks effectief bij borstkanker.

In **hoofdstuk 5** wordt een studie beschreven waarin onderzocht wordt wat het effect van trastuzumab-behandeling is op de opname van $^{111}$In-trastuzumab. Een eerder artikel beschreef $^{111}$In-trastuzumab scintigrafie in 17 patiënten met een HER2 positief uitgezaaide borstkanker[5]. Om het effect van trastuzumab-behandeling op orgaanaccumulatie, radiatiedosimetrie en tumoropname van $^{111}$In-trastuzumab te evalueren, presenteren we hier aanvullende analyses van dezelfde patiënten die zowel voorafgaand aan, als tijdens behandeling met trastuzumab, een scintigrafie-procedure ondergingen. Patiënten kregen zes kuren van 3 weken met trastuzumab (2 mg/kg wekelijks na een oplaaddosis van 4 mg/kg) en paclitaxel (175 mg/m$^2$ 3-wekelijks) toegediend. $^{111}$In-trastuzumab werd geïnjecteerd op dag één van cyclus één ($t = 0$) en dag 15 van cyclus vier ($t = 1$). Whole-body scintigrafie werd verricht op vier momenten tussen 15 minuten en 7 dagen na de injectie met $^{111}$In-trastuzumab. Het verschil in tumor- en orgaanopname werd bepaald door middel van radiatiedosimetrie en uitgedrukt in residentietijden (gedefinieerd als oppervlakte onder de curve van radioactiviteit versus tijd). Bij 12 van de 17 patiënten konden beide scintigrafie-procedures genalyseerd worden. In totaal werden er 25 tumorlaesies gevisualiseerd, allen aantoonbaar bij beide scintigrafie-procedures. De residentietijden van de opname van de tracer in normale organen bleven gelijk tussen $t = 0$ en $t = 1$, met uitzondering van een toename in het bloedcompartiment ($P = 0{,}014$). De residentietijden van de opname van de tracer in de tumoren verminderde met 19,6% ± 53,8% ($P = 0{,}03$). Verandering van de residentietijd was niet gerelateerd aan tumorrespons zoals gemeten met conventionele beeldvorming. Ondanks behandeling met trastuzumab was het dus nog steeds goed mogelijk HER2 positieve tumoren af te beelden.

In **hoofdstuk 5B** worden de bevindingen met $^{89}$Zr-trastuzumab PET bij een bijzondere patiënt beschreven. Deze patiënte werd 2 jaar eerder gediagnosticeerd met twee primaire borstkankers waarvan er één wel en de andere niet HER2 tot overexpressie bracht. Op CT bleek zij meerdere uitzaaiingen te hebben, die allen moeilijk bereikbaar waren voor een biopt. Op $^{89}$Zr-trastuzumab PET werd er traceropname gezien in meerdere uitzaaiingen. De patiënt werd behandeld voor een HER2 positief uitgezaaide borstkanker met paclitaxel en trastuzumab waar de uitzaaiingen goed op reageerden.

De klinische haalbaarheid van $^{89}$Zr-bevacizumab PET bij primaire borstkanker wordt beschreven in **hoofdstuk 6**. Deze studie werd uitgevoerd om $^{89}$Zr-bevacizumab opname in borstkankers te evalueren. Bij patiënten met primaire borstkanker werd een $^{89}$Zr-bevacizumab PET scan van de borsten en de oksels verricht voorafgaand aan de operatie. $^{89}$Zr-bevacizumab opname werd gekwantificeerd als de maximum standaard uptake value ($SUV_{max}$) en gecorreleerd met de VEGF-A expressie van de tumor gemeten met Enzyme-Linked Immuno Sorbent Assay (ELISA). Op de PET scan werden 25 van de 26 tumoren gevisualiseerd. De $SUV_{max}$ was hoger in tumoren (1,85 ± 1,22, range 0,52-5,64) dan in het normale borstweefsel (0,59 ± 0,37; range, 0,27-1,69; $P < 0{,}001$). De enige niet gedetecteerde tumor was relatief klein ( diameter 10 mm). VEGF-A levels van 17 analyseerbare tumoren waren in alle gevallen hoger dan in het normale borstweefsel van dezelfde patiënte, en $^{89}$Zr-bevacizumab uptake correleerde met VEGF-A tumorspiegels (r = 0,49). Tumor

specifieke beeldvorming van VEGF-A maakt het mogelijk het grootste deel van de primaire borstkankers af te beelden.

Eén van de therapieën waarbij moleculaire beeldvorming als vroege voorspeller zou kunnen dienen is bij het gebruik van een remmer van Heat Shock Protein-90 (HSP90). De HSP90 remmer NVP-AUY922 verlaagt de expressie van vele oncogene eiwitten die van HSP90 afhankelijk zijn (inclusief HER2), en blokkeert vaatnieuwvorming indirect door het verlagen van hypoxia inducible factor 1α (HIF-1α) waardoor VEGF-A excretie afneemt. In **hoofdstuk 7** wordt een fase 2 studie met de HSP90 remmer NVP-AUY922 bij patiënten met uitgezaaide borstkanker beschreven. NVP-AUY922, 70 mg/m$^2$ werd eenmaal per week intraveneus toegediend aan patiënten met uitgebreide ER of HER2-positieve borstkanker. Analyse bestond uit $^{18}$F-fluordeoxyglucose (FDG), $^{89}$Zr-trastuzumab of $^{89}$Zr-bevacizumab PET scans, verricht voor behandeling en na respectievelijk 4 en 8 weken (FDG) en 3 weken ($^{89}$Zr-trastuzumab of $^{89}$Zr-bevacizumab). Responsevaluatie gebeurde volgens RECIST 1.0. De FDG, $^{89}$Zr-trastuzumab en $^{89}$Zr-bevacizumab verdeling werd gekwantificeerd door het berekenen van de $SUV_{max}$. In bloed werden seriële HSP70 monsters en de extracellulaire vorm van HER2 (HER2-ECD) gemeten. In totaal werden 16 patiënten behandeld met NVP-AUY922 (10 met HER2 en 6 met ER positieve borstkanker. Er was één patiënt met een partiële tumorrespons (HER2 positief); zeven patiënten hadden stabiele ziekte (3 HER2 positief, 4 ER positief). Verandering van de $SUV_{max}$ van individuele laesies op $^{89}$Zr-trastuzumab PET na 3 weken was heterogeen en gerelateerd aan de respons op de CT scan na 8 weken ($r^2 = 0,69$; $P = 0,006$). $^{89}$Zr-bevacizumab PET en FDG PET opname verandering correleerde niet met de tumorrespons op de CT scan. Nieuwe PET tracers zoals $^{89}$Zr-trastuzumab kunnen dus inzicht geven in de respons op nieuwe medicijnen zoals HSP90 remmers bij HER2 positieve borstkanker.

Samenvattend kan worden gesteld dat het optimaliseren van kankertherapie door het aanpassen van chemotherapiebehandelingen mogelijk is, en dat het gebruik van moleculaire beeldvorming met radioactief gelabelde antilichamen een rol kan gaan spelen bij de ontwikkeling van nieuwe doelgerichte anti-kanker behandelingen. Het onderzoek met radioactief gelabelde antilichamen dat beschreven is in dit proefschrift laat zien dat de techniek klinisch toepasbaar is bij patiënten met borstkanker.

# Referenties

1. Lower EE, Glass E, Blau R, et al: HER-2/neu expression in primary and metastatic breast cancer. Breast Cancer Res Treat 2009; 113:301-306.
2. Niikura N, Liu J, Hayashi N, et al: Loss of human epidermal growth factor receptor 2 (HER2) expression in metastatic sites of HER2-overexpressing primary breast tumors. J Clin Oncol 2012; 30:593-599.
3. Slamon DJ, Clark GM, Wong SG, Levin WJ, Ullrich A, McGuire WL. Human breast cancer: correlation of relapse and survival with amplification of the HER-2/neu oncogene. Science 1987; 235:177-82.
4. Masood S, Bui MM. Prognostic and predictive value of HER2/neu oncogene in breast cancer. Microsc Res Tech 2002; 59:102-8.
5. Perik PJ, Lub-De Hooge MN, Gietema JA et al. Indium-111-labeled trastuzumab scintigraphy in patients with human epidermal growth factorreceptor 2-positive metastatic breast cancer. J Clin Oncol 2006; 24:2276-2282

# Dankwoord

# Dankwoord

Allereerst wil ik alle patiënten bedanken die op een heel moeilijk moment in hun leven hebben besloten bij te dragen aan de studies beschreven in dit proefschrift. Zonder hen was het niet mogelijk geweest dit proefschrift te schrijven.

Veel dank gaat uit naar het promotieteam, bestaande uit promotor prof. dr. Liesbeth de Vries, en copromotores dr. Carolien Schröder, dr. Adriënne Brouwers en dr. Marjolijn Lub-de Hooge.

Beste Liesbeth, iedereen die bij jou gepromoveerd is weet dat je kritische en snelle kijk op manuscripten onmisbaar zijn. Het was fijn dat je me betrok bij verschillende gynaecologische projecten, we samen zwangere patiënten met borstkanker behandelden, en ik de kans kreeg om een paar maanden als ANIOS gynaecologie in het Martini Ziekenhuis te werken.

Beste Carolien, bedankt voor je snelle en goede kijk op de manuscripten. Met veel plezier deed ik op de woensdagmiddagen mee met jouw poli. Het was prettig om op deze manier veel te leren van de 'reguliere' oncologie.

Beste Adriënne, heel wat uren hebben we samen doorgebracht in de computerruimte van de nucleaire geneeskunde. Het was fijn dat je altijd tijd maakte om de scans samen te beoordelen.

Beste Marjolijn, dank je dat jij vanuit de farmacologische kant een verfrissende blik had, waardoor de verschillende studies uiteindelijke veel interessanter werden.

De leden van de leescommisie, prof. dr. R.A.J.O. Dierckx, prof. dr. J.G.W. Kosterink en prof. dr. E. Vellenga, dank ik hartelijk voor de snelle beoordeling van dit proefschrift, zodat ik nog voor mijn verlof mijn proefschrift mag verdedigen.

Het Multidisciplinair Oncologisch laboratorium wil ik bedanken voor alle hulp en gezelligheid. Met name het imaging team wil ik bedanken voor de nuttige discussies (dr. Hetty Timmer-Bosscha, Anton, Thijs, Michel, Frederike, Martine, Titia, Hilde, Frank-Jan, Eva). Linda en Silke, bedankt voor de vele labelingen, ELISA's, en scoringen.

De afdeling Medische Oncologie bedankt voor alle (administratieve) ondersteuning (Gerry Sieling, Gretha Beuker, Bianca Smit) en voor de nuttige discussies over de verschillende projecten (dr. An Reyners, prof. dr. Jourik Gietema, prof. dr. Geke Hospers, dr. Sjoukje Oosting en dr. Thijs Oude Munnink)

De afdeling Nucleaire geneeskunde en Moleculaire Beeldvorming bedankt voor alle ondersteuning bij het maken (en uitwerken) van de verschillende scans. Eerder beginnen of langer doorgaan om er toch nog een Zr-scan of injectie tussen te krijgen was nooit een probleem (dr. Johan de Jong, Paul van Snick, Hans ter Veen, Clara Lemstra, Gert Luurtsema en Klaas Willem Sietsma).

De afdeling radiologie bedankt voor het beoordelen van alle scans (drs. Sybille van der Meulen, drs. Fons Bongaerts).

De afdeling pathologie bedankt voor de hulp met kleuringen en scoren (dr. Jos Bart, prof. dr. Harry Hollema, Tineke van der Sluis).

De afdeling chirurgie bedankt voor de hulp bij het includeren van patiënten, de 'EDD meetings' waren altijd gezellig (dr. Jaap de Vries, dr. Liesbeth Jansen, Arieke Prozee, drs. Kees Meijer en Marjan Beernink).

De afdeling gynaecologische oncologie bedankt voor alle samenwerking en het verzamelen van weefsel (prof. dr. Marian Mourits, prof. dr. Ate van der Zee, dr. Henriëtte Arts, Harry Klip, Klaske ten Hoor en dr. Welmoed Reitsma.

Mijn onderzoekstijd was nooit zo leuk geweest zonder mijn kamergenoten en maatjes van boven en het Triade. Bedankt voor de (ijzige) weekendjes weg, alle borrels, quizzen, schaatswedstrijdjes en etentjes. Anton, Michel, Martine, Hink, Rob, Titia, Frederike, Niek, Hilde, Sophie, Jolien, Jolien, Sjoukje, Grytsje en Lars.

De afdeling intensive care van het Medisch Spectrum Twente en de afdeling gynaecologie van het Deventer Ziekenhuis, bedankt voor jullie belangstelling tijdens de afrondende fase van dit proefschrift.

Lieve vrienden en familie, lieve papa en mama, bedankt voor jullie interesse in mijn onderzoek gedurende het hele traject.

Lieve paranimfen, bedankt voor jullie hulp en interesse voor mijn promotietraject. Lieve Wendy, je hebt zelfs je vakantie verzet om erbij te kunnen zijn. Dank je wel! Lieve Richtje, fijn dat je mijn paranimf wilt zijn.

Lieve Marcel, we konden altijd lachen om de laatste zin van het dankwoord bij andere proefschriften. Nu zijn we het zelf. Dankjewel!